Методы анализа поверхности

Электронная спектроскопия, сканирующая зондовая микроскопия

А.Н. Чайка, А.М. Ионов

- **РОССИЙСКАЯ АКАДЕМИЯ НАУК**
- **ИНСТИТУТ ФИЗИКИ ТВЕРДОГО ТЕЛА**

План

Возможности электронной спектроскопии

Сканирующая зондовая микроскопия

Пример исследования низкоразмерных структур с использованием комплекса методик: графен/SiC/Si(001)

Исторический экскурс

Заключение

Электронная спектроскопия

Возможности электронной спектроскопии

- исследование атомной и электронной структуры соединений, поверхностей и границ раздела;
- определение химического состава многокомпонентных соединений;
- изучение динамических процессов на поверхности;
- изучение взаимосвязи электронной и атомно-кристаллической структуры поверхности изучаемых объектов с их свойствами

Получение чистой поверхности

Основные методы

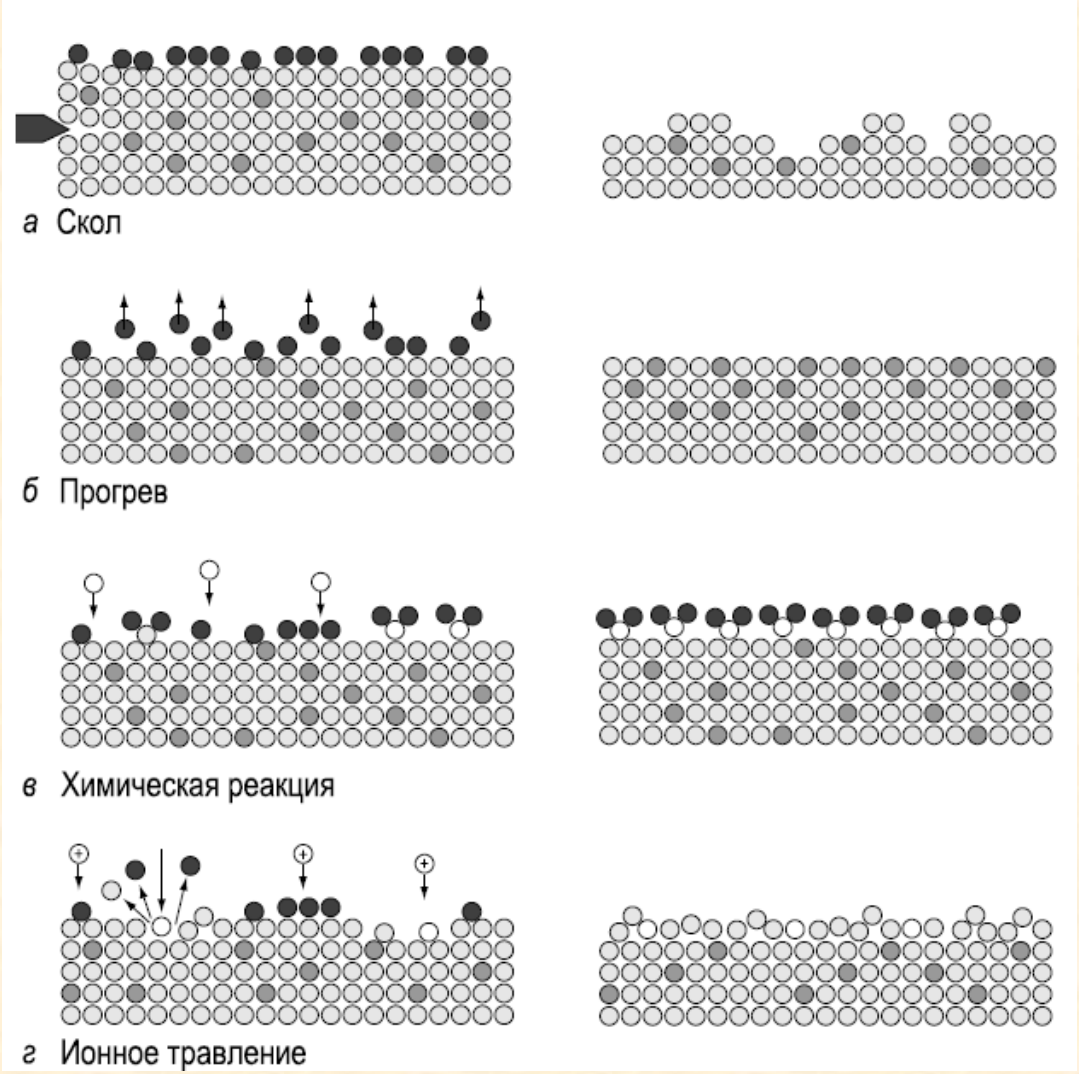

Один монослой адсорбата «прилипает» к поверхности за 1 секунду при давлении $p=1x10^{-6}$ Торр.

Для получения чистой поверхности и анализа ее структуры давление в камере должно бытьне выше $1x10^{-9}$ Торр

Методы физики поверхности
(список далеко не полон)

Оже-электронная спектроскопия (AES) – *химический состав поверхности*

Фотоэлектронная спектроскопия (UPS, XPS) – *электронная структура поверхности, состав*

Дифракция медленных электронов (LEED) – *изображение обратной решетки, упорядочение атомов поверхности*

Спектроскопия поглощения (EXAFS) – *структура, ориентация химических связей*

Как правило, нет прямой информации об атомной структуре поверхности; усредненная информация по площади зондирования пучком фотонов или электронов, невысокая локальность методов

Микроскопия медленных электронов – прямая визуализация поверхности с субмикронным разрешением

Сканирующая зондовая микроскопия - *исследование структуры и свойств поверхности с атомным разрешением*

Дифракция медленных электронов

Схема 4-сеточной установки ДМЭ

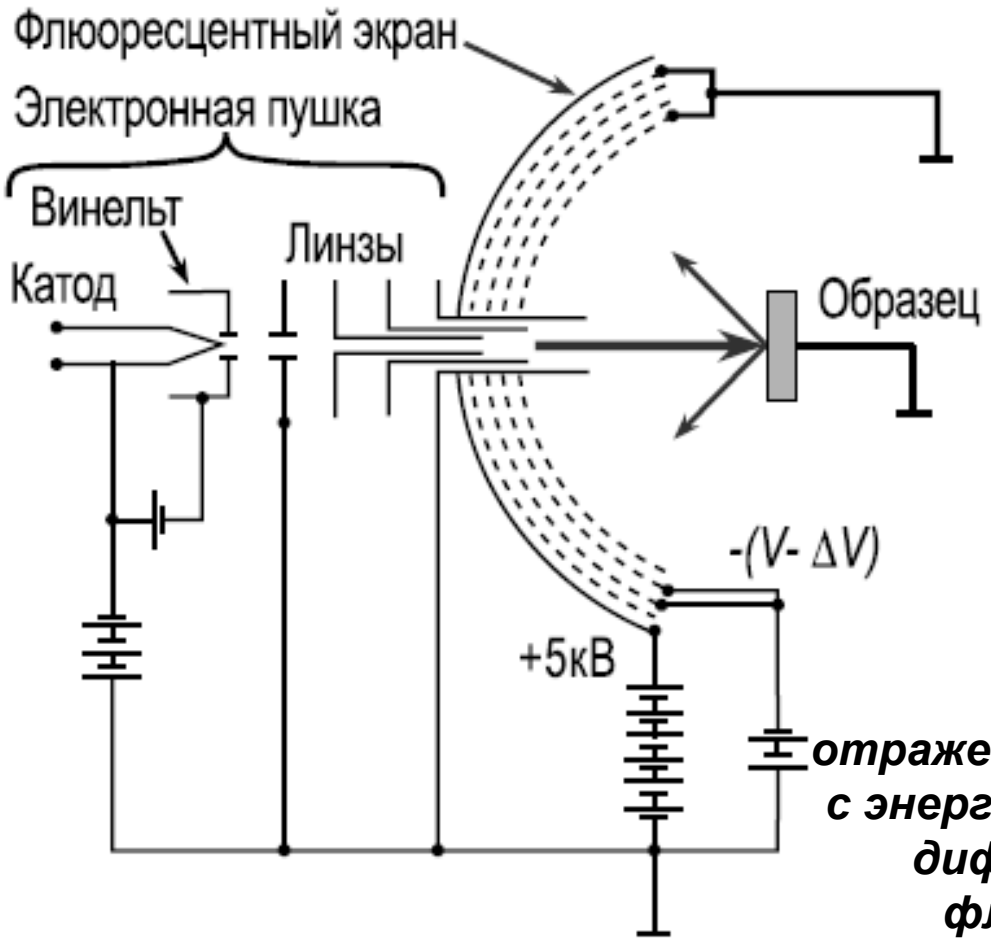

ДМЭ
Si(111)-7×7

отраженные от образца электроны с энергиями 10--100 эВ формируют дифракционную картину на флюоресцентном экране

Электронная спектроскопия

Оже-электронная спектроскопия AES

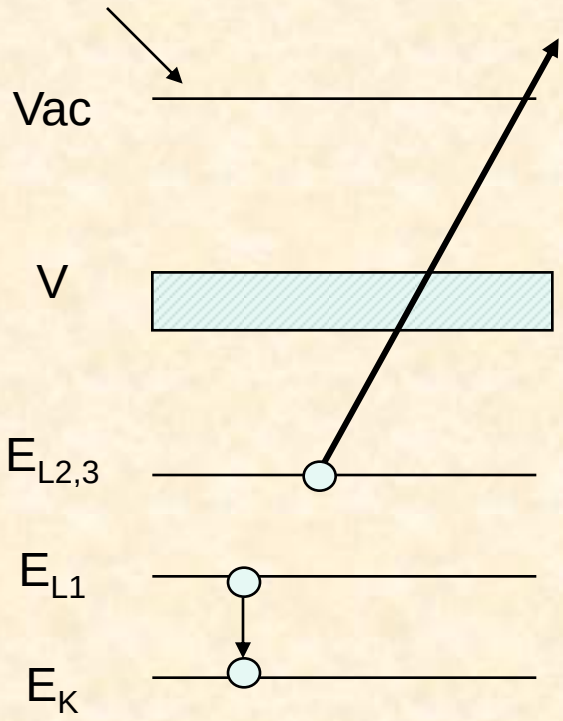

$KE = E_K - E_{L1} - E_{L23} - \Phi$

Рентгеновская фото-электронная спектроскопия XPS

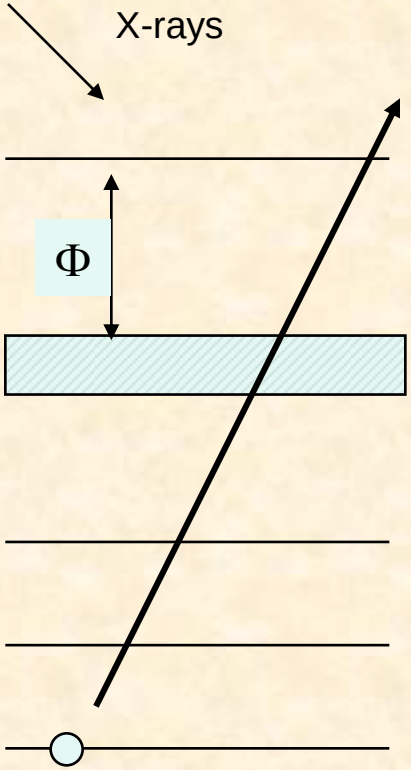

$KE = h\nu - E_K - \Phi$

Ультрафиолетовая фотоэлектронная спектроскопия UPS

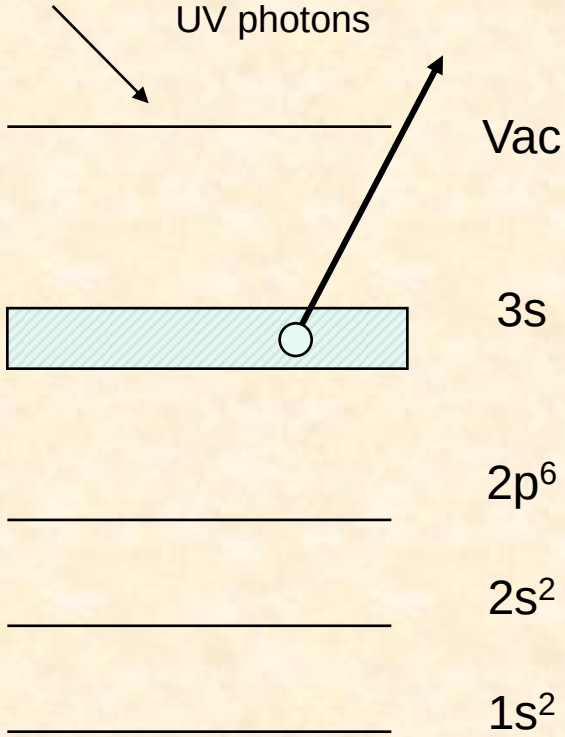

$KE = h\nu - E_V - \Phi$

Схема электронного спектрометра

УФ источник

ДМЭ

Электронная пушка ОЭС, СХПЭ

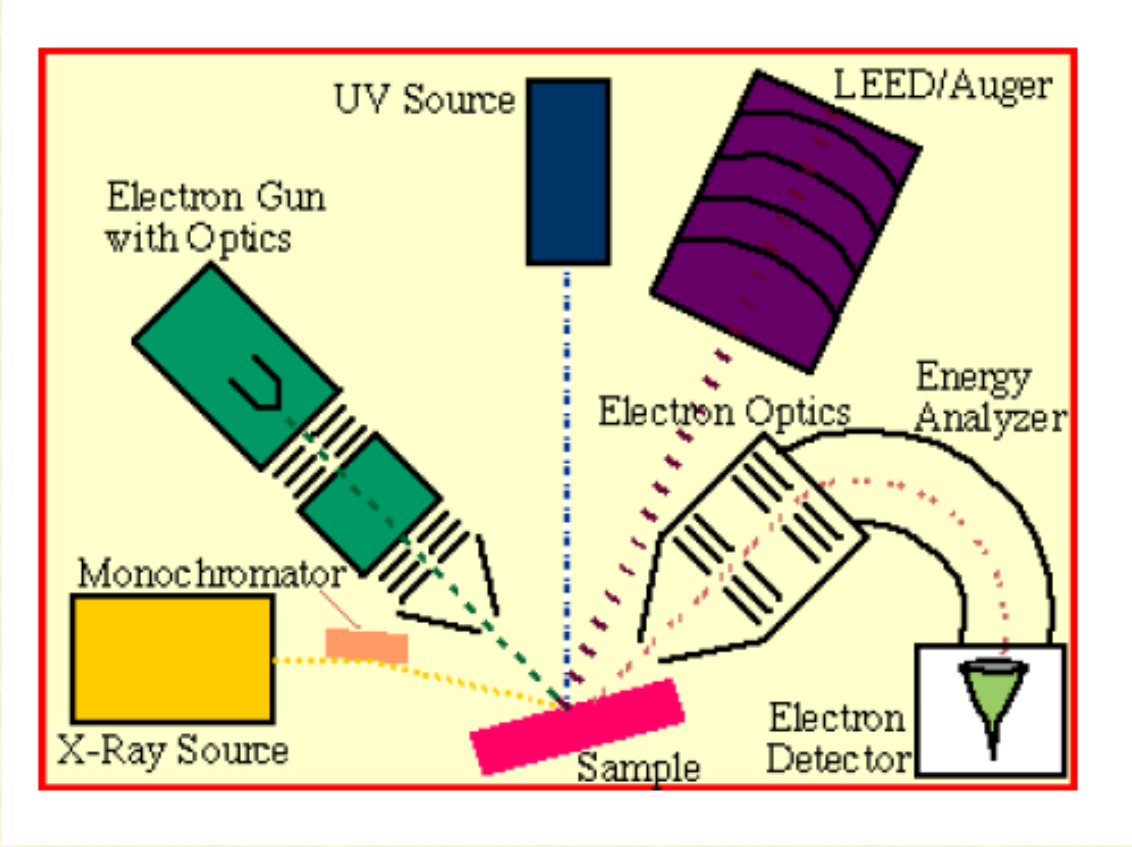

Анализатор

Рентгеновский источник

Детектор

Образец

Электронный спектрометр ESCALAB-5 с низкотемпературным криоманипулятором

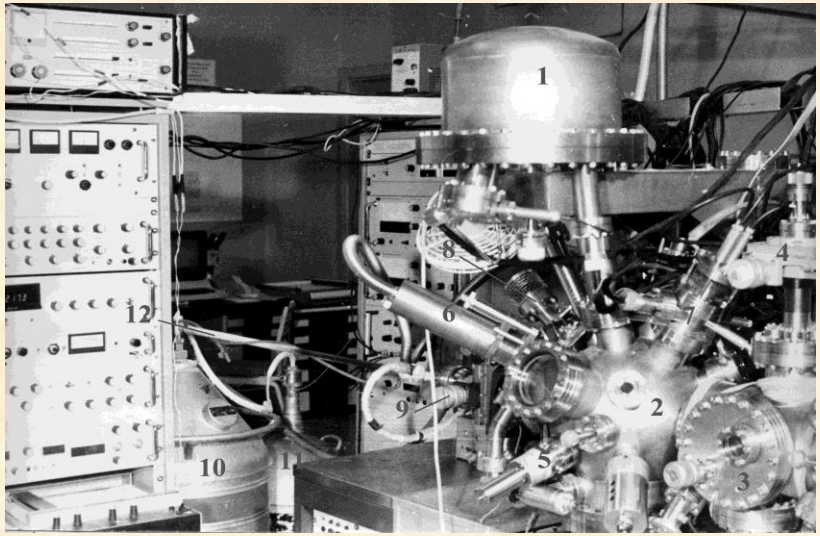

Электронный спектрометр ESCALAB-5 в ИФТТ РАН

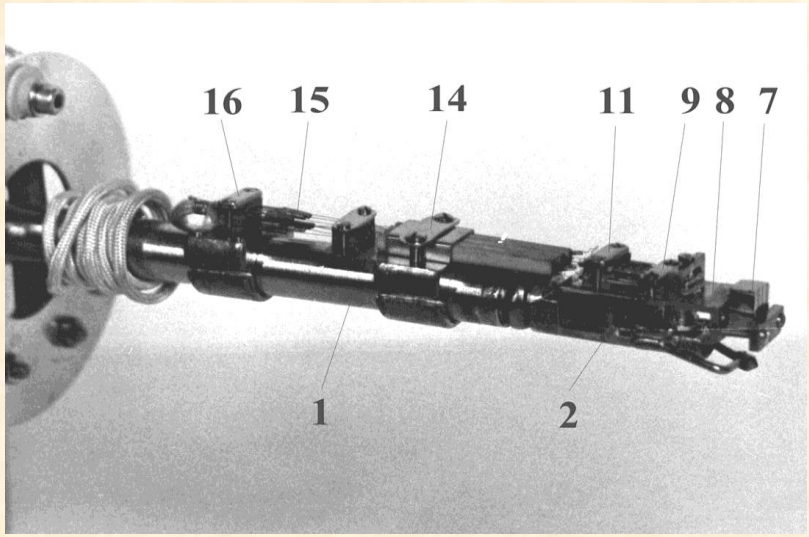

Низкотемпературный криоманипулятор

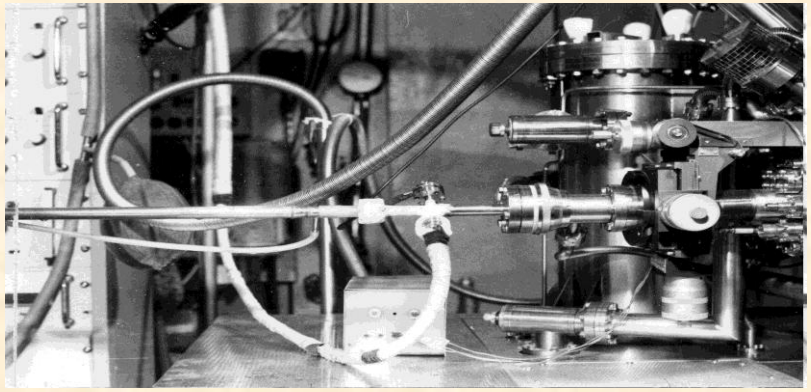

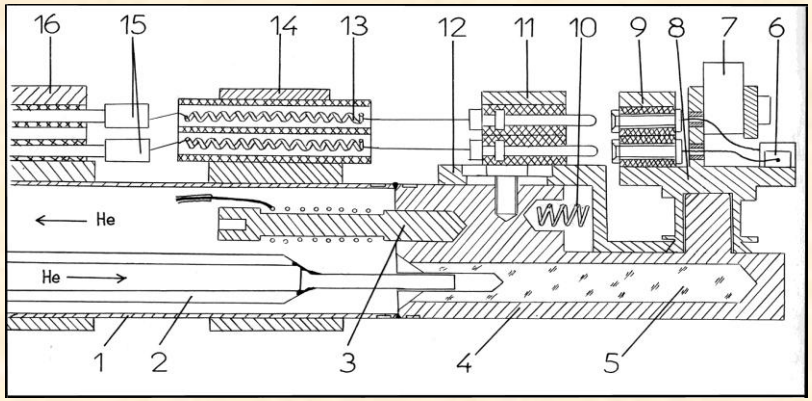

KRATOS AXIS Ultra DLD
(ИФТТ РАН)

X-ray spectroscopy

UPS spectroscopy

AES+SEM

AES and XPS mapping

LEED

Фотоэлектронная спектроскопия

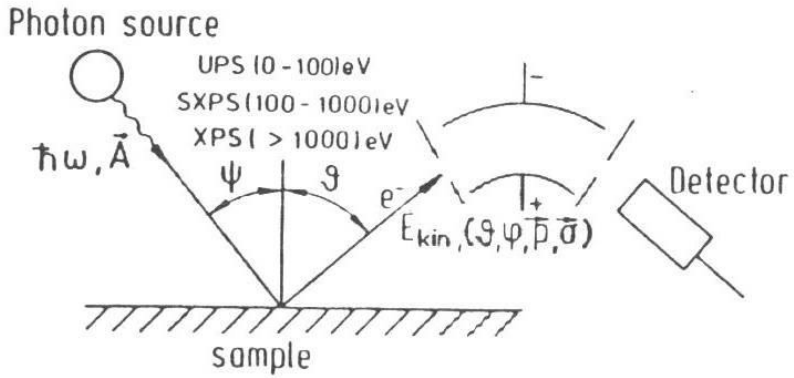

PES spectra

$E_{kin}=h\nu-\Phi-E_B$

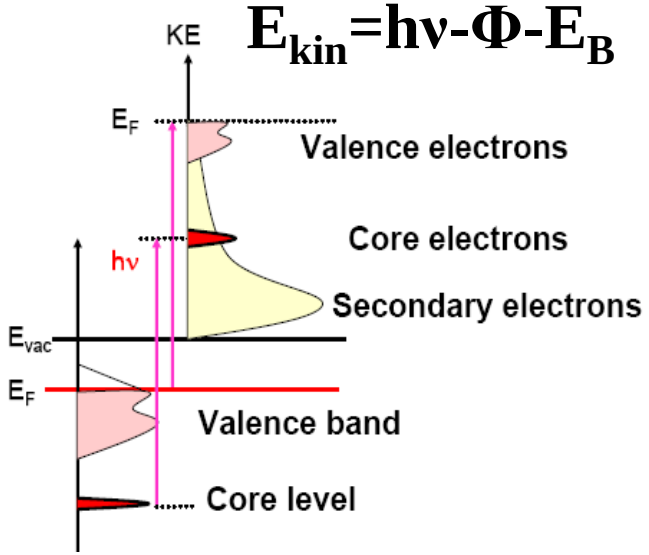

При изменении энергии фотонов меняется кинетическая энергия электронов, выбитых с остовного уровня, и поверхностная чувствительность метода

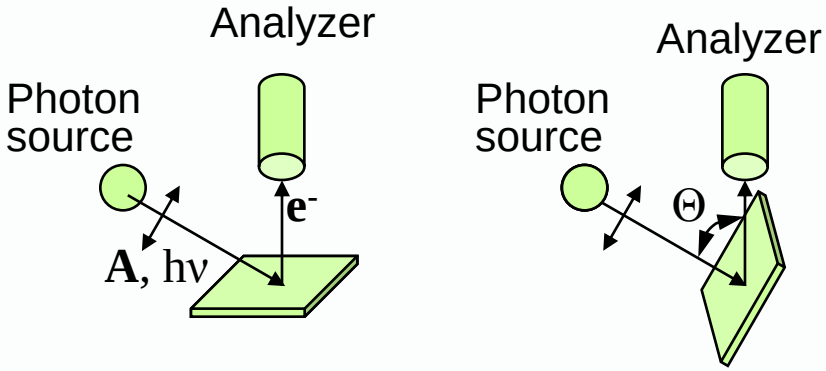

При линейной поляризации фотонов можно подобрать угол эмиссии электронов, при котором вектор поляризации направлен вдоль определенных химических связей

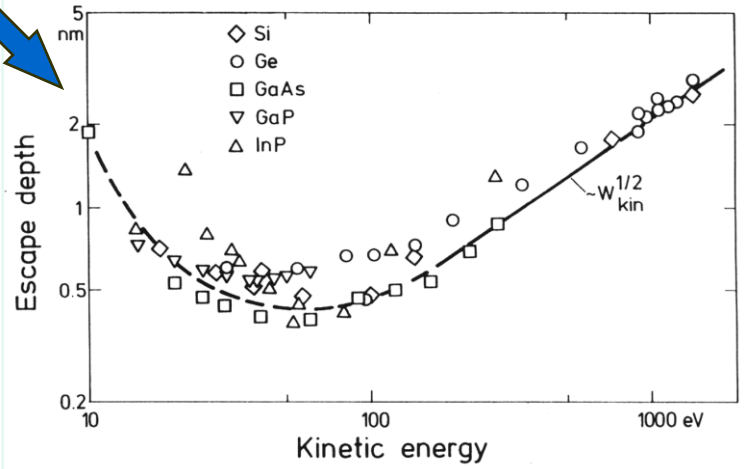

Atomic Spectra

- **Electron excitation**
  - The excitation can occur at different degrees
    - low E tends to excite the outmost e^-'s first
    - when excited with a high E (photon of high *v*) an e^- can jump more than one levels
    - even higher E can tear inner e^-'s away from nuclei
  - An e^- at its excited state is not stable and tends to return its ground state
  - If an e^- jumped more than one energy levels because of absorption of a high E, the process of the e^- returning to its ground state may take several steps, - i.e. to the nearest low energy level first then down to next …

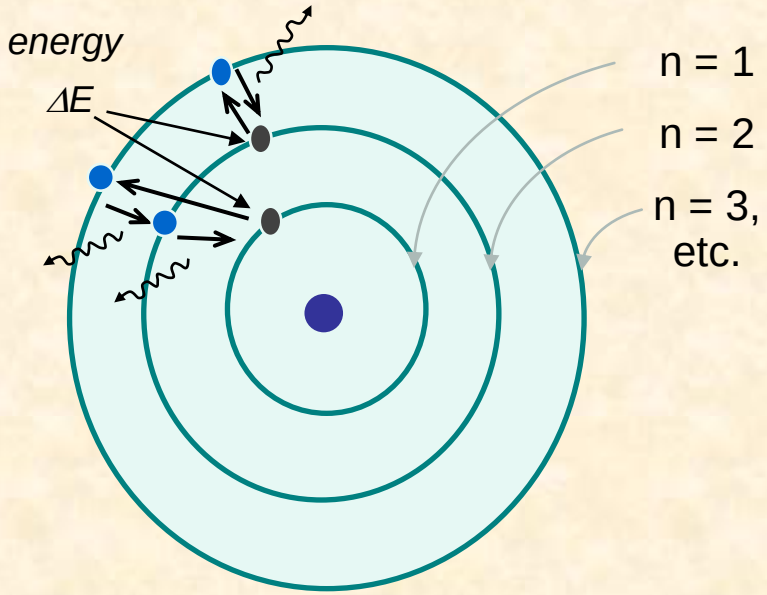

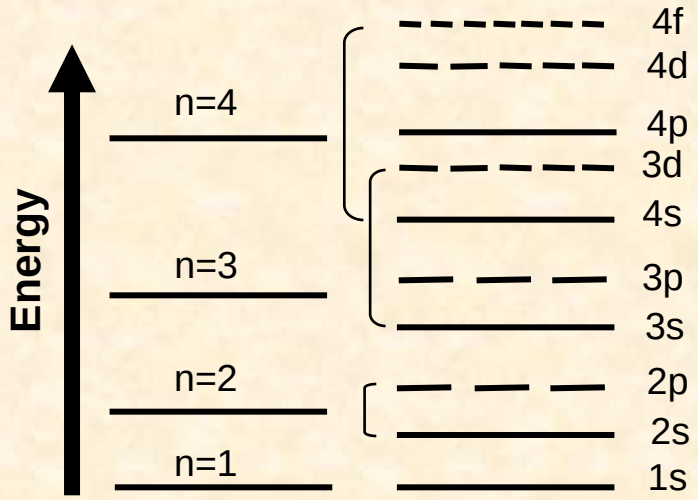

РФЭС спектры остовных уровней

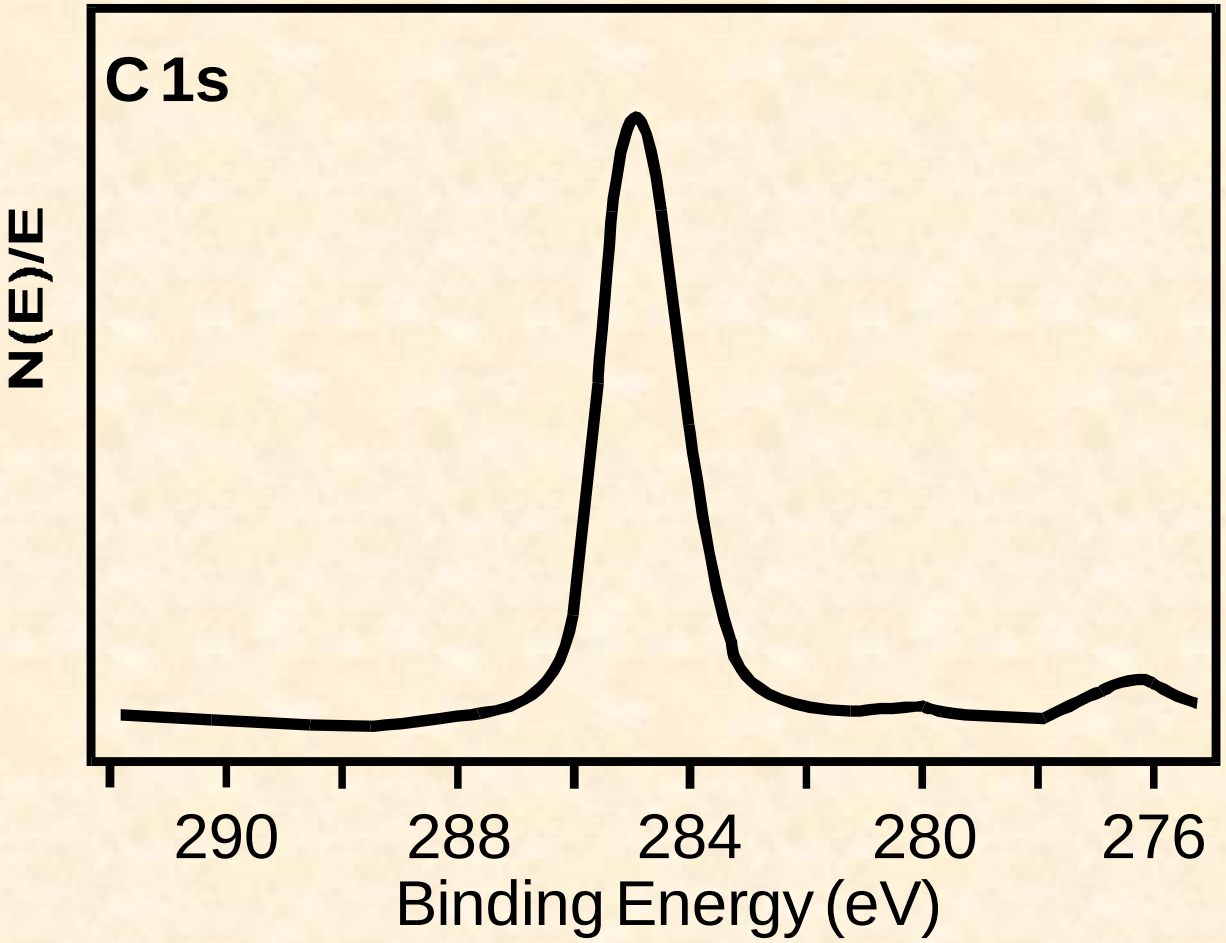

Orbital=s

l=0

s=+/-1/2

ls=1/2

***S* - состояния**

РФЭС спектры остовных уровней

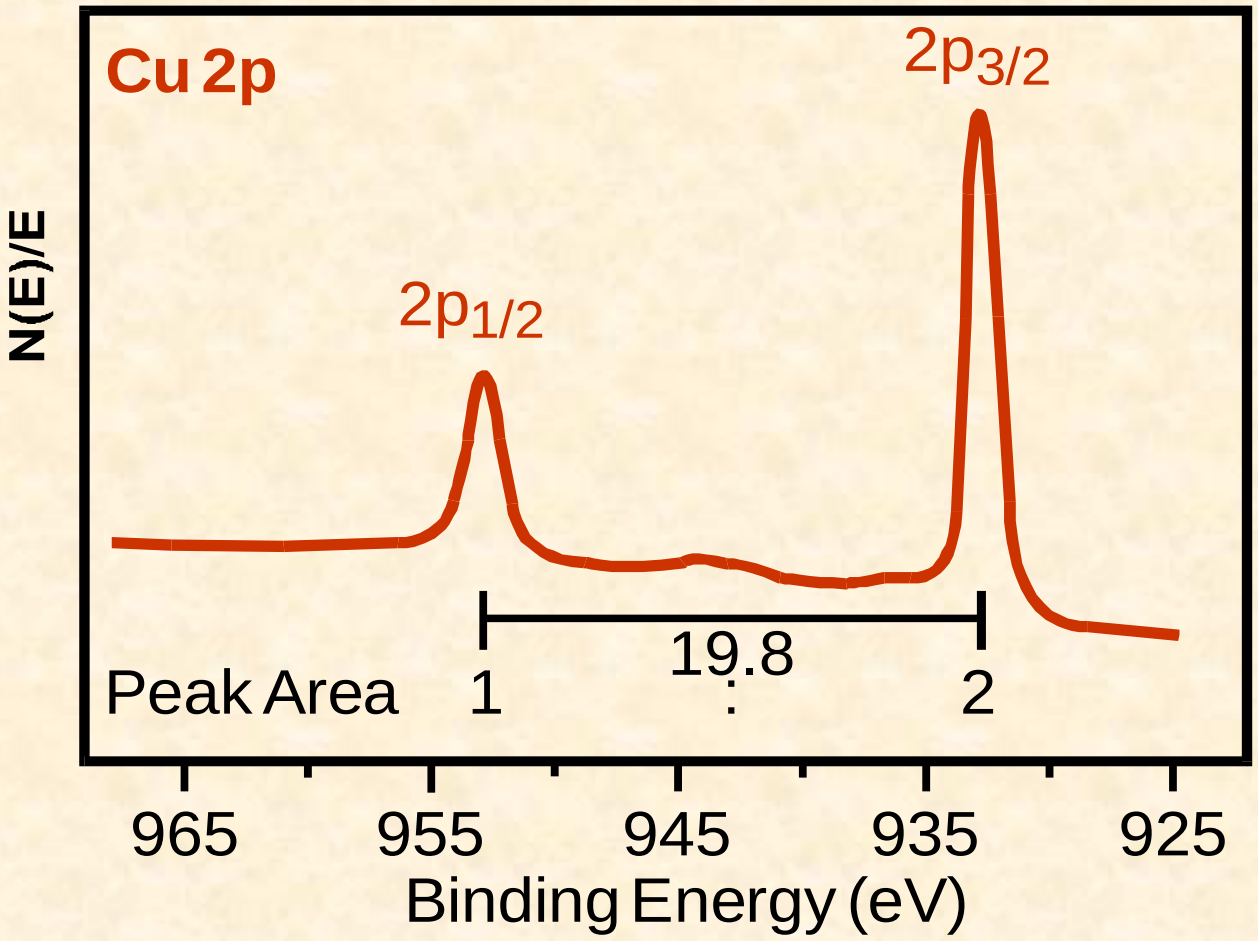

Orbital=p

l=1

s=+/-1/2

ls=1/2,3/2

***p* - состояния**

РФЭС спектры остовных уровней

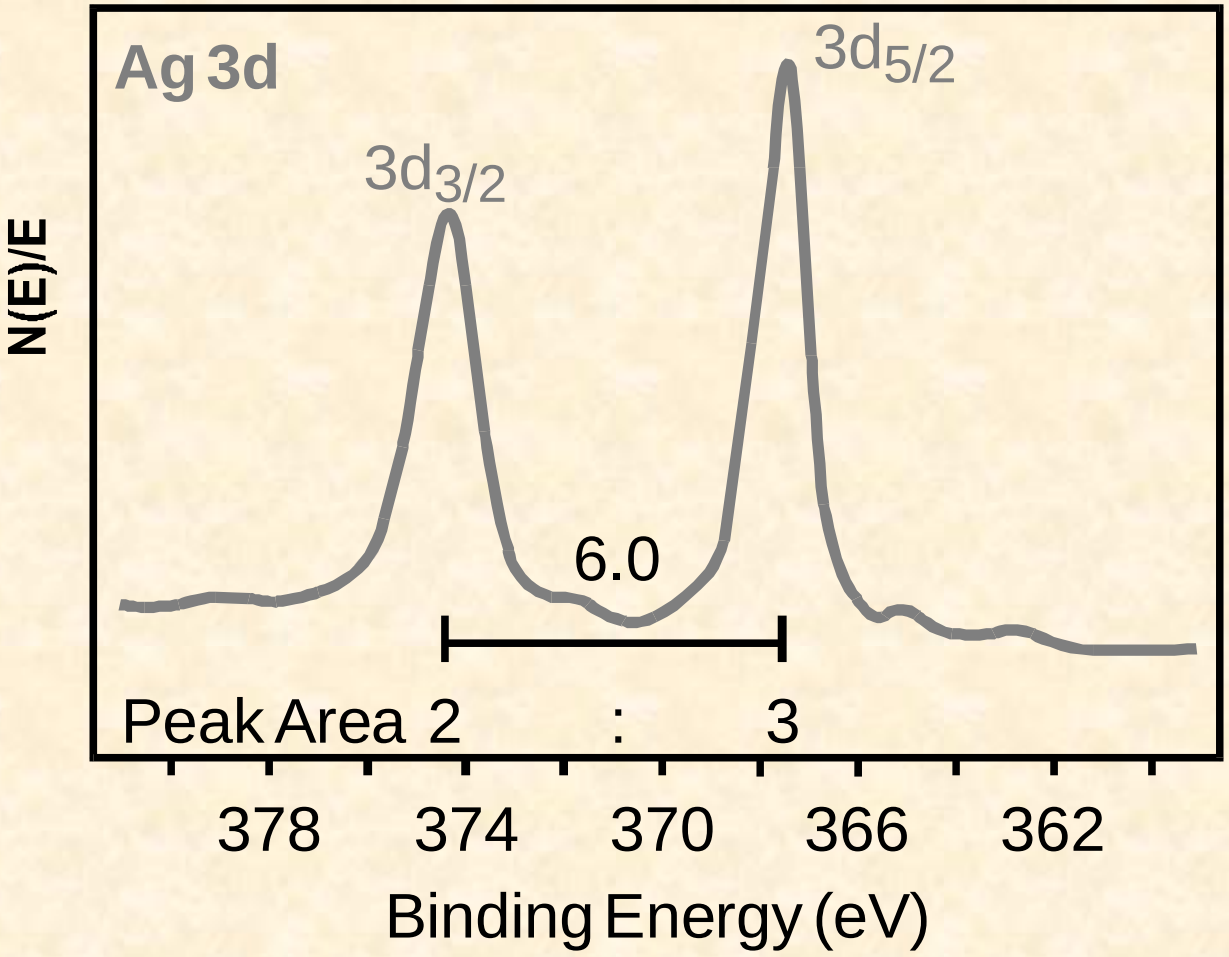

Orbital=d

l=2

s=+/-1/2

ls=3/2,5/2

***d* - состояния**

РФЭС спектры остовных уровней

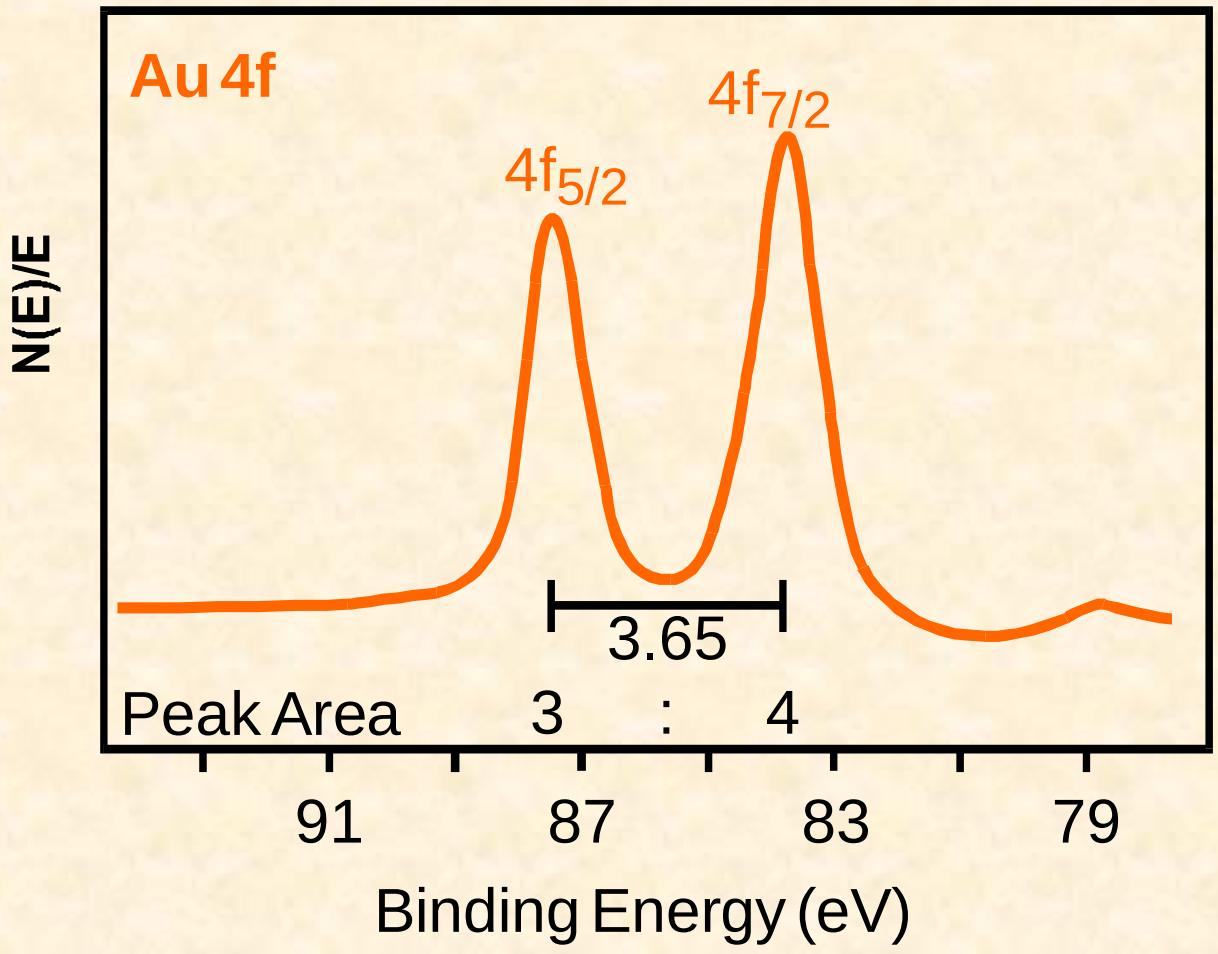

Orbital=f

l=3

s=+/-1/2

ls=5/2,7/2

***f* - состояния**

РФЭС спектры многокомпонентных соединений

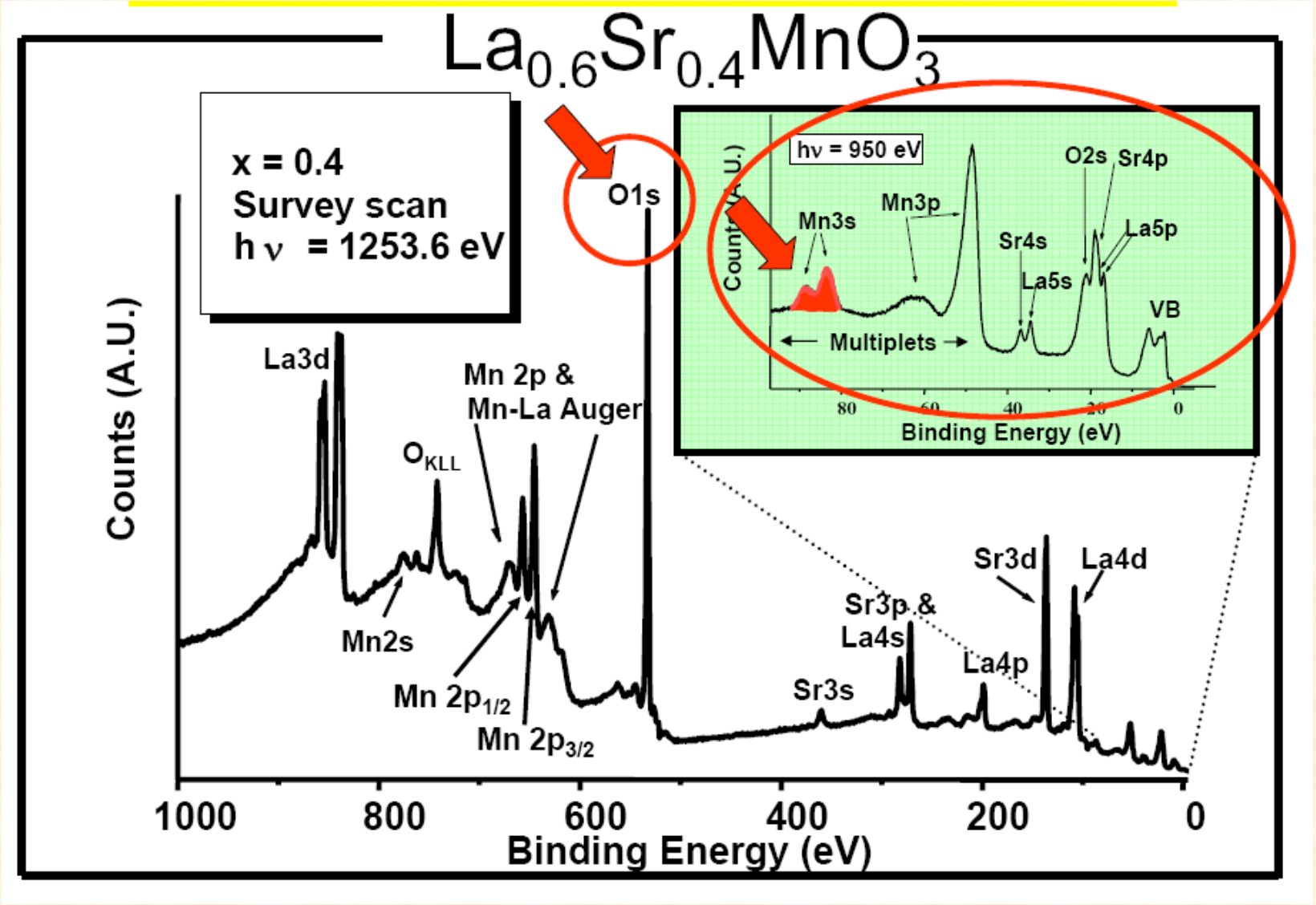

Определение элментного состава по РФЭС спектрам: сплав Cu-Ni

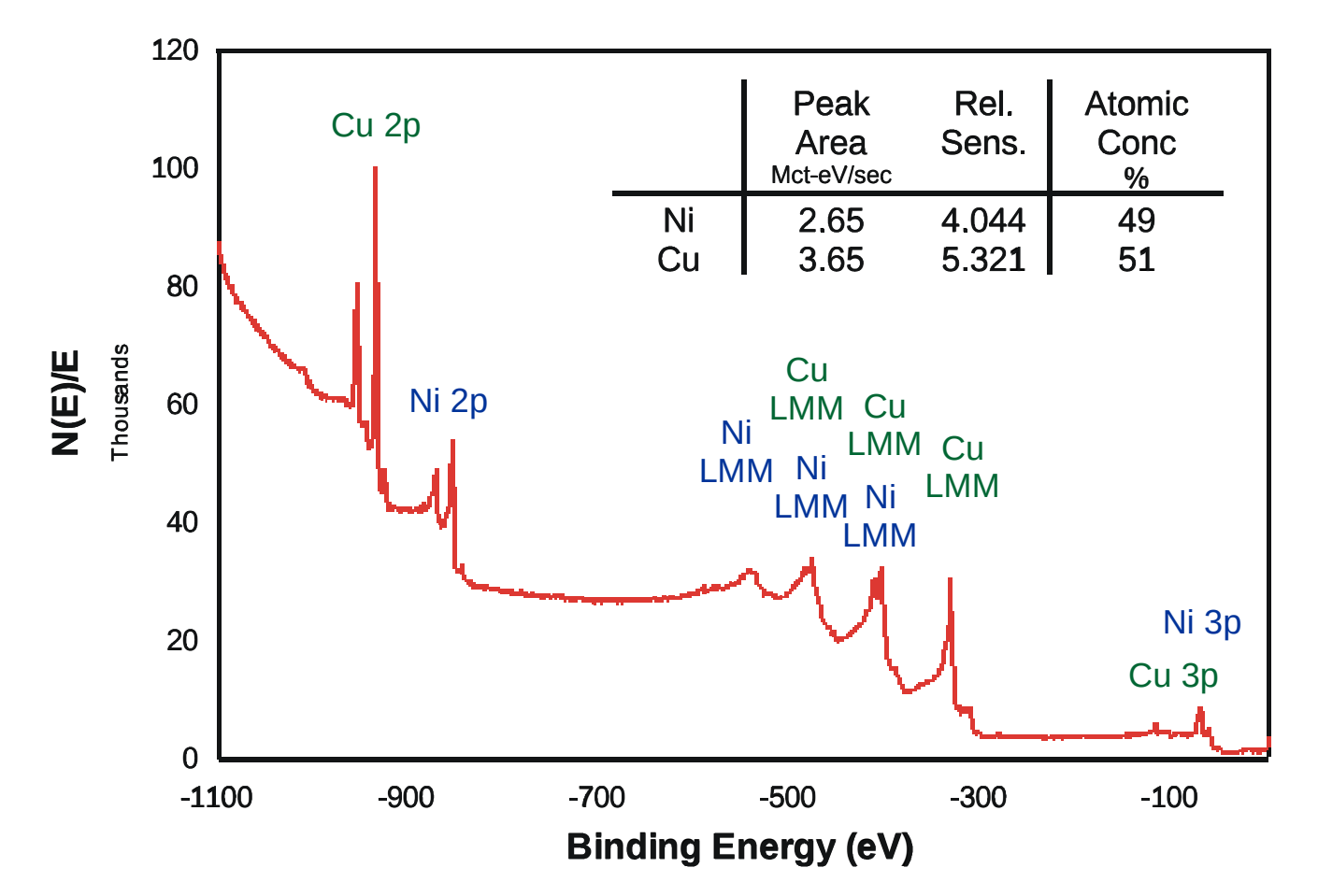

по интенсивностям линий и сечениям фотоионизации можно определить концентрации элементов в многокомпонентных соединениях

Химический сдвиг спектров остовных уровней: *оксид кремния на Si(001)*

Charge transfer, e^-- e^- coulomb integral:

$$Shift \approx q_{Si} K_{Si2p,Si3p} =$$

$$\int \varphi^*_{2p}(\vec{r}_1)\varphi^*_{3p}(\vec{r}_2)\frac{e^2}{r_{12}}\varphi_{2p}(\vec{r}_1)\varphi_{3p}(\vec{r}_2)dV_1dV_2$$

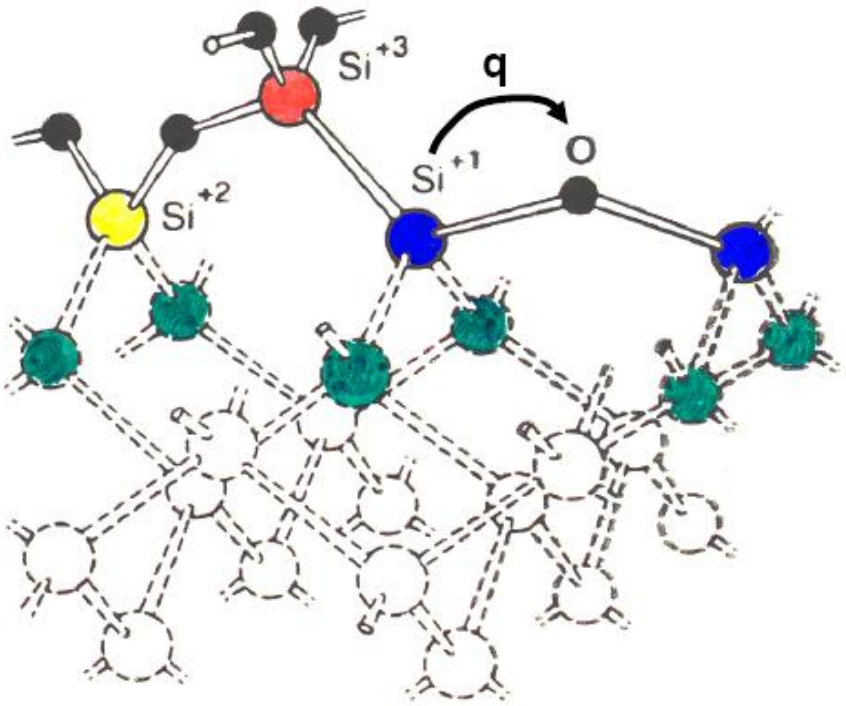

Himpsel et al., Phys. Rev. B 38, 6086 ('88)

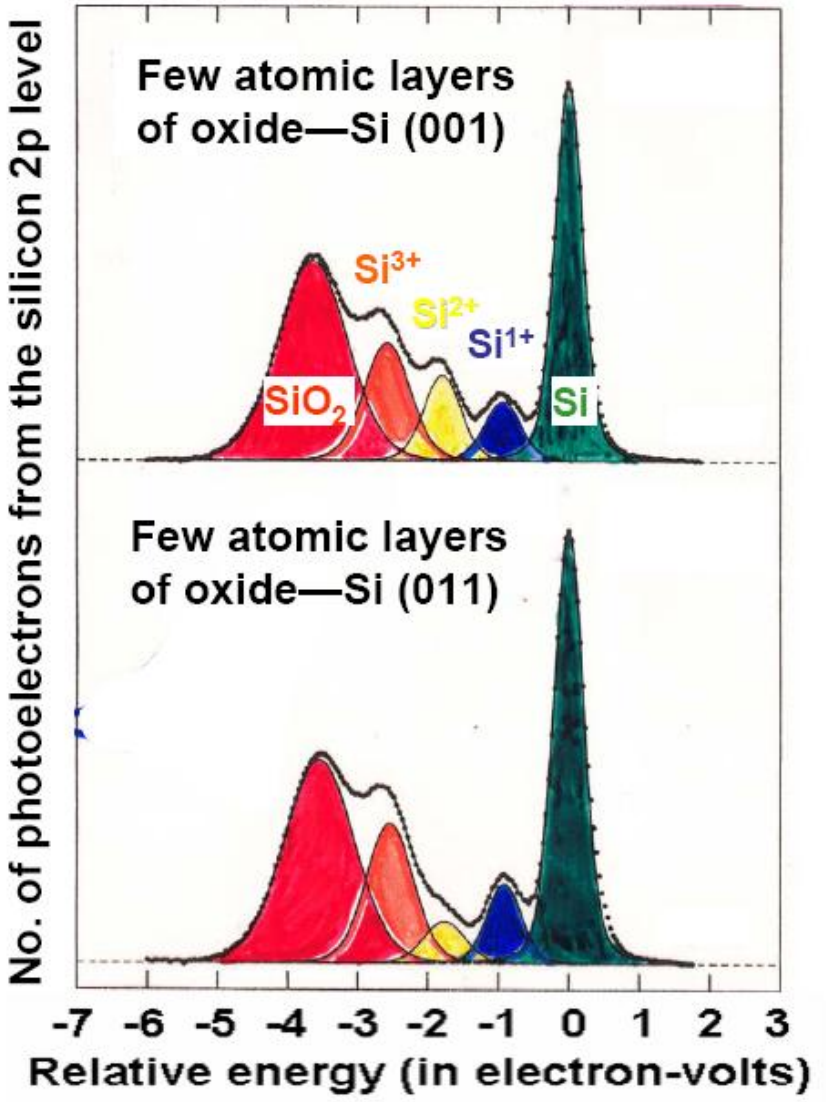

Химический сдвиг РФЭС спектров *Si 2p* в различных соединениях

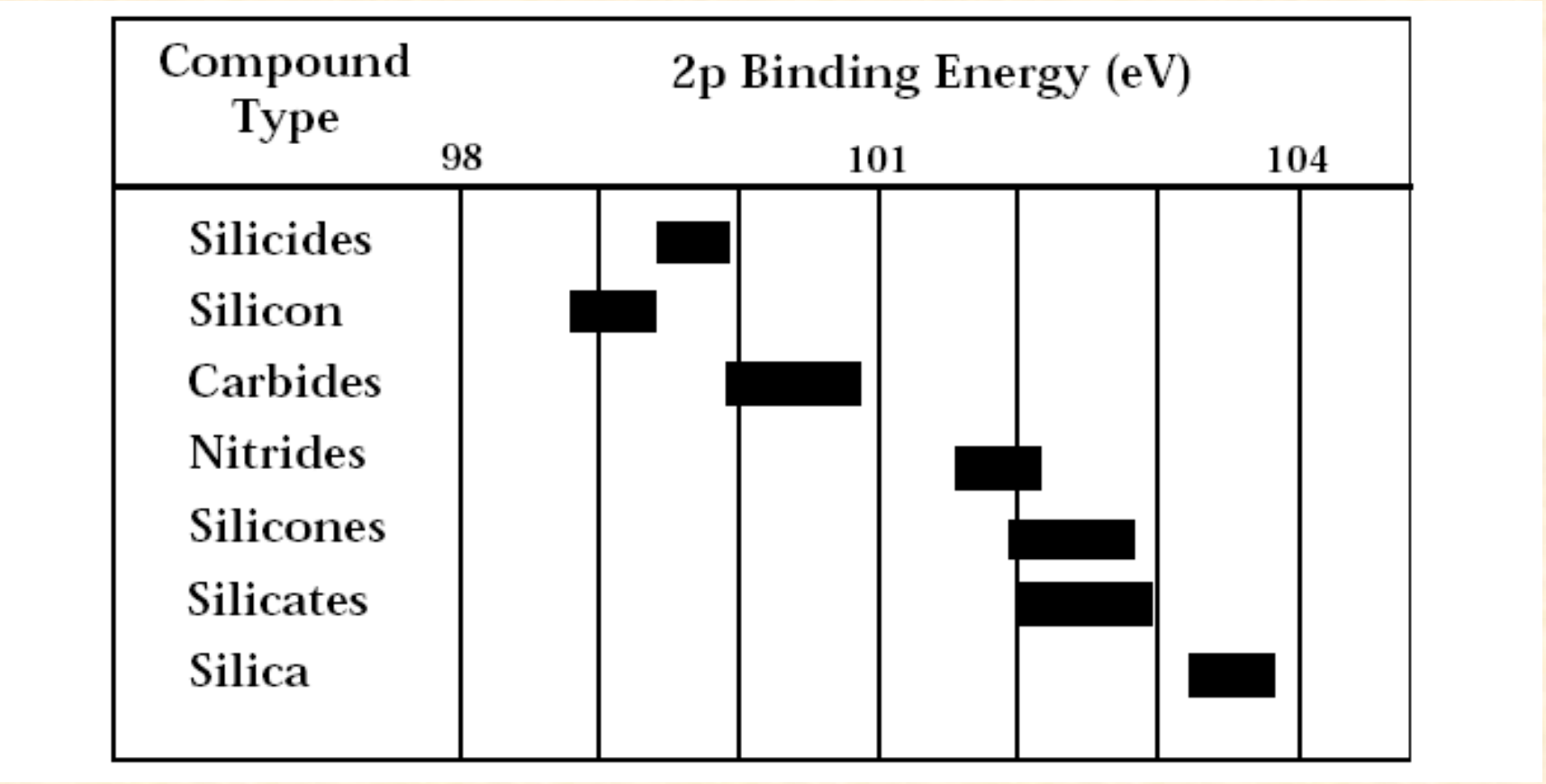

энергетический сдвиг спектров остовных уровней может достигать нескольких эВ, что позволяет идентифицировать химические соединения

Химический сдвиг РФЭС спектров C 1s в различных соединениях

Functional Group		*Binding Energy (eV)*
hydrocarbon	C-H, C-C	285.0
amine	C-N	286.0
alcohol, ether	C-O-H, C-O-C	286.5
Cl bound to C	C-Cl	286.5
F bound to C	C-F	287.8
carbonyl	C=O	288.0

энергетический сдвиг спектров остовных уровней может достигать нескольких эВ, что позволяет идентифицировать химические соединения

Металлорганические комплексы на основе порфиринов

Порфирины – молекулярные комплексы для нанотехнологий:
Решение проблемы управляемого фотосинтеза;
Создание элементов и устройств на основе отдельных молекул

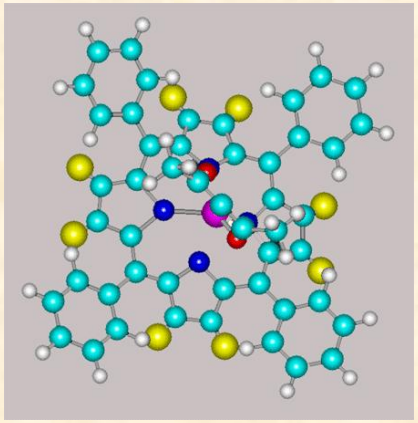

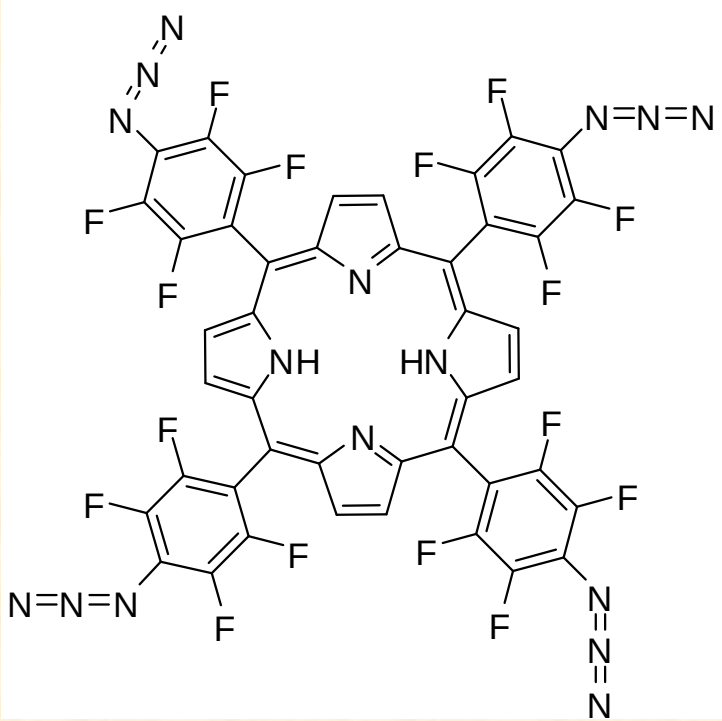

5,10,15,20-тетракис(4’-азидотетра-фторфенил) порфирин

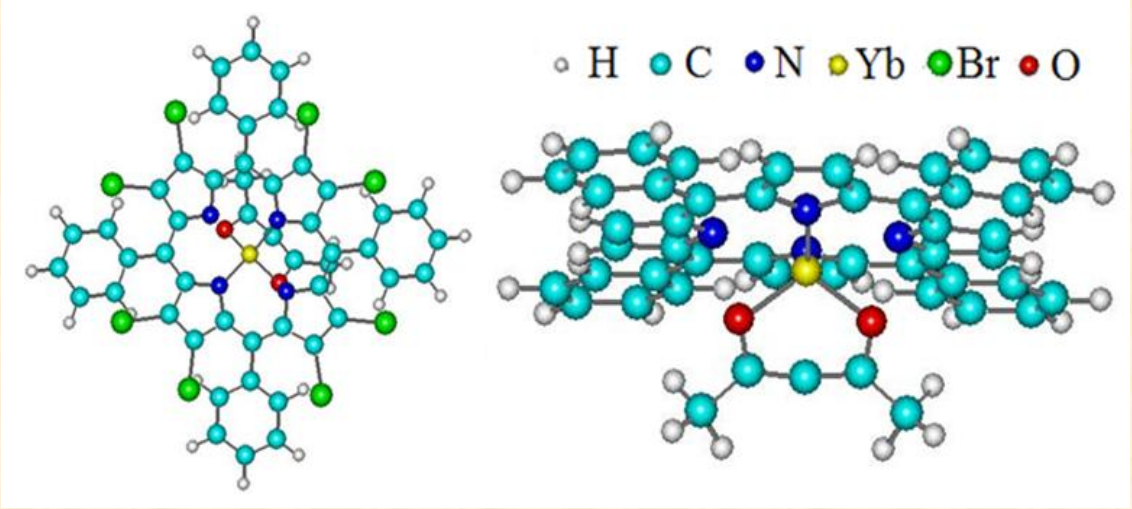

- Иттербиевые металлокомплексы тетрафенилпорфирина:

слева Yb(acac)TPPBr$_8$ вид сверху; справа Yb(acac)TPP вид сбоку

Электронная структура *N 1s* состояний в металлорганических пленках

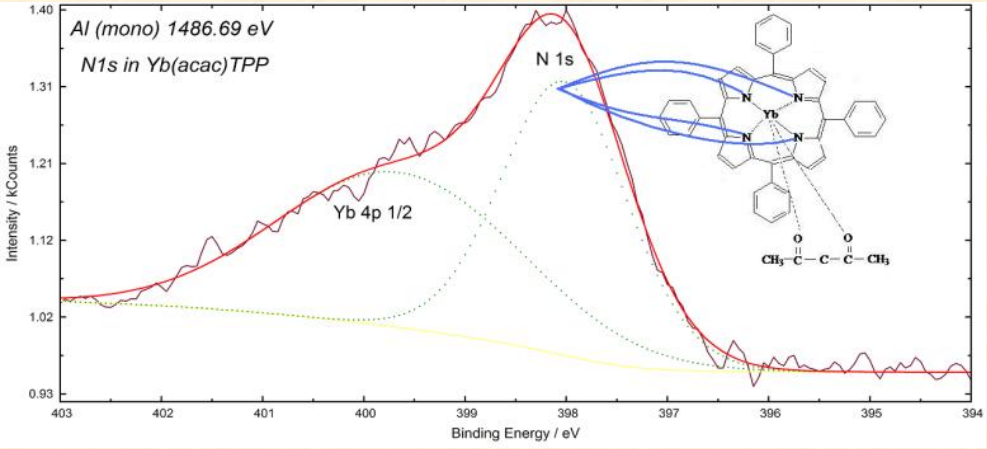

Неэквивалентные положения азота N1s в молекуле Тетракис(4’-азидотетра-фторфенил) порфирине

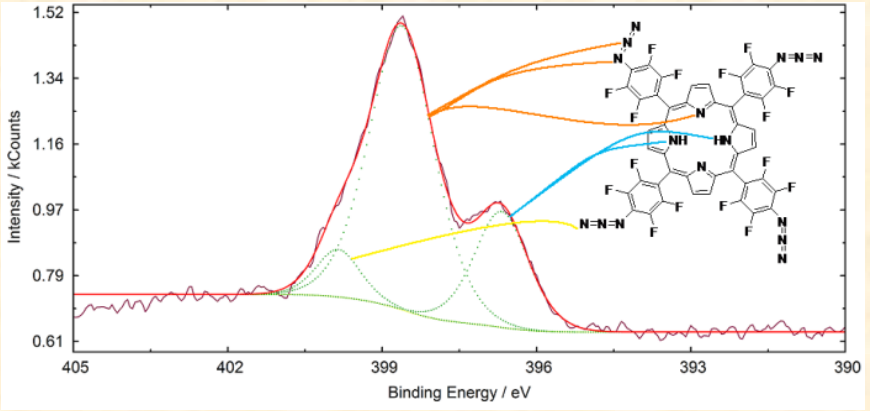

Перераспределение электронной плотности между азотом пиррольной и аза-группы в молекулах TPP и $Yb(acac)TPPBr_8$

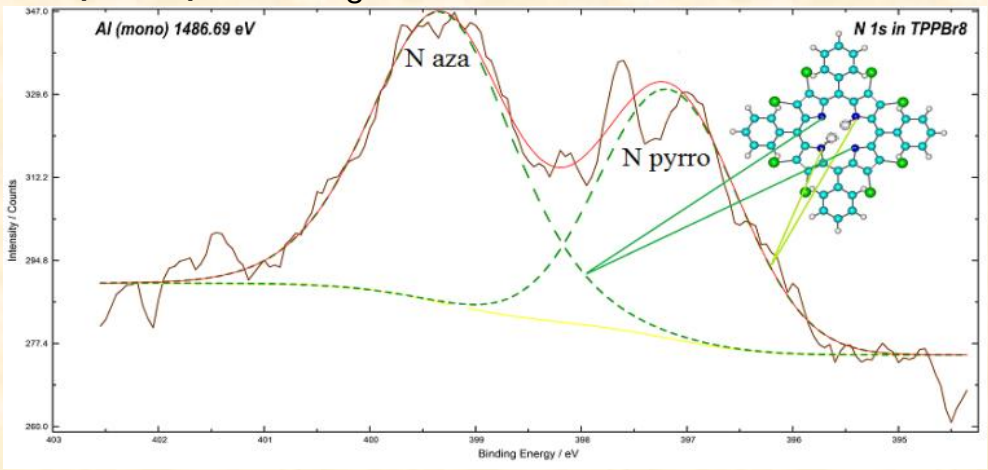

Электронная структура *C 1s* состояний в металлорганических пленках

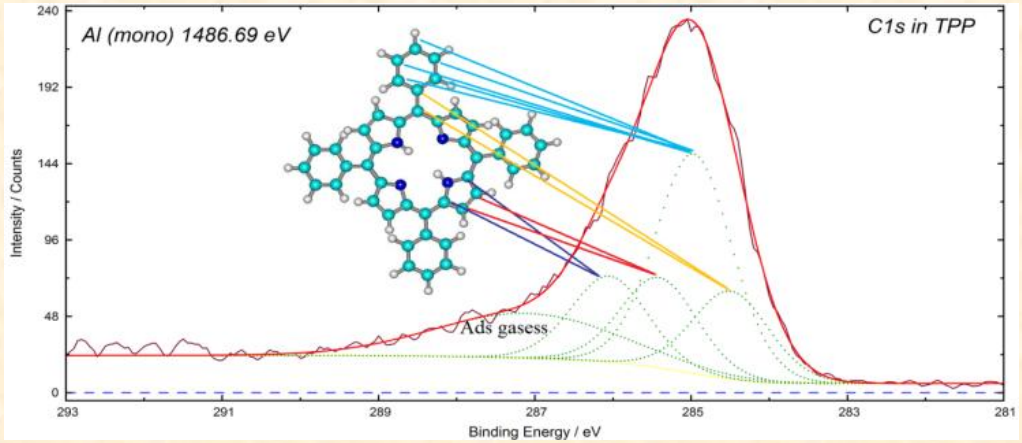

Неэквивалентные положения углерода в молекулах TPP и Yb(acac)TPPBr_8 (ароматическое, пиро- и аза-)

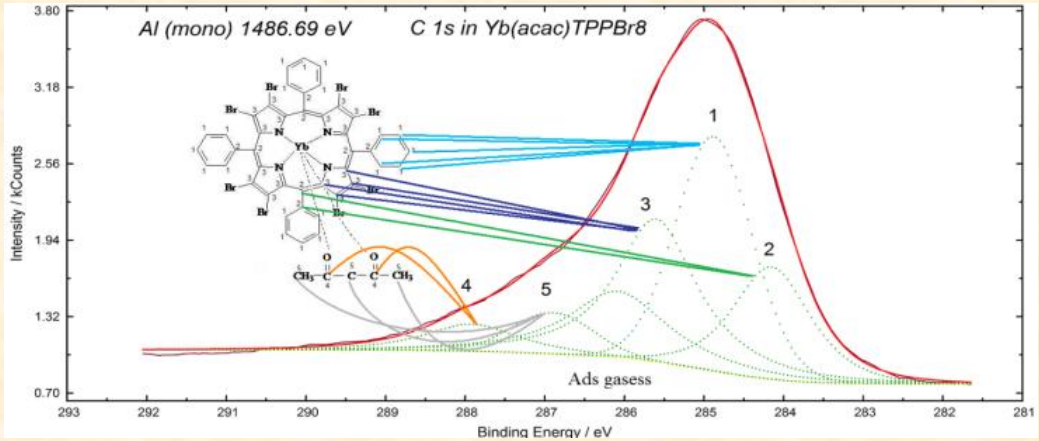

Неэквивалентные положения углерода в молекуле тетракис (4'-азидотетра-фторфенил) порфирине

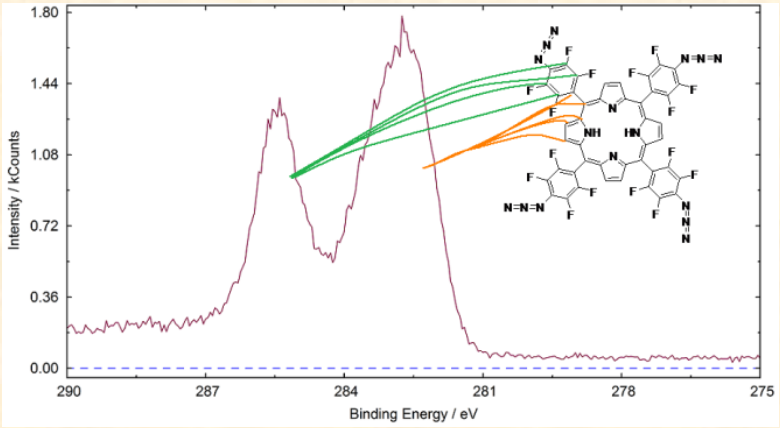

Микроанализ и картирование

Small area analysis and XPS Imaging

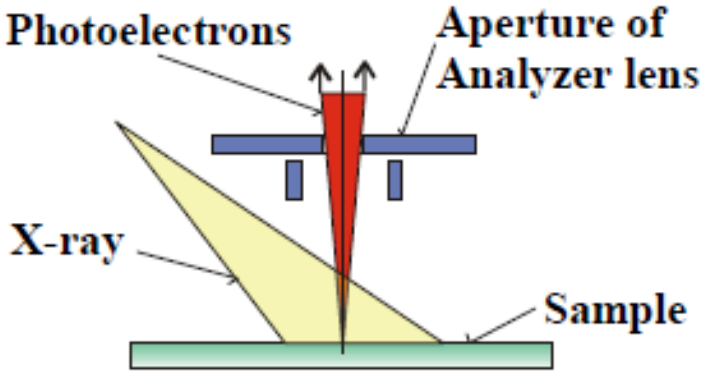

Spot size determined by the analyser

Both monochromated and dual anode x-ray sources can be used

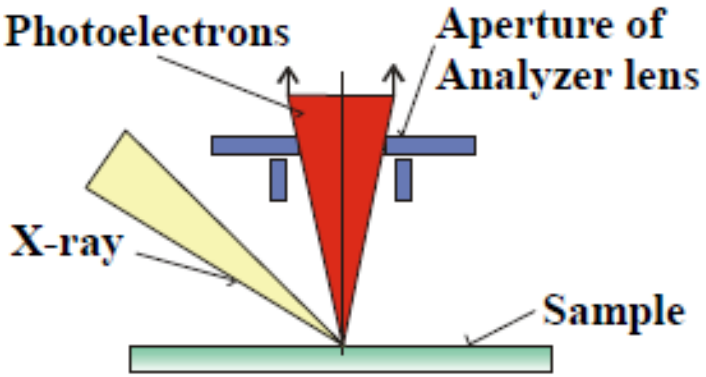

Spot size determined by the x-ray beam

РФЭС картирование

XPS Elemental Map of ITO circular patterns

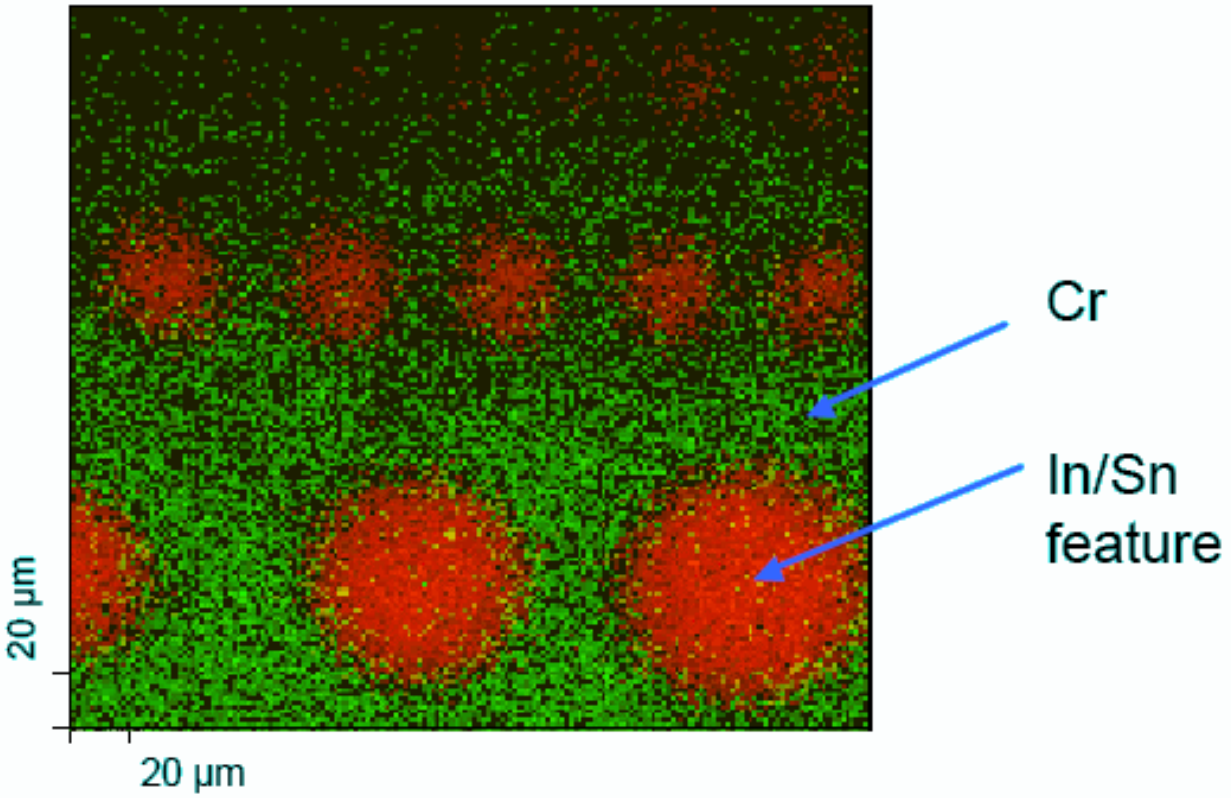

Анализ распределения элементов по глубине

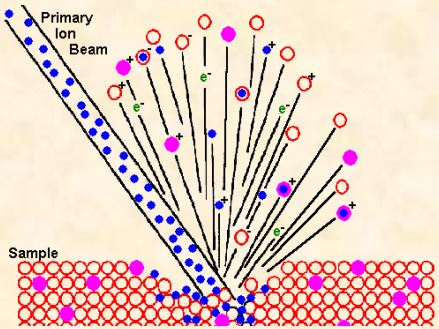

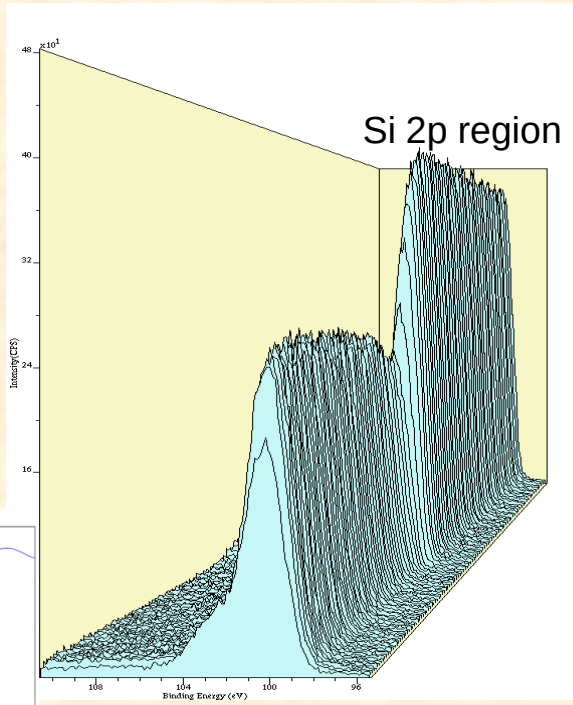

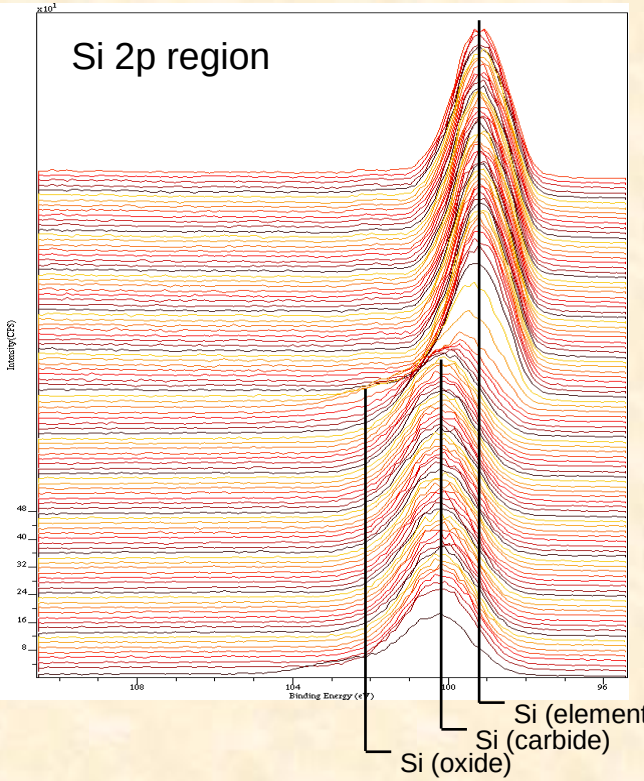

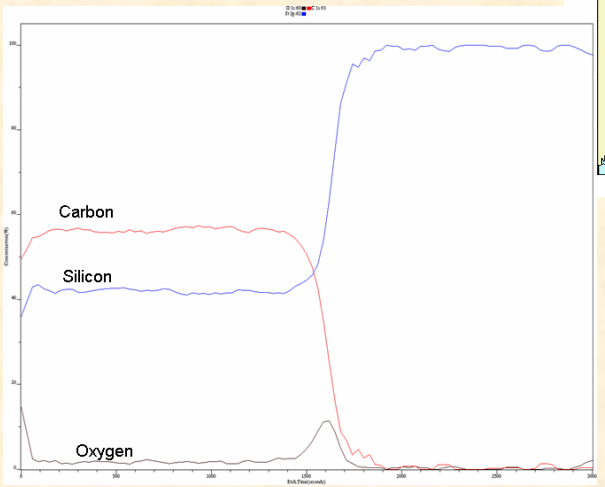

SiC

SiO_2

Si substrate

Поверхностная чувствительность

Длина свободного пробега

$I(z)=I_0\exp(-z/l)$

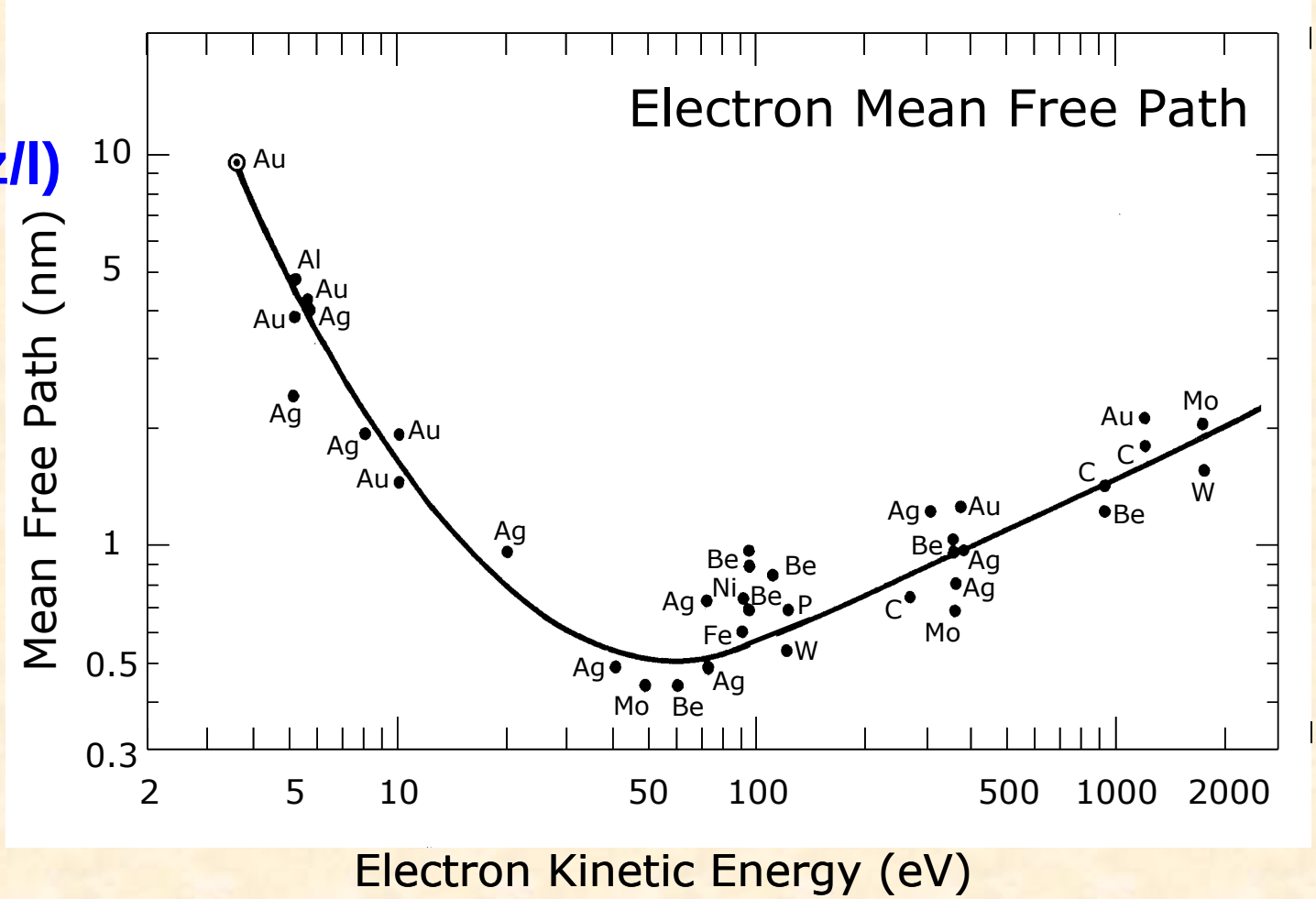

Изменение поверхностной чувствительности в эксперименте

Electron inelastic attenuation length in solids—the "universal curve"
Photoemission is a surface sensitive experiment

Изменение угла

Changing angle:
1st way to vary surface sensitivity

$$I(z) = I_0 e^{-\frac{z}{\Lambda_e \sin\Theta}}$$

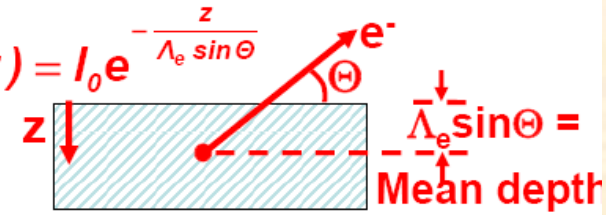

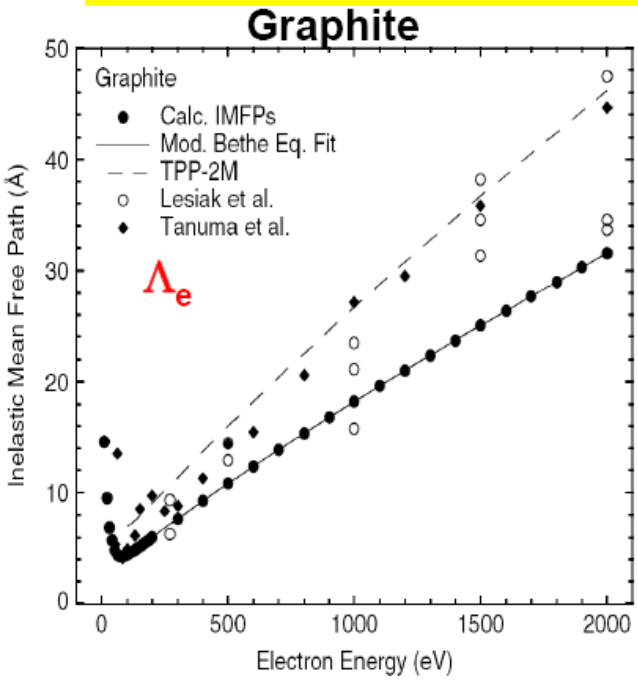

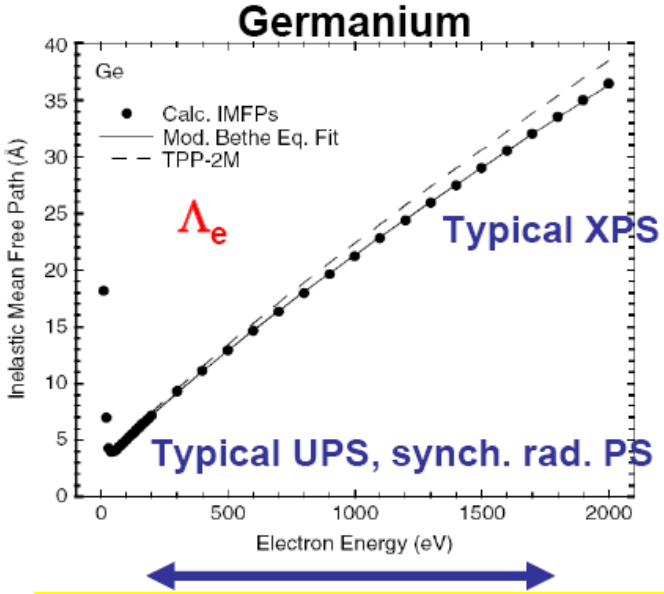

Изменение энергии квантов

Changing photon energy:
2nd way to vary surface sensitivity

Источники синхротронного излучения

DESY, Hamburg

BESSY, Berlin

BESSY, Berlin

Elettra, Trieste

Max-Lab, Lund

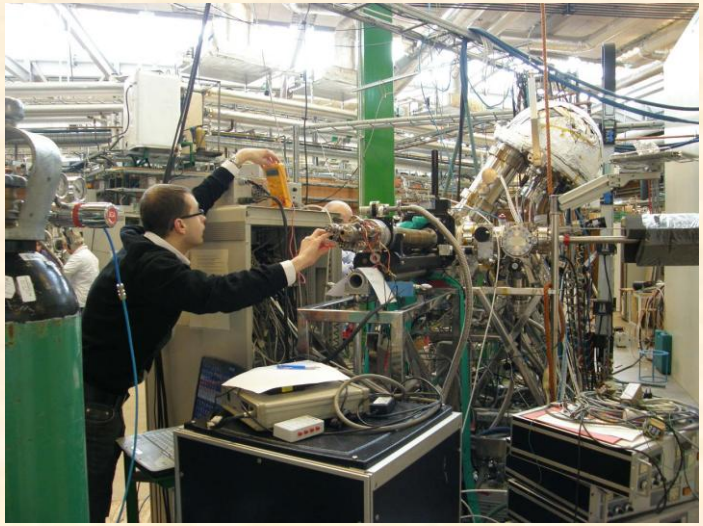

изменяемая энергия фотонов;

высокая интенсивность;

высокое энергетическое разрешение

Surface core level shifts of Si(111)7×7

surface sensitive

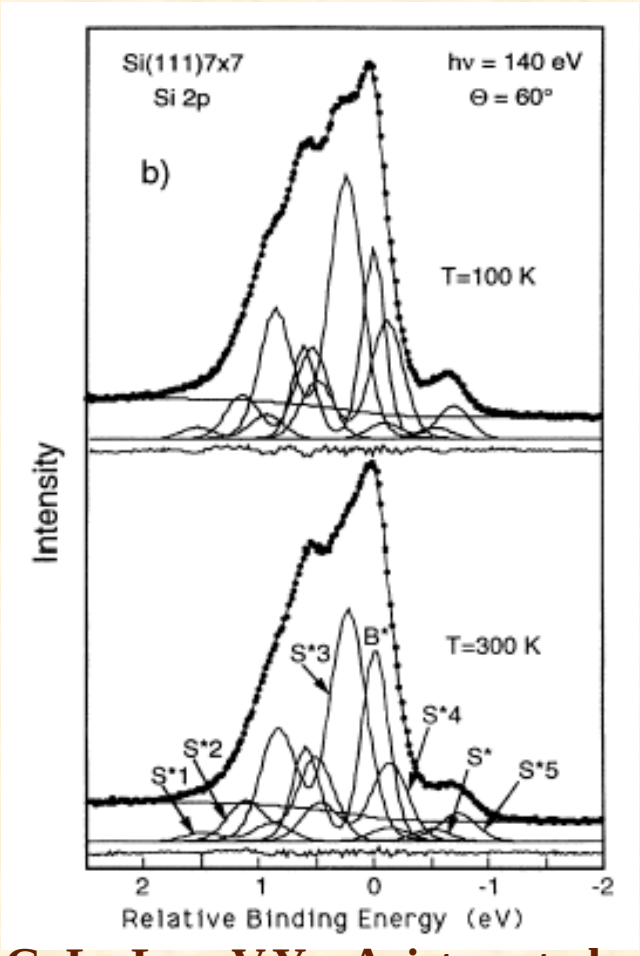

G. Le Lay, V.Yu. Aristov et al.,
Phys. Rev. B 50 (1994) 14277

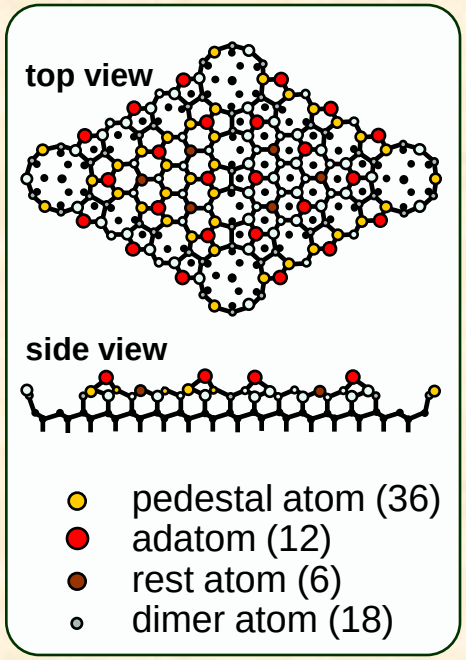

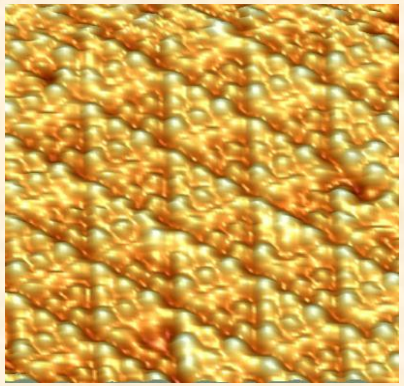

bulk sensitive

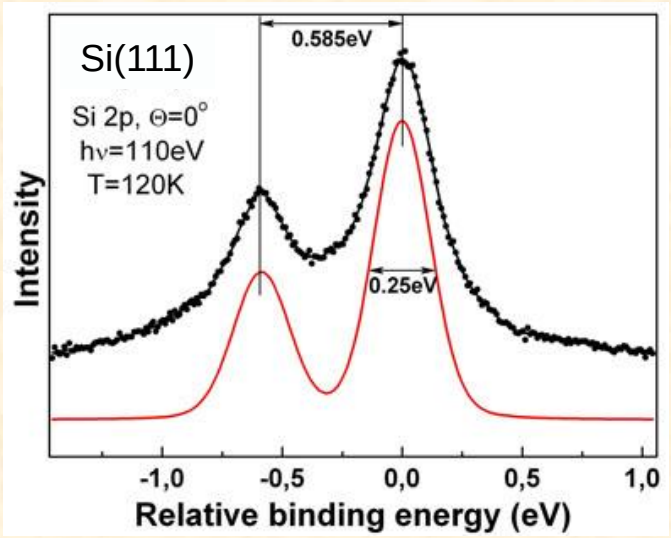

S1 – shakeup, S2 – adatoms, S3 - pedestal atoms, S4 – dimer atoms, S5 - rest atoms

УФЭС с угловым разрешением (ARPES)

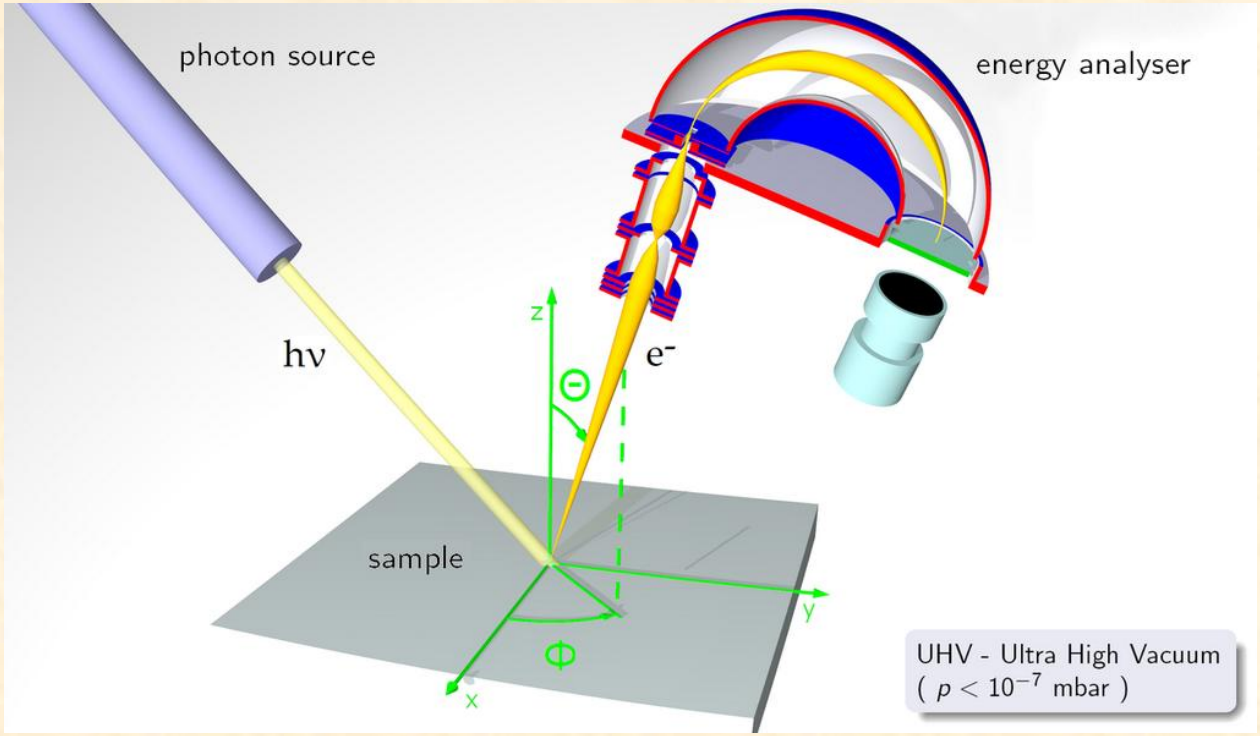

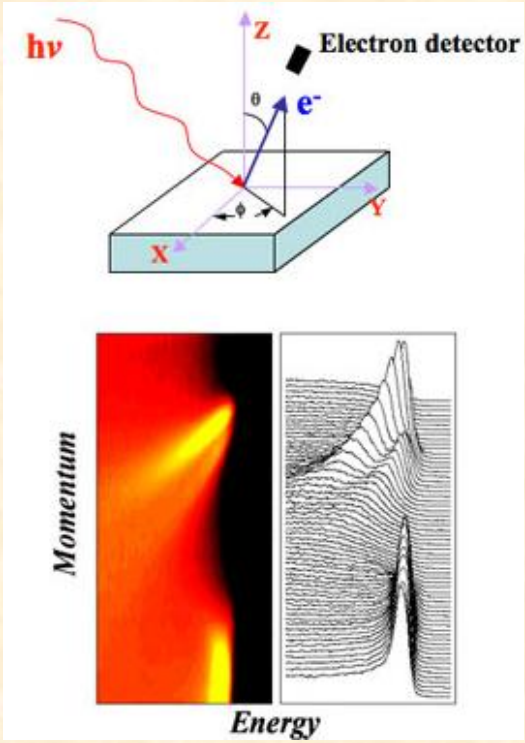

Измеряя N(E) для электронов, вылетающих под различными углами к поверхности, можно построить зависимости E(k)

Визуализация поверхности

Микроскопия медленных электронов (LEEM)

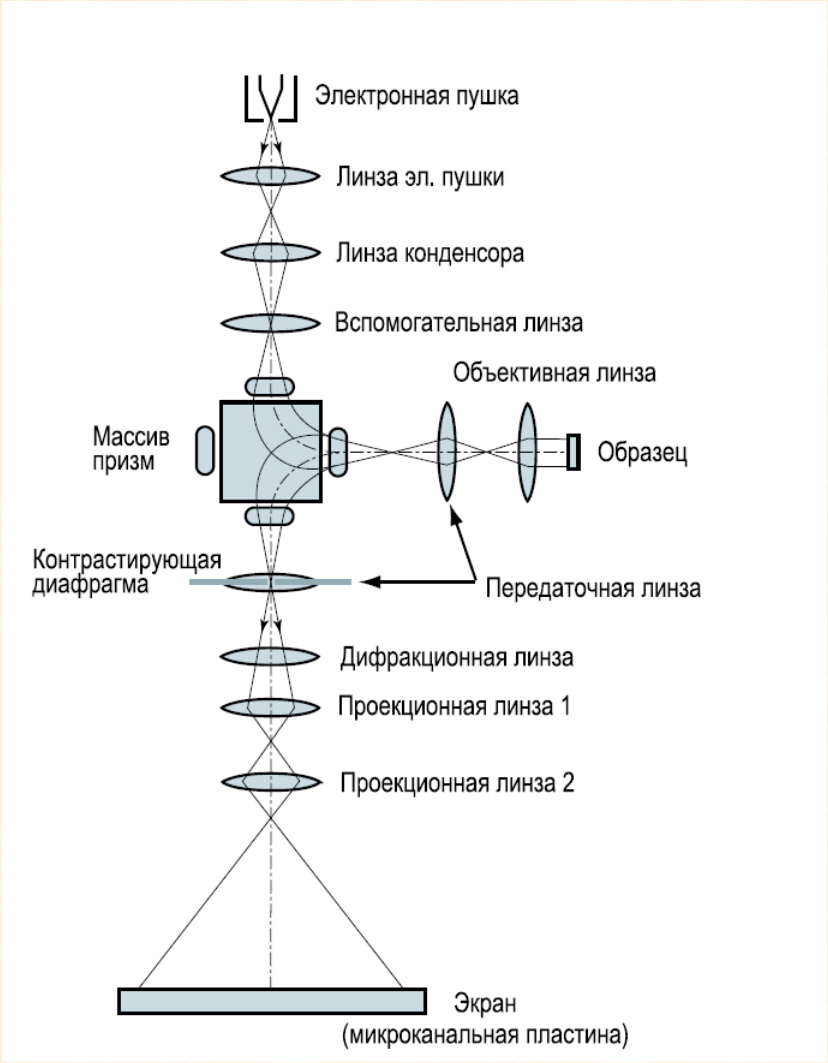

Электроны низких энергий (до 100 эВ) падают на исследуемую поверхность, отраженные электроны используются для формирования изображения.

Пространственное разрешение достигает десятков нанометров.

Контраст обусловлен изменением отражательной способности из-за различия в структуре поверхности.

Si(111), 7×7→1×1 transition

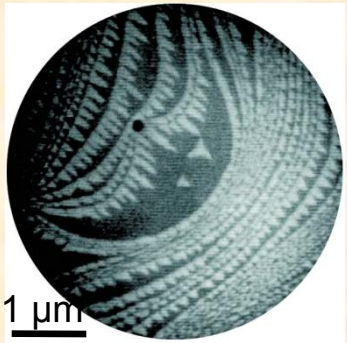

Сканирующие зондовые методы исследования и модификации поверхности

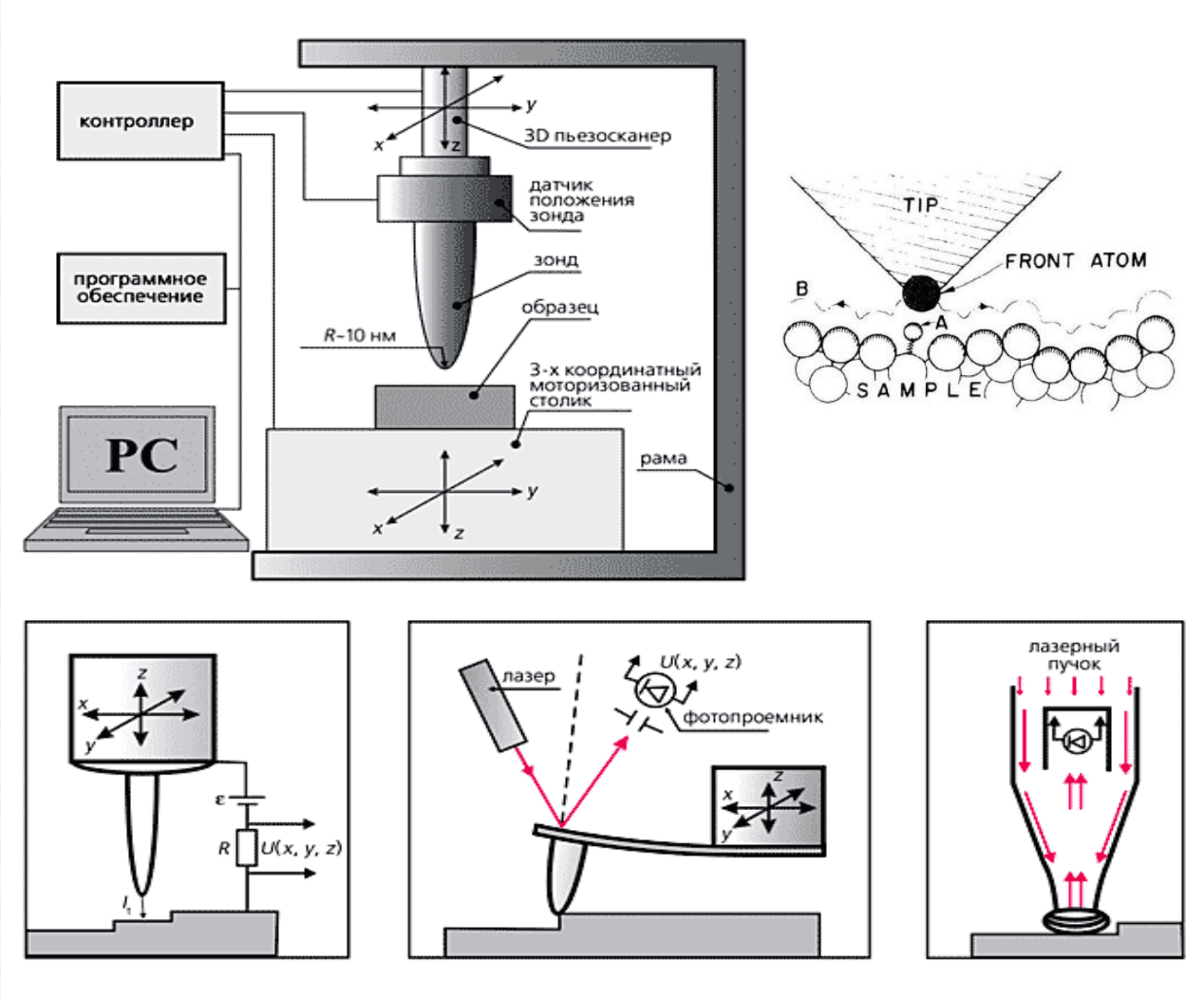

STM *AFM* *NSOM*

Сканирующая зондовая микроскопия

Scanning Probe Microcopy

- Scanning Tunneling Microscopy(STM): topography, local DOS
- Atomic Force Microscopy (AFM): topography, force measurement
- Lateral Force Microscopy (LFM): friction
- Magnetic Force Microscopy (MFM): magnetism
- Electrostatic Force Microscopy (EFM): charge distribution
- Nearfield Scanning Optical Microscopy (NSOM): optical properties
- Scanning Capacitance Microscopy (SCM): dielectric constant, doping
- Scanning Thermal Microscopy (SThM): temperature
- Ballistic Electron Emission Microscopy (BEEM): interface structure
- Spin-polarized STM (SP-STM): spin structure
- Scanning Electro-chemical Microscopy (SECM): electrochmistry
- Scanning Tunneling Potentiometry (SPM): potential surface
- Photon Emission STM (PESTM): chemical identification

Силы и взаимодействия в СЗМ

ток (STM)

силы (AFM, MFM)

оптический сигнал (NSOM)

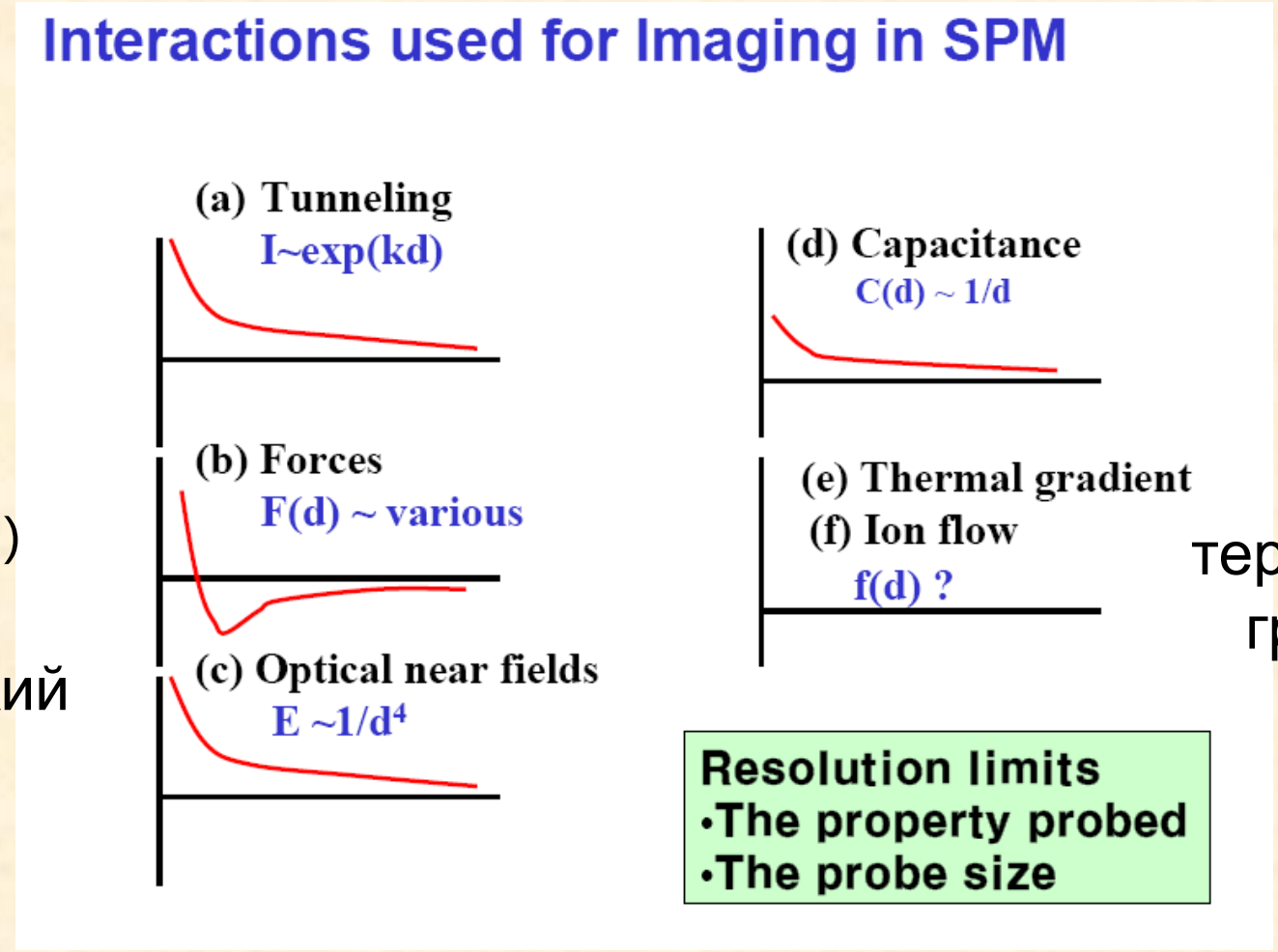

емкость (SCM)

термический градиент (SThM)

The principle of STM

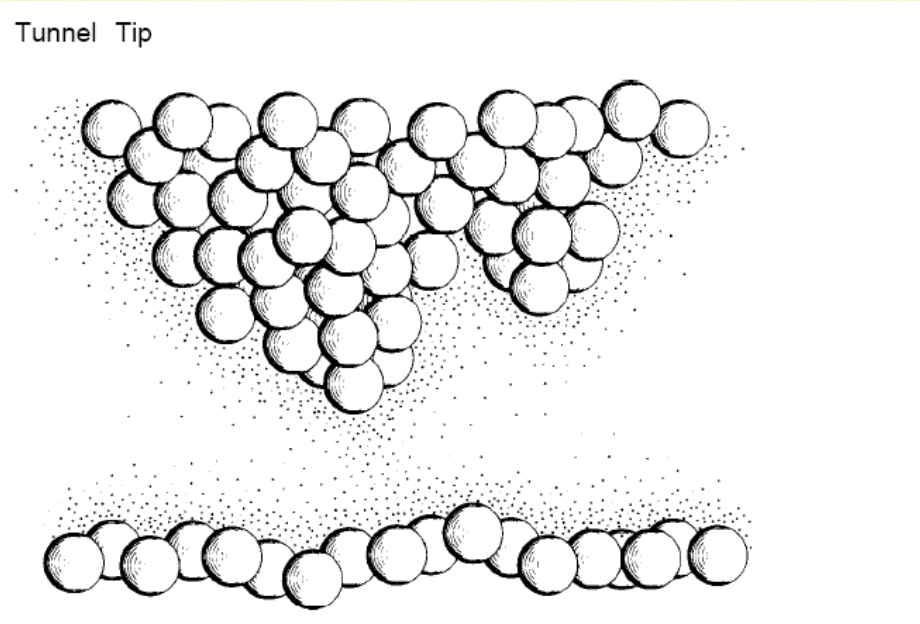

G. Binnig, H. Rohrer, *Nobel Lecture, 1986*

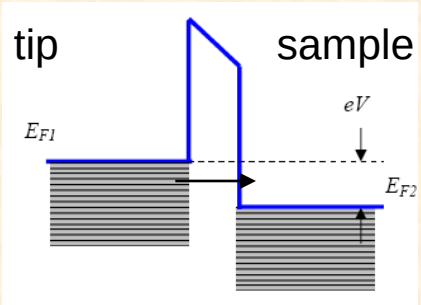

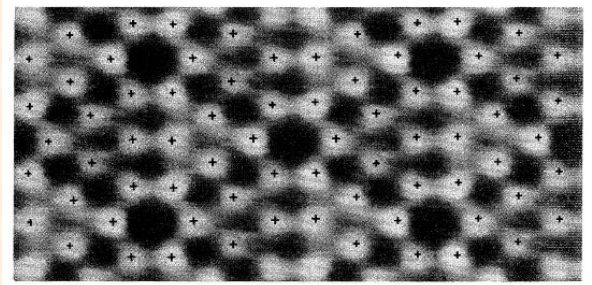

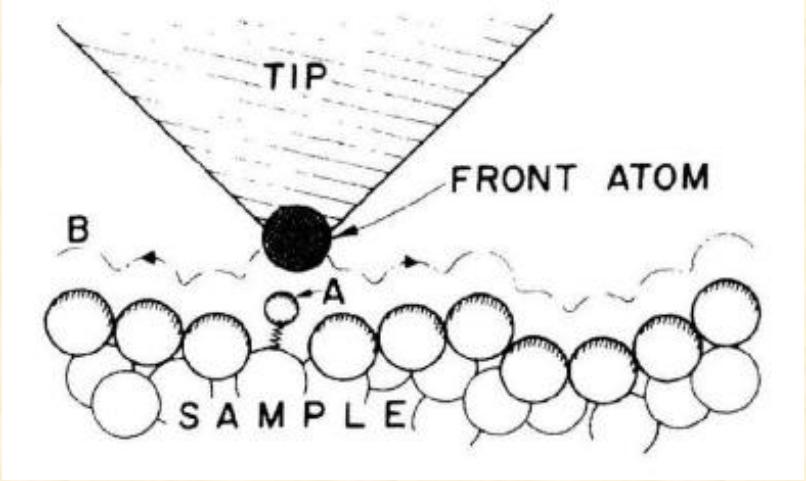

$$I \propto (V/d)\rho_s\rho_t \exp(-A\varphi^{1/2}d)$$

A=1.025 (eV)$^{-1/2}$Å^{-1},
V - bias voltage,
φ - barrier height (~4 eV),
d - tip-sample distance,
ρ_s and ρ_t – density of electron states of the sample and tip

$$d_2 - d_1 = 0.1nm \Rightarrow I_2/I_1 \sim 10$$

Более 90% туннельного тока может протекать через один атом на острие иглы. Пространственное разрешение менее 1 Å.

Электронный спектрометр RIBER LAS-3000 и RT STM GPI-300 *(ИФТТ РАН)*

LAS-3000 (RIBER)

RT STM GPI-300

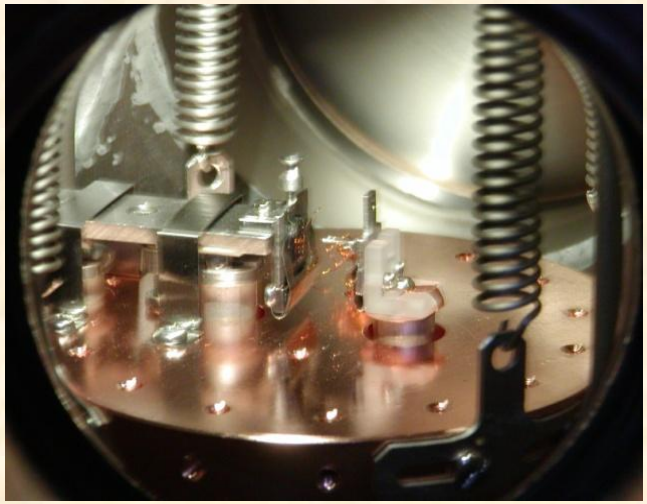

UHV STM

300 K, $p<6\times10^{-11}$ Torr

СТМ-эксперимент с использованием монокристаллического зонда W[001]

SEM image of a W[001] tip

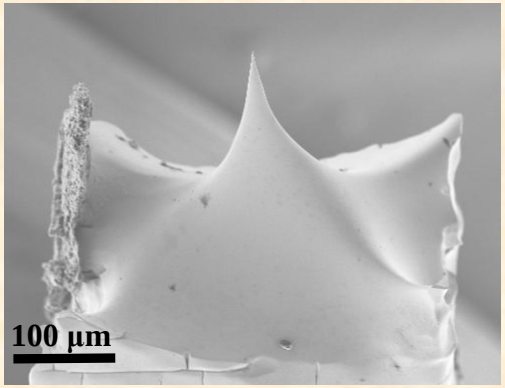

TEM characterization

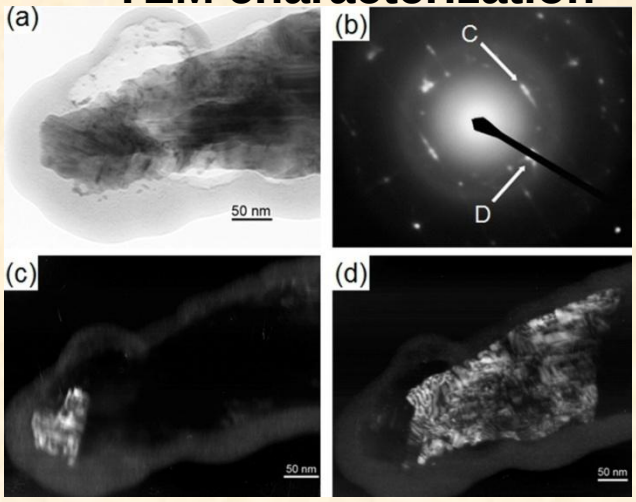

(a) bright field TEM image of a W[001] tip; (c,d) dark field images of the apex showing {110} (c) and {100} (d) planes

A. Chaika *et al., Sci. Rep. 4, 3742 (2014)*

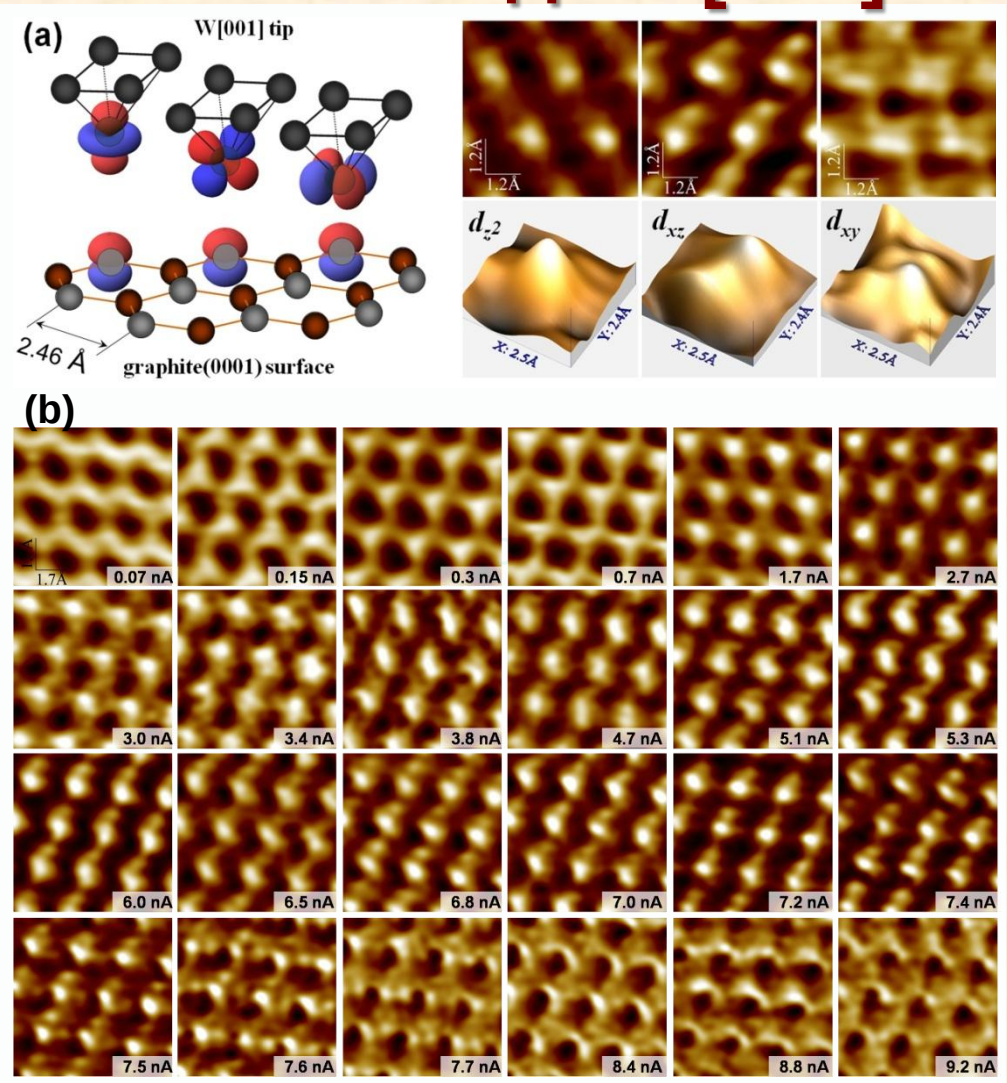

(a) model and STM images measured at certain tunneling parameters; (b) gap resistance dependence at ***U*=-35 mV**

A. Chaika *et al., EPL 92 (2010) 46003*

СТМ-эксперимент с использованием монокристаллического зонда W[001]

SEM image of a W[001] tip

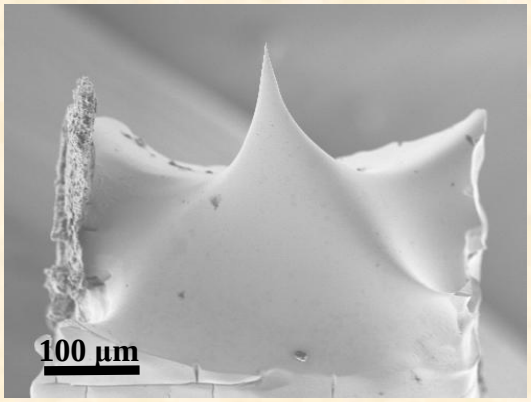

TEM images of the apex

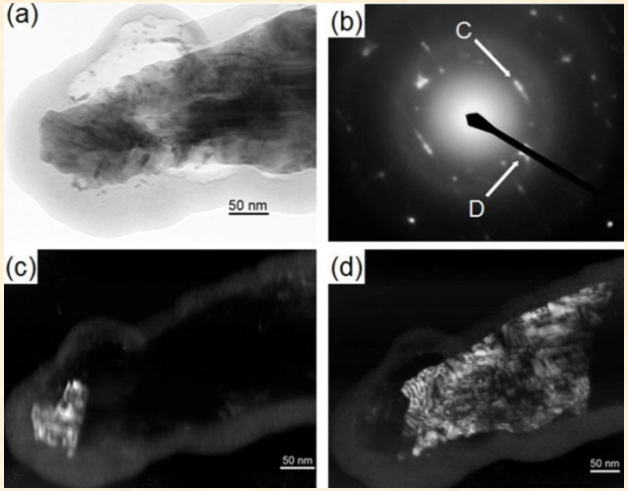

Dark field TEM images show that the tip apex is grained by {110} (c) and {100} (d) planes

STM experiments on HOPG

DFT

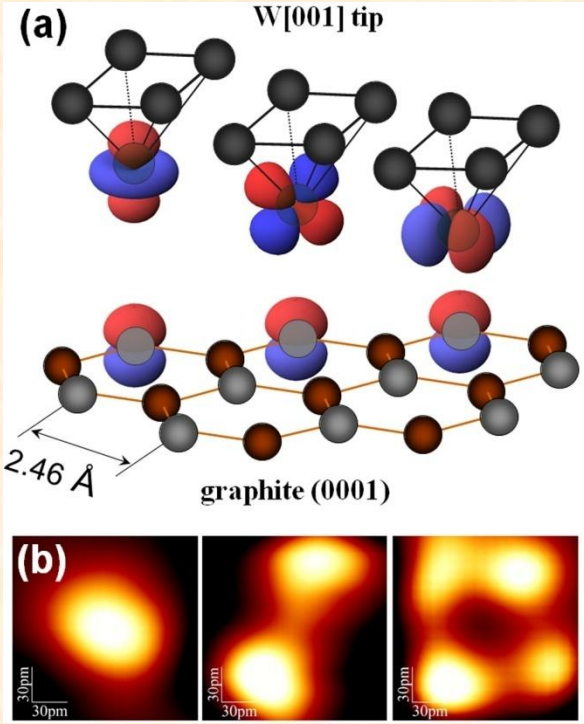

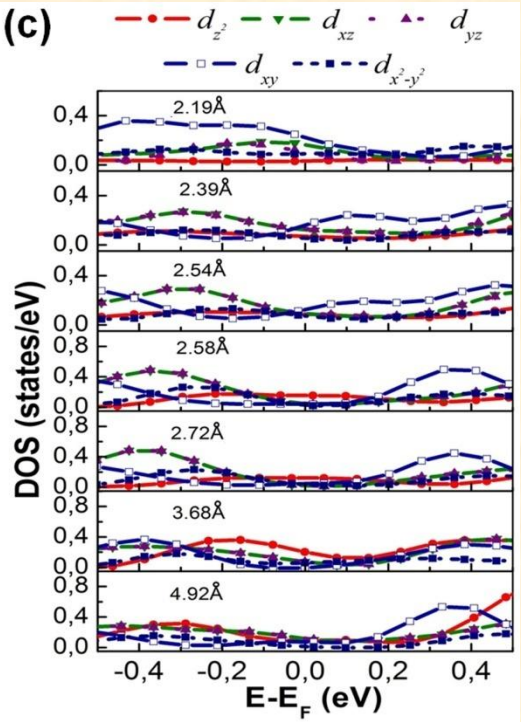

A. Chaika *et al.*,
EPL 92 (2010) 46003;
Appl. Surf. Sci. 267 (2013) 219
Sci. Rep. 4, 3742 (2014)

PDOS for constrained and fully relaxed W-graphite systems, DFT calculations

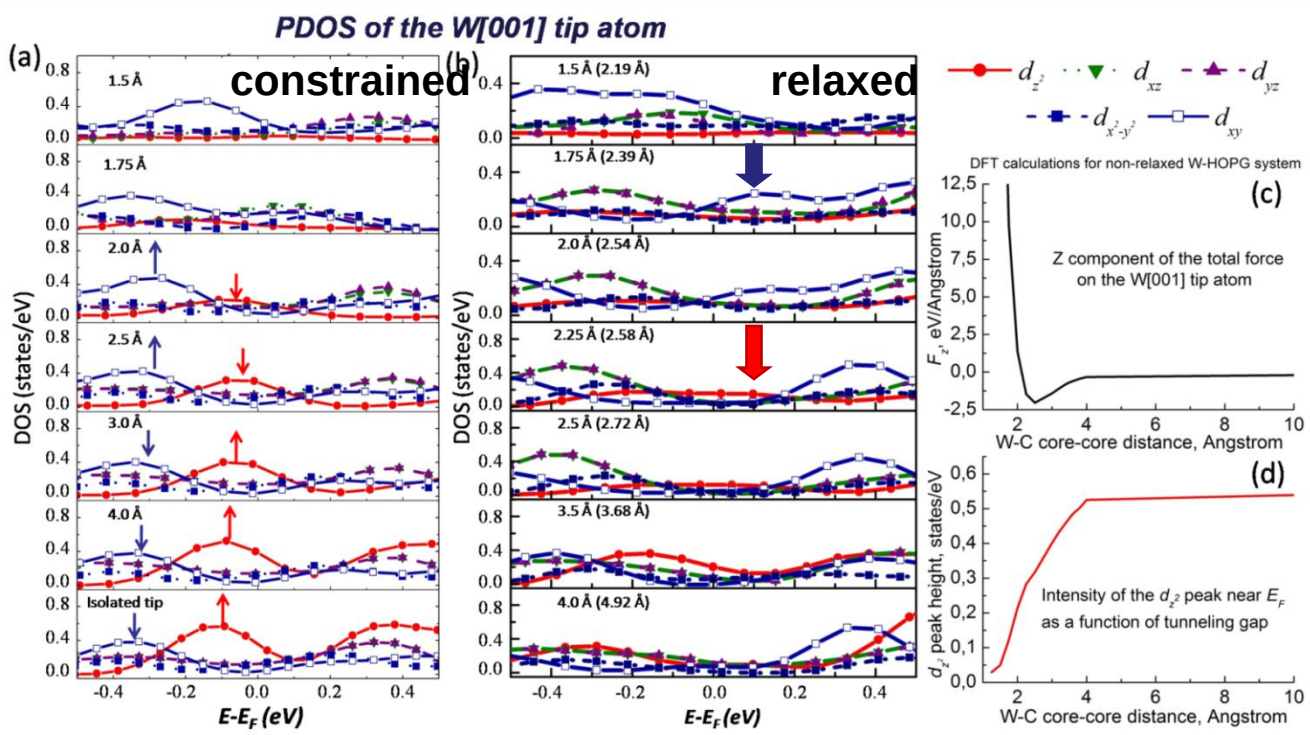

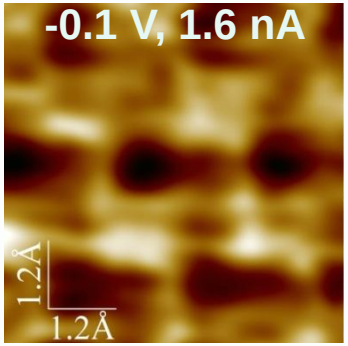

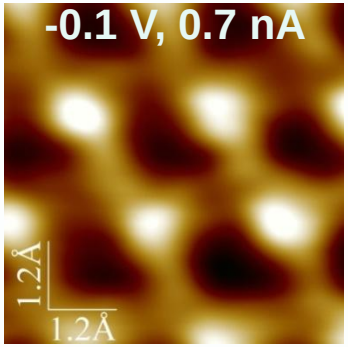

(a,b) PDOS of the W[001] tip atom interacting with the surface atom calculated for constrained (a) and fully-relaxed slabs (b) at different tip-surface distances. **(c)** The total force on the tip atom as a function of the tip-sample distance and **(d)** the height of the d_{z2} peak near the Fermi level.

The tip d_{z2} orbital is suppressed at d<3 Å, the d_{xy} orbital dominates at d=2–2.5Å. X and Y axes in calculations and experiments coincided with the {001} directions.

Сравнение данных CTM и ACM

AFM experiments on HOPG with polycrystalline tungsten tips

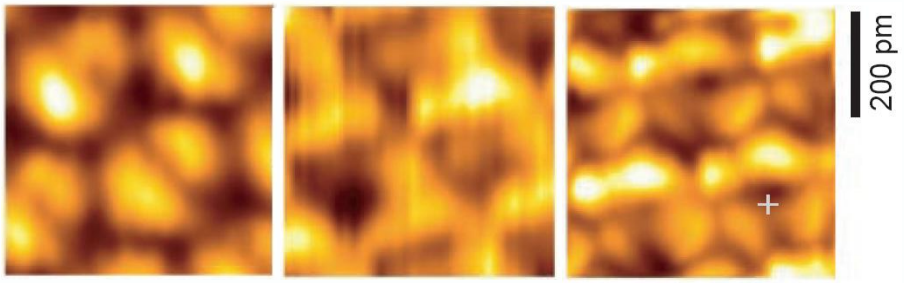

Explanation: direct imaging orbital structure of the front tip atom for three different apex orientations

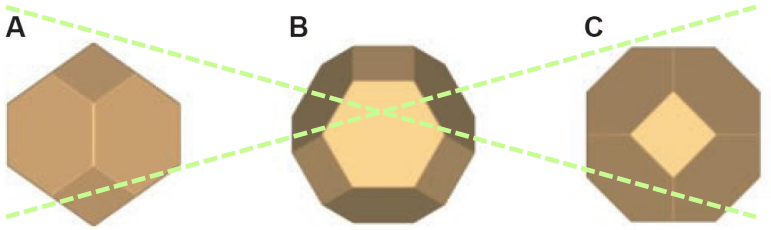

S. Hembacher, F. J. Giessibl, J. Mannhart, *Science 305, 380 (2004)*

STM experiments with unchanged single crystalline W[001] tip

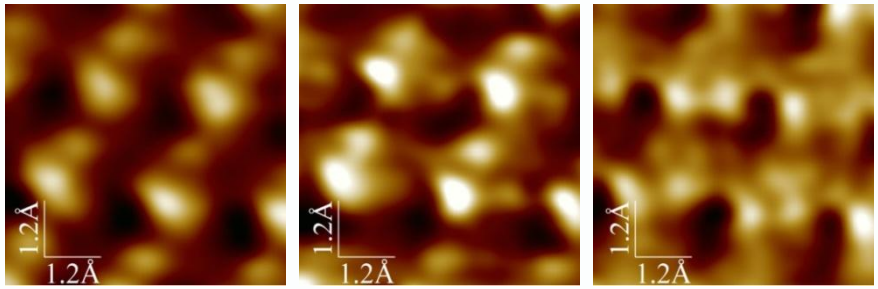

Explanation: direct imaging of the W[001] tip atom electronic structure modified by tip-sample interaction

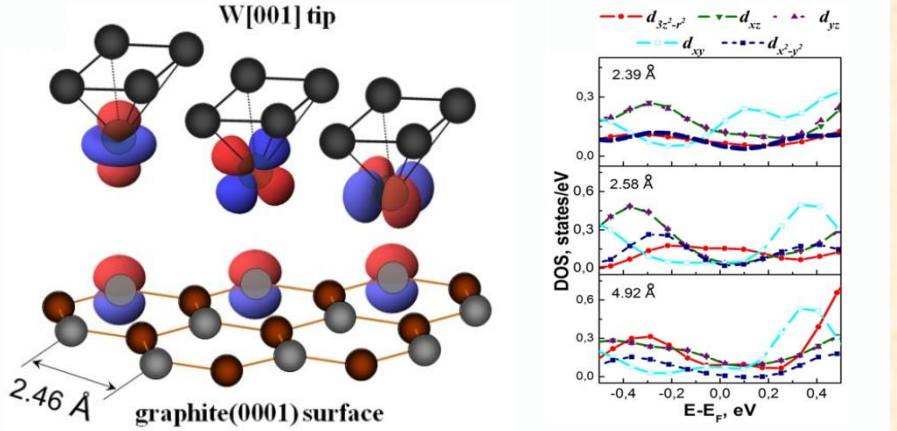

A. Chaika *et al., EPL 92 (2010) 46003; Appl. Surf. Sci. 267 (2013) 219*

VOLUME 70, NUMBER 10 PHYSICAL REVIEW LETTERS 8 MARCH 1993

Direct Observation of Surface Chemical Order by Scanning Tunneling Microscopy

M. Schmid, H. Stadler, and P. Varga
Institut für Allgemeine Physik, Technische Universität Wien, A-1040 Wien, Austria
(Received 4 August 1992)

We present the first scanning tunneling microscopy (STM) study which allows clear discrimination of two chemical species in a metal alloy. Special tunneling conditions, which we attribute to an adsorbate at the STM tip, cause a difference in corrugation between Pt and Ni atoms of 0.3 Å. The STM data reveal chemical short-range order at the surface, which is in agreement with embedded atom simulations and can be understood as small domains of an $L1_0$ ordered phase.

We present the first STM study which allows clear discrimination of two chemical species in a metal alloy. Special tunneling conditions, whuch we attribute to an adsorbate at the STM tip, cause a difference in corrugation between Pt and Ni atoms of 0.3 Å

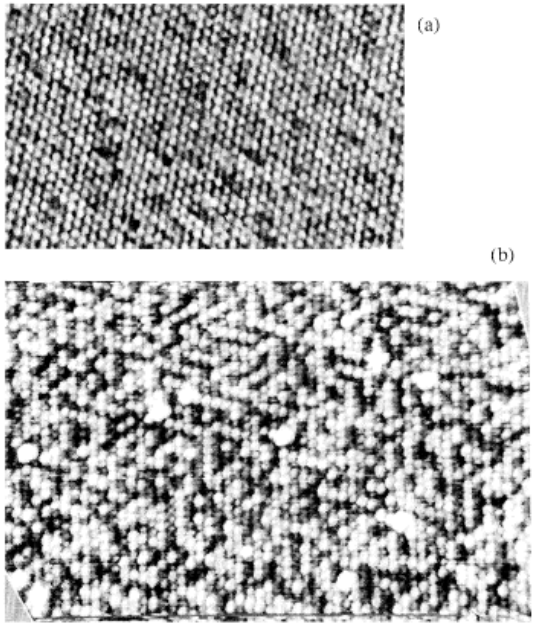

FIG. 1. STM constant current topographs of the (111) surface of a $Pt_{25}Ni_{75}$ single crystal. Tunneling voltage/current and sample treatment: (a) 0.5 mV/7 nA, thoroughly cleaned; (b) 5 mV/16 nA, less cleaning. Image sizes are 100 Å×70 Å and 125 Å×100 Å. Both images have been slightly high-pass filtered; image (b) has been distorted to correct for drift and creep of the STM.

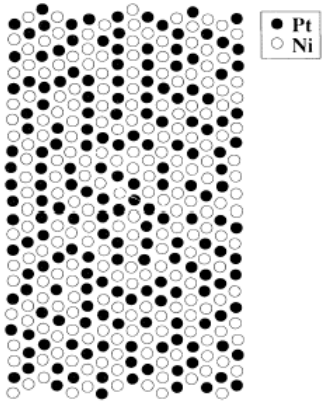

FIG. 3. Atomic arrangement on the (111) surface calculated by Monte Carlo simulations with embedded atom potentials. Bulk composition is assumed as 37% Pt and 63% Ni; temperature is 420 K.

Спин-поляризованная микроскопия
Spin Polarized STM

R. Wiesendanger,
Rev. Mod. Phys. 81 (2009) 1495

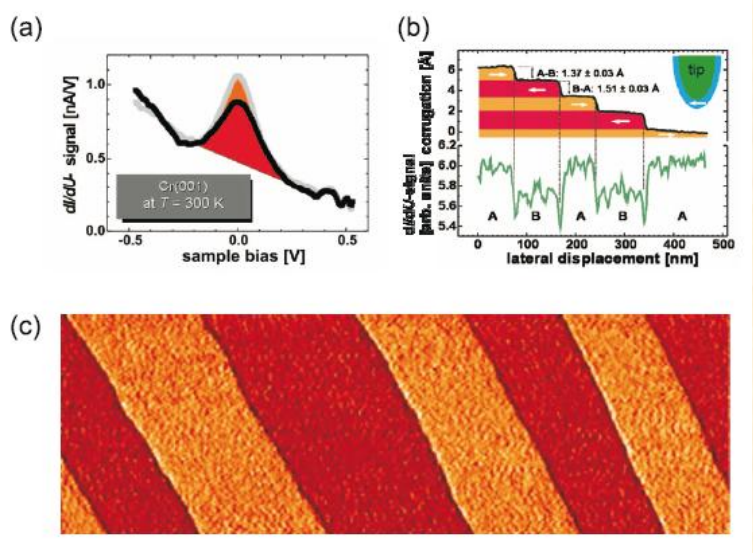

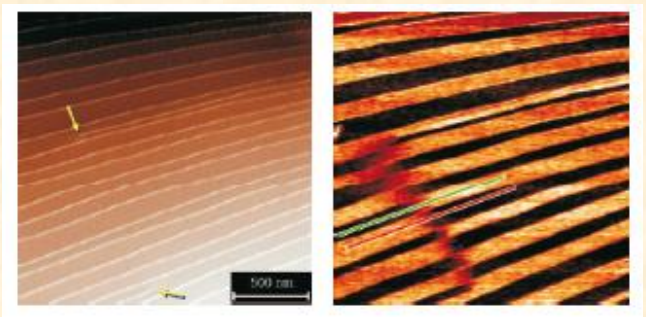

топография

магнитный контраст

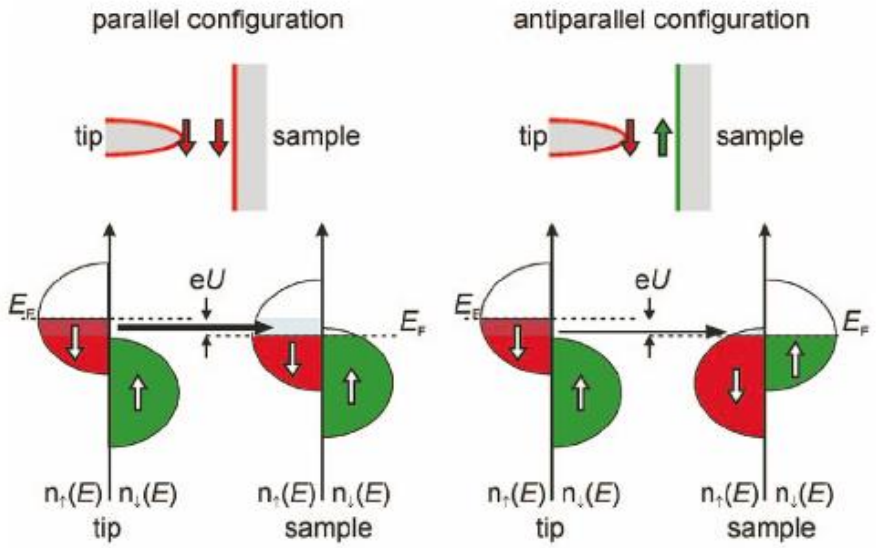

$$I_{SP}(U_0) \propto I_0 \cdot [1 + P_{tip} \cdot P_{sample} \cdot \cos(\vec{m}_{tip}, \vec{m}_{sample})]$$

FIG. 5. (Color) Principle of spin-polarized scanning tunneling microscopy (SP-STM): the spin-polarized tunneling current flowing between a magnetic tip and a magnetic sample depends on the relative alignment of the local magnetization of tip and sample as well as on the spin polarization of the electronic states of tip and sample contributing to the tunneling current.

Манипулирование атомами ксенона

D. M. Eigler and E. K. Schweizer,
Nature 344, 524 (1990)

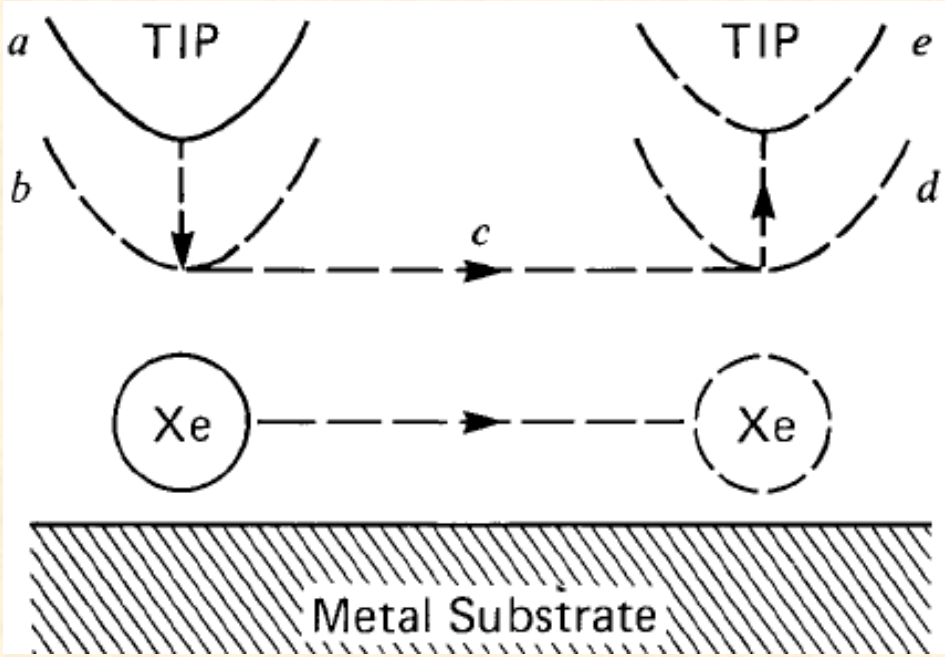

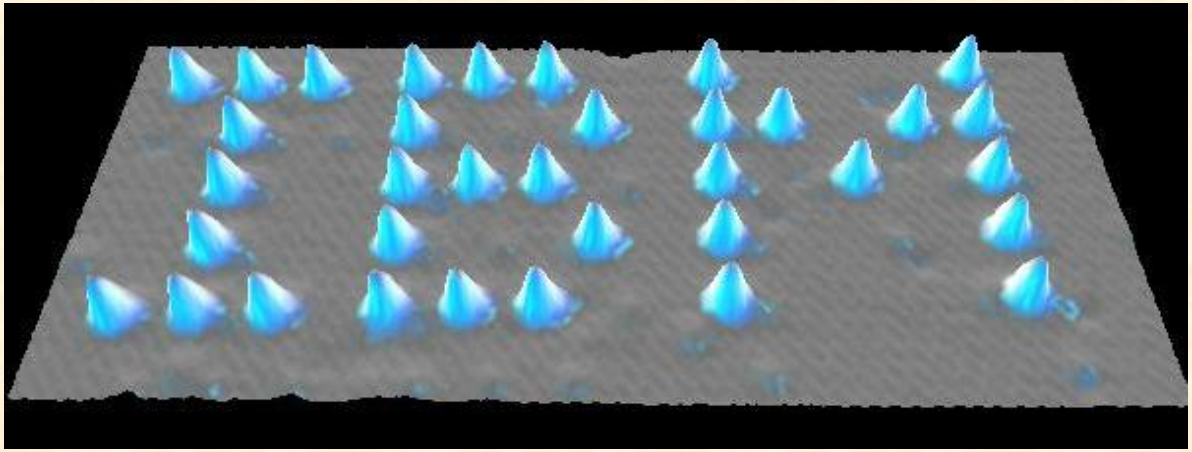

Манипулирование атомами железа на поверхности меди

«квантовые кораллы»

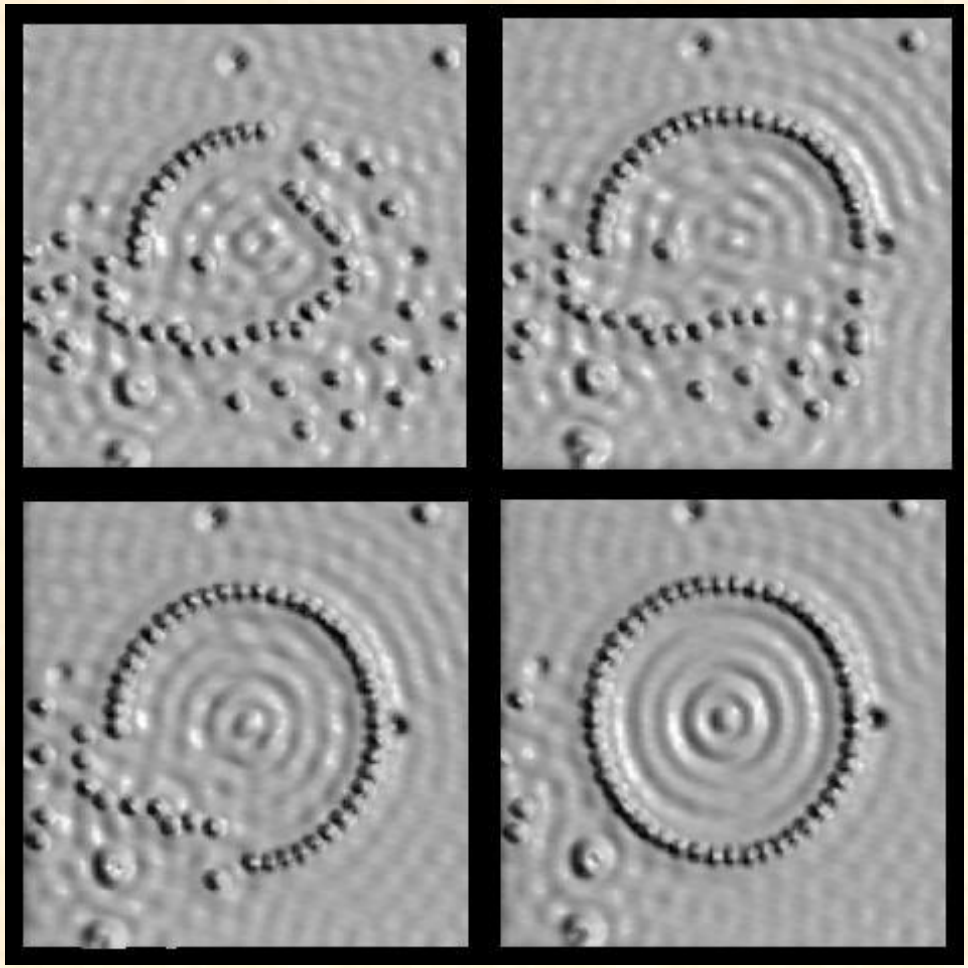

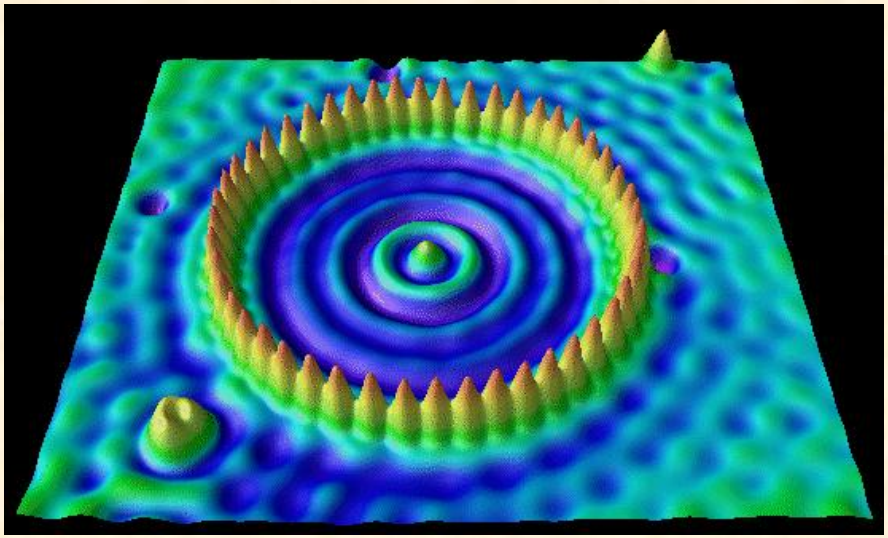

M.F. Crommie, C.P. Lutz, D.M. Eigler,

Nature 363 (1993) 524-527

Imaging standing waves in a 2-Dimensional electron-gas

Бесконтактная АСМ с атомным и субатомным разрешением

First atomic resolution in UHV conditions,
F.J. Giessibl, Science, 1995

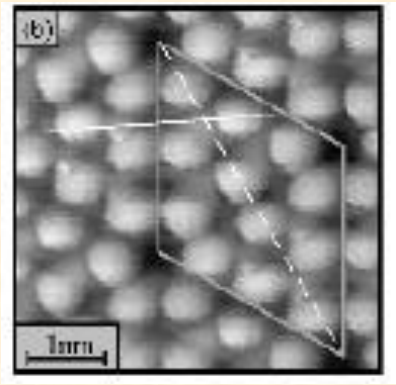

M. A. Lantz et al.,
Phys. Rev. Lett. 84, 2642 (2000)

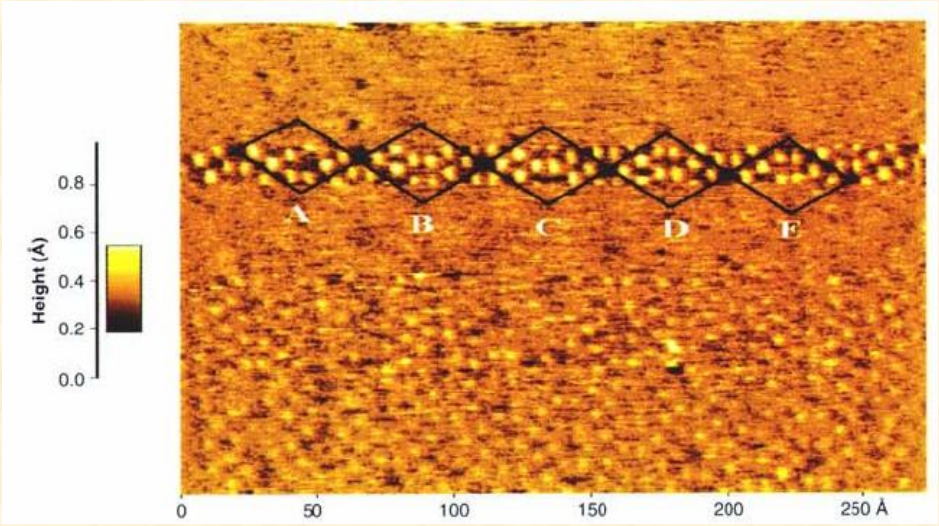

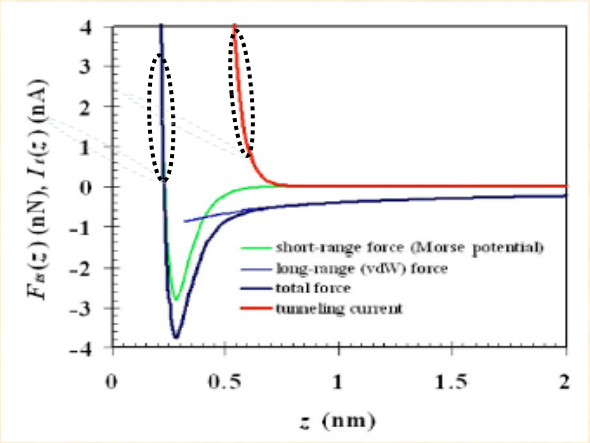

First subatomic resolution in SPM
Si(001) tip over Si(111)7×7

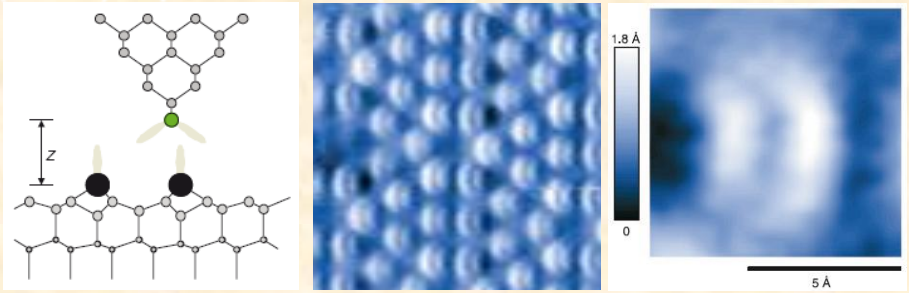

F.J. Giessibl et al., *Science 289, 244 (2000)*

Химическая идентификация атомов с помощью АСМ

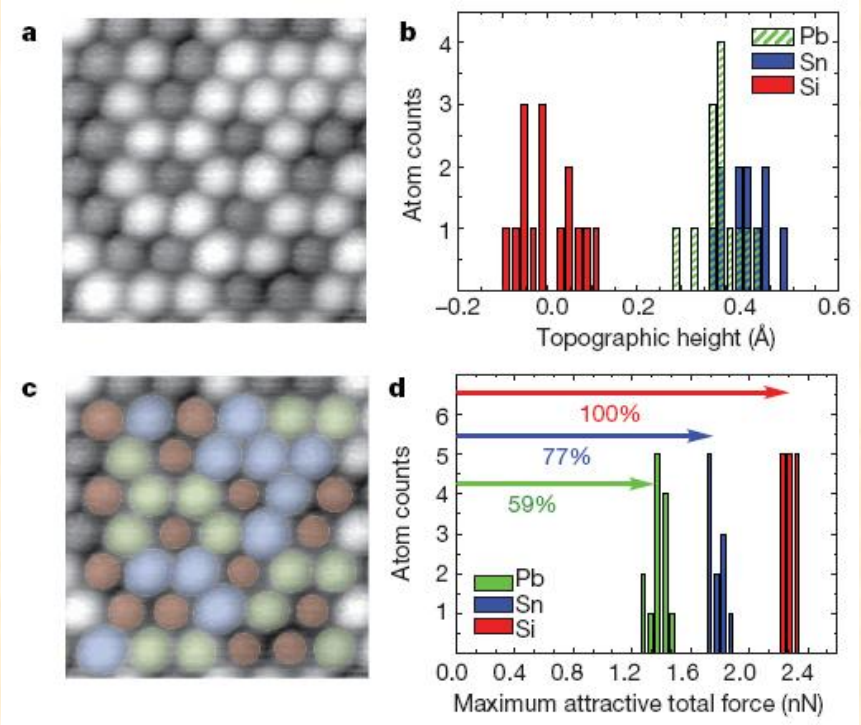

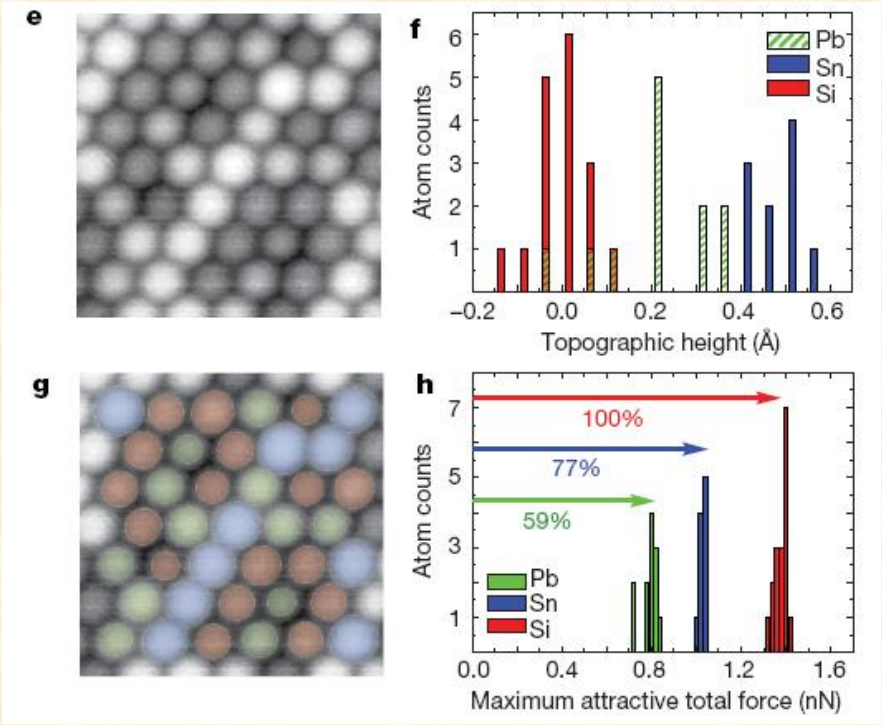

Y. Sugimoto et al., Nature 446 (2007) 64-67

Графен на поверхности SiC/Si(001)

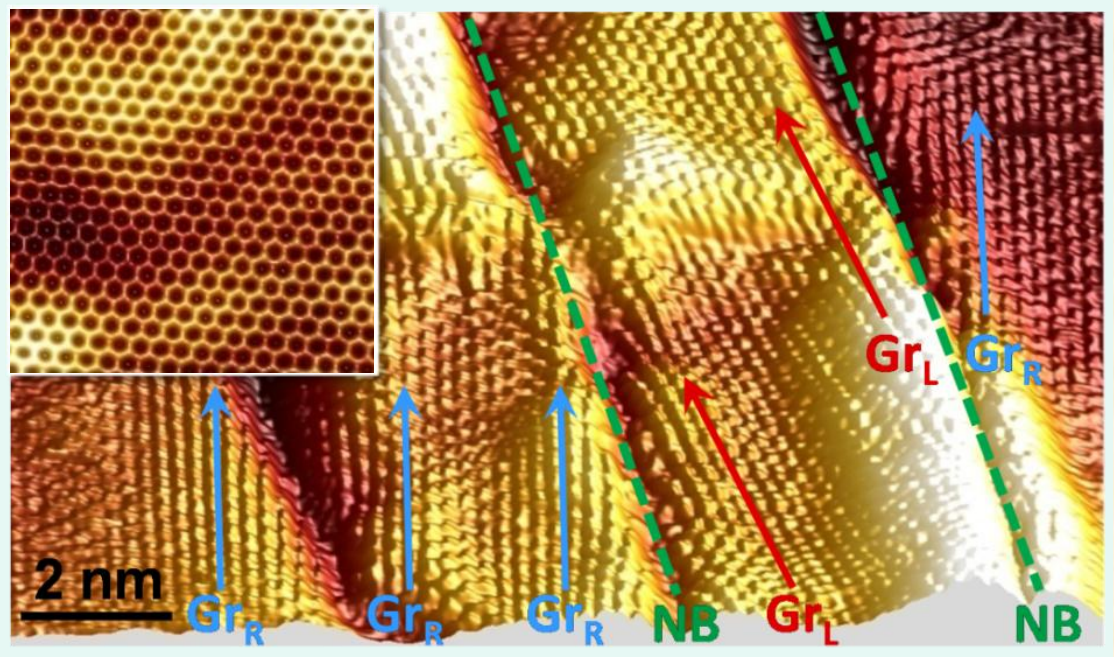

Graphene

2D honeycomb lattice of carbon atoms

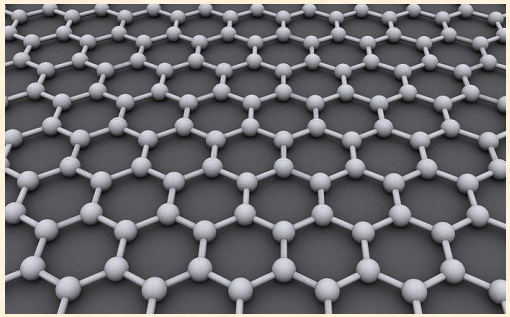

atomic-scale rippling in free-standing form
(A. Fasolino, J. Los, M. Katsnelson, Nature Mater. 6 (2007) 858)

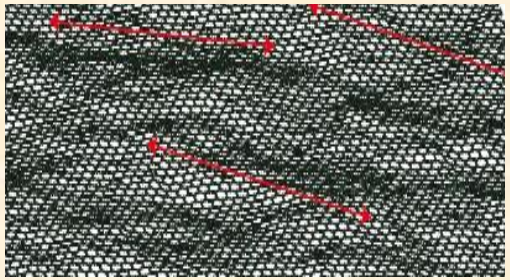

linear dispersion at the K-points,
(P. Wallace, 1947; J. McClure, 1957)

high carrier mobility
Quantum Hall effect at RT
(K. Novoselov et al., Science 306 (2004) 666, …)

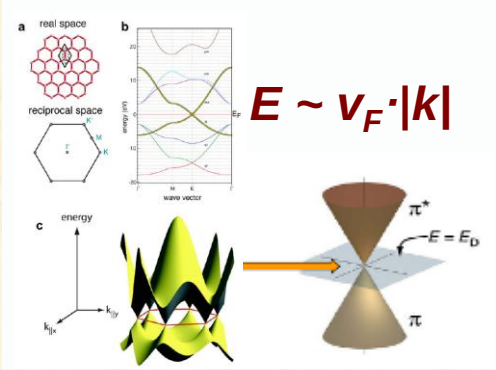

Nobel Prize in Physics 2010

Andrei Geim, Konstantin Novoselov

Graphene fabrication

Exfoliation

high quality graphene for basic research

K. Novoselov *et al*., Science 306 (2004) 666

Synthesis on single-crystalline three-fold symmetrical substrates:

(a) metallic surfaces

Ni(111), Ru(0001), Ir(111), …

first works on metal graphitization *– H. Lyon, G. Somorjai et al., Phys. Rev. Lett. 15 (1965) 491; J. Chem. Phys. 46 (1967) 2539;*
monolayer graphene*- A.Tontegode, Prog. Surf. Sci. 38 (1991) 201*

strong interaction with the substrate, substrate conductivity

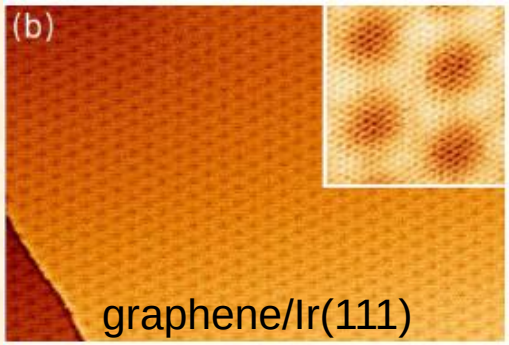

PRL 102, 056808 (2009)

(b) semiconductors

hexagonal SiC – A. J. van Bommel et al., Surf. Sci. 48 (1975) 463-472

suitable for electronics

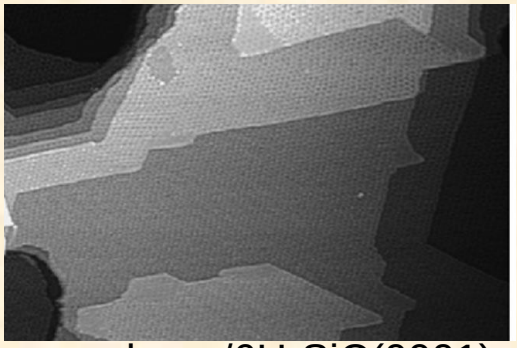

graphene/6H-SiC(0001)
JAP 92, 2479 (2002)

Graphene synthesis on α-SiC in vacuum

Ultrathin Epitaxial Graphite: 2D Electron Gas Properties and a Route toward Graphene-based Nanoelectronics

Claire Berger,† Zhimin Song, Tianbo Li, Xuebin Li, Asmerom Y. Ogbazghi, Rui Feng, Zhenting Dai, Alexei N. Marchenkov, Edward H. Conrad, Phillip N. First, and Walt A. de Heer*

School of Physics, Georgia Institute of Technology, Atlanta, Georgia 30332-0430

Received: October 7, 2004

J. Phys. Chem. B, Vol. 108, No. 52, 2004

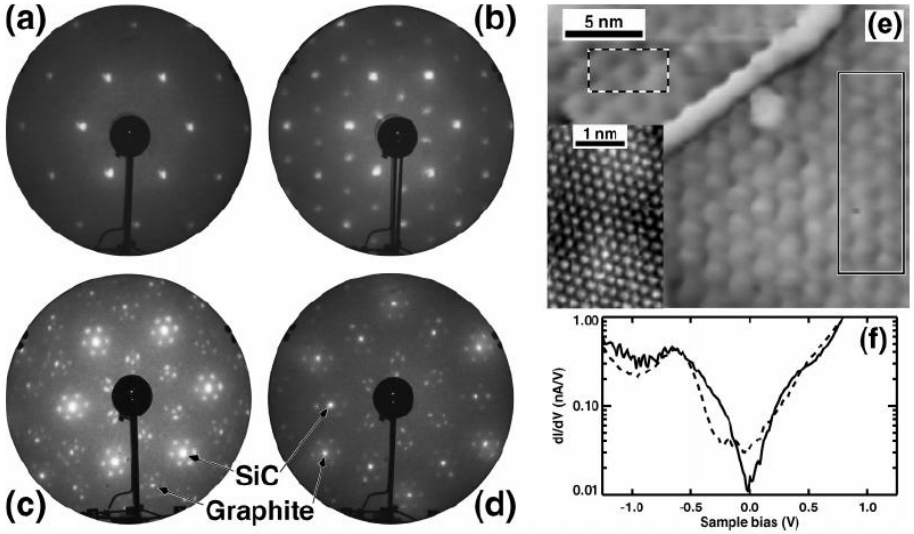

PRL 103, 226803 (2009) PHYSICAL REVIEW LETTERS week ending 27 NOVEMBER 2009

First Direct Observation of a Nearly Ideal Graphene Band Structure

M. Sprinkle,[1] D. Siegel,[2] Y. Hu,[1] J. Hicks,[1] A. Tejeda,[3,4] A. Taleb-Ibrahimi,[5] P. Le Fèvre,[4] F. Bertran,[4] S. Vizzini,[6,7] H. Enriquez,[6,7] S. Chiang,[6,8] P. Soukiassian,[6,7] C. Berger,[1,9] W. A. de Heer,[1] A. Lanzara,[2] and E. H. Conrad[1]

[1]*The Georgia Institute of Technology, Atlanta, Georgia 30332-0430, USA*
[2]*Department of Physics, University of California, Berkeley, California 94720, USA and Advanced Light Source, Lawrence Berkeley National Laboratory, Berkeley, California 94720, USA*
[3]*Institut Jean Lamour, CNRS–Université de Nancy–UPV-Metz, 54506 Vandoeuvre les Nancy, France*
[4]*Synchrotron SOLEIL, L'Orme des Merisiers, Saint-Aubin, 91192 Gif sur Yvette, France*
[5]*UR1 CNRS/Synchrotron SOLEIL, Saint-Aubin, 91192 Gif sur Yvette, France*
[6]*Commissariatà l'Energie Atomique, SIMA, DSM-IRAMIS-SPCSI, Saclay, 91191 Gif sur Yvette, France*
[7]*Département de Physique, Université de Paris-Sud, 91405 Orsay, France*
[8]*Department of Physics, University of California-Davis, California 95616-8677, USA*
[9]*CNRS/Institut Néel, BP166, 38042 Grenoble, France*

(Received 29 July 2009; published 24 November 2009)

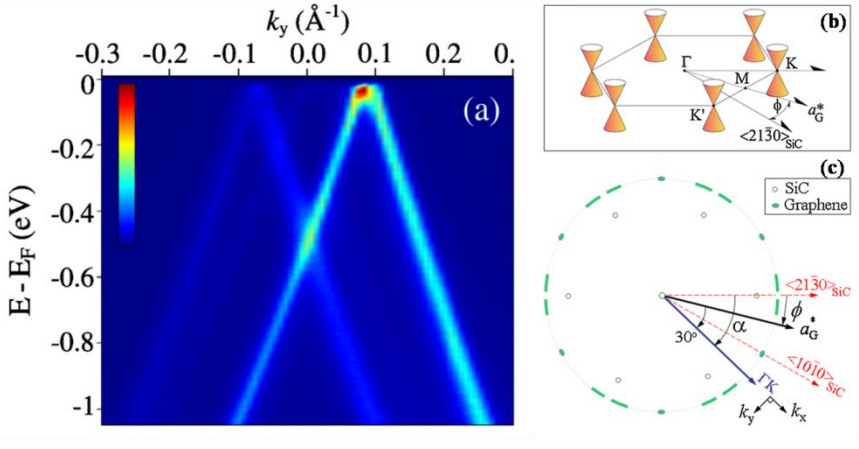

C. Berger et al.,
J. Phys. Chem. B 108, 19912 (2004)

M. Sprinkle et al.,
Phys. Rev. Lett. 103, 226803 (2009)

Nearly perfect linear dispersions at the K-points even for multilayer graphene on the SiC(000-1) but substrates are very expensive for mass production

Fabrication of SiC wafers

α-SiC

a-SiC boules (ingots):

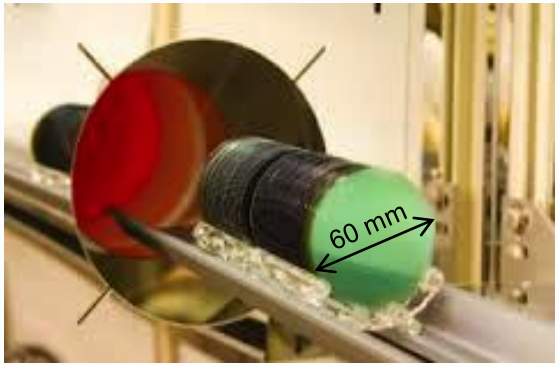

a-SiC wafers:

relatively small size;
expensive (~2000 $ each);
high quality

β-SiC

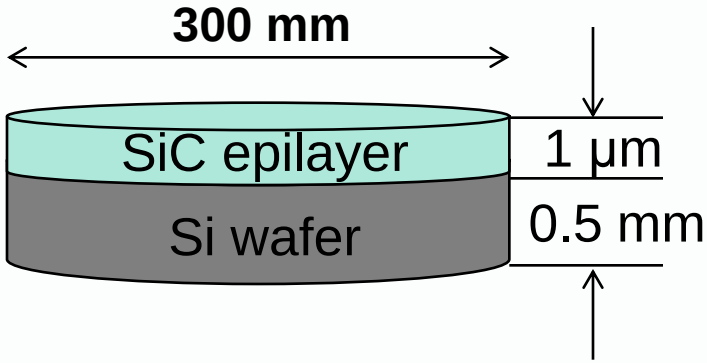

cubic-SiC/Si wafers:

large size wafers;
cheap and commercially available;
compatible with Si technologies

SiC(001) surface reconstructions

- Deposition of Si atoms onto preliminary cleaned SiC(001) surface
- Sublimation of deposited Si atoms by annealing in UHV ($p<1\times10^{-10}$ *Torr*)
- Fabrication of various silicon- and carbon-rich reconstructions with increasing temperatures

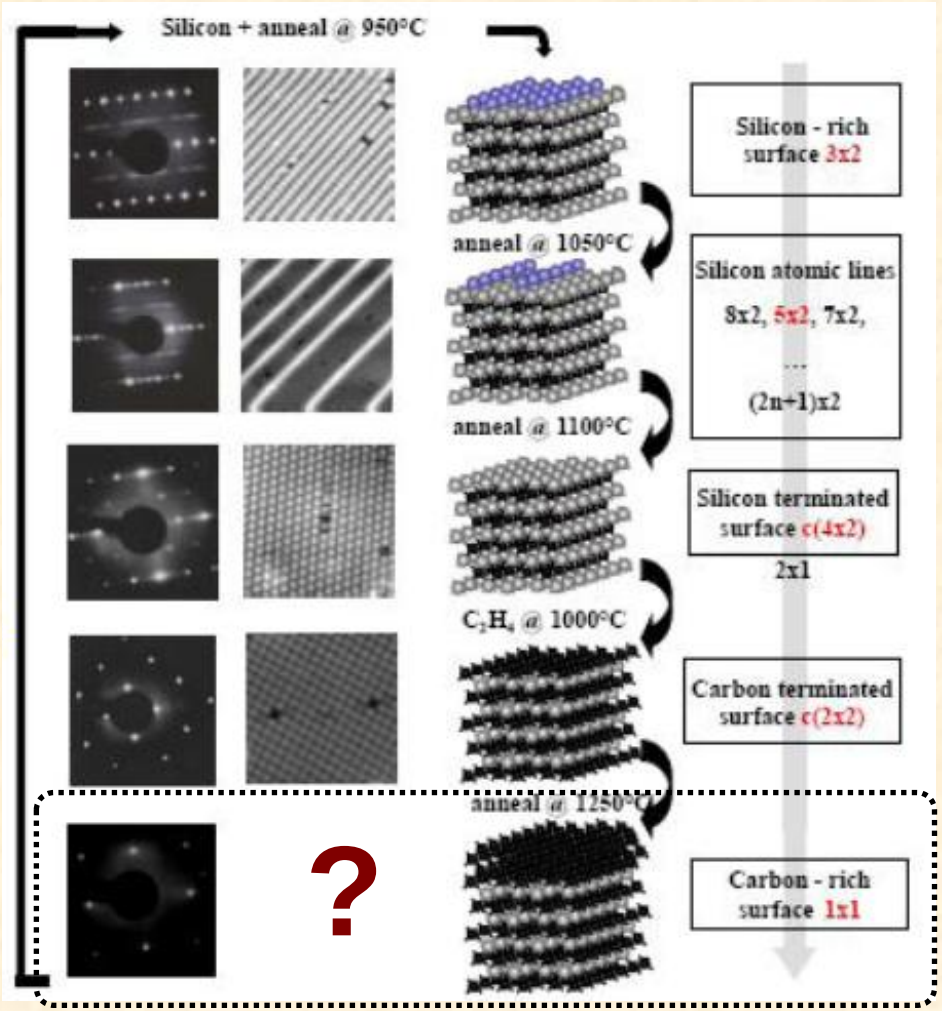

adapted from
P. Soukiassian and H. Enriquez,
J. Phys.: Condens. Matter 16 (2004) 1611

V. Derycke et al., Surf. Sci. 446 (2000) L101;
V. Derycke et al., Phys. Rev. Lett. 81 (1998) 5868;
F. Semond et al., Phys. Rev. Lett. 77 (1997) 2013;
V. Aristov et al., Phys. Rev. Lett. 79 (1997) 3700;
P. Soukiassian et al., Phys. Rev. Lett. 78 (1997) 907;
L. Douillard et al., Surf. Sci. 401 (1998) L395.

SiC(001) surface transformation during heating in UHV

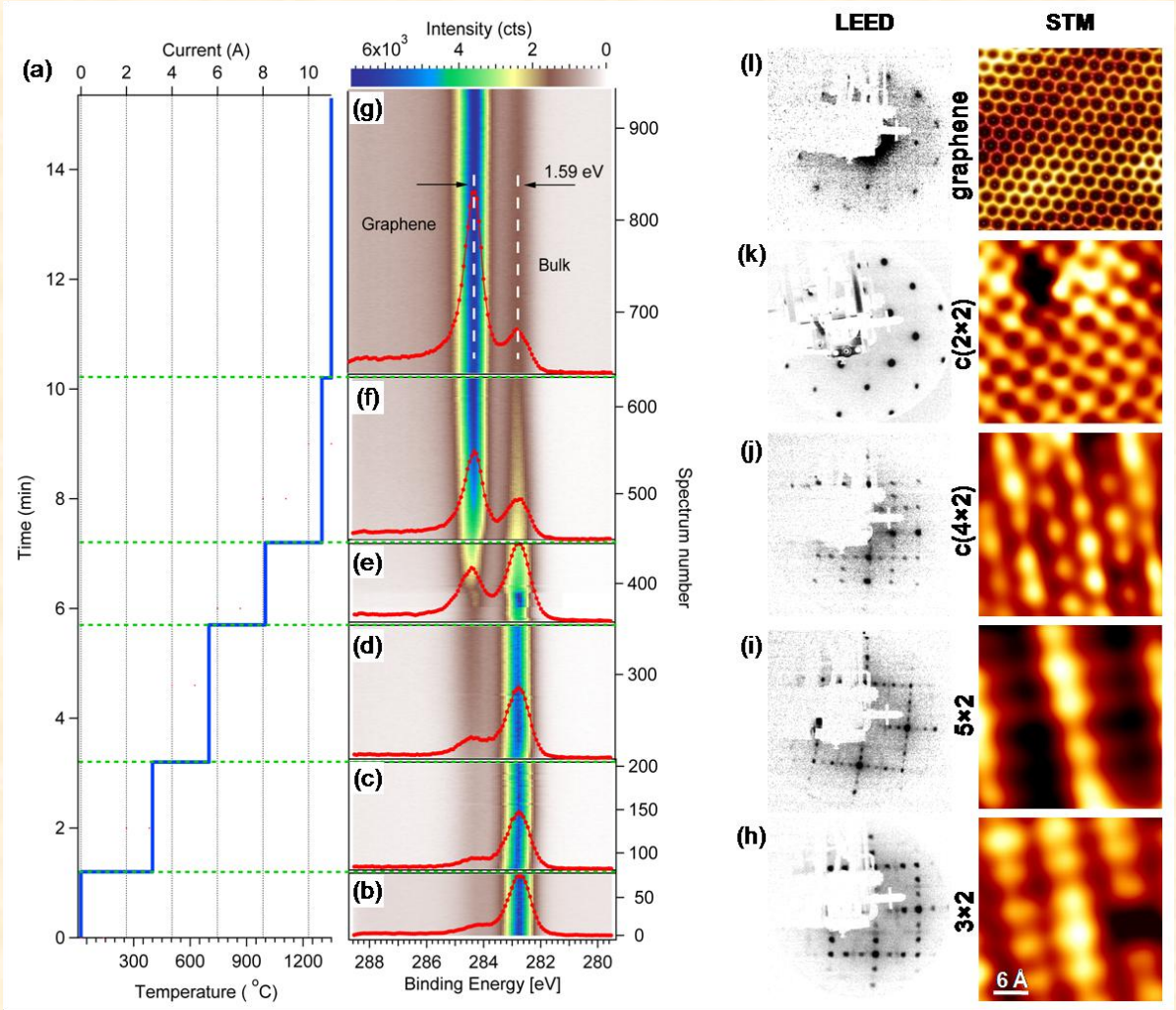

C 1s core level spectra were measured *in-situ* in a snapshot mode (1s/spectrum) during the sample heating using the Argus spectrometer at PETRA III (DESY, Hamburg);

LEED and STM data were obtained using the RT STM GPI-300 after successive heating the same SiC(001) sample

Graphitization of SiC(001) at t>1300°C

A.N. Chaika, V. Y. Aristov, O.V. Molodtsova,
***Progress in Materials Science 89* (2017) 1-30**

LEEM studies of graphene/SiC(001)

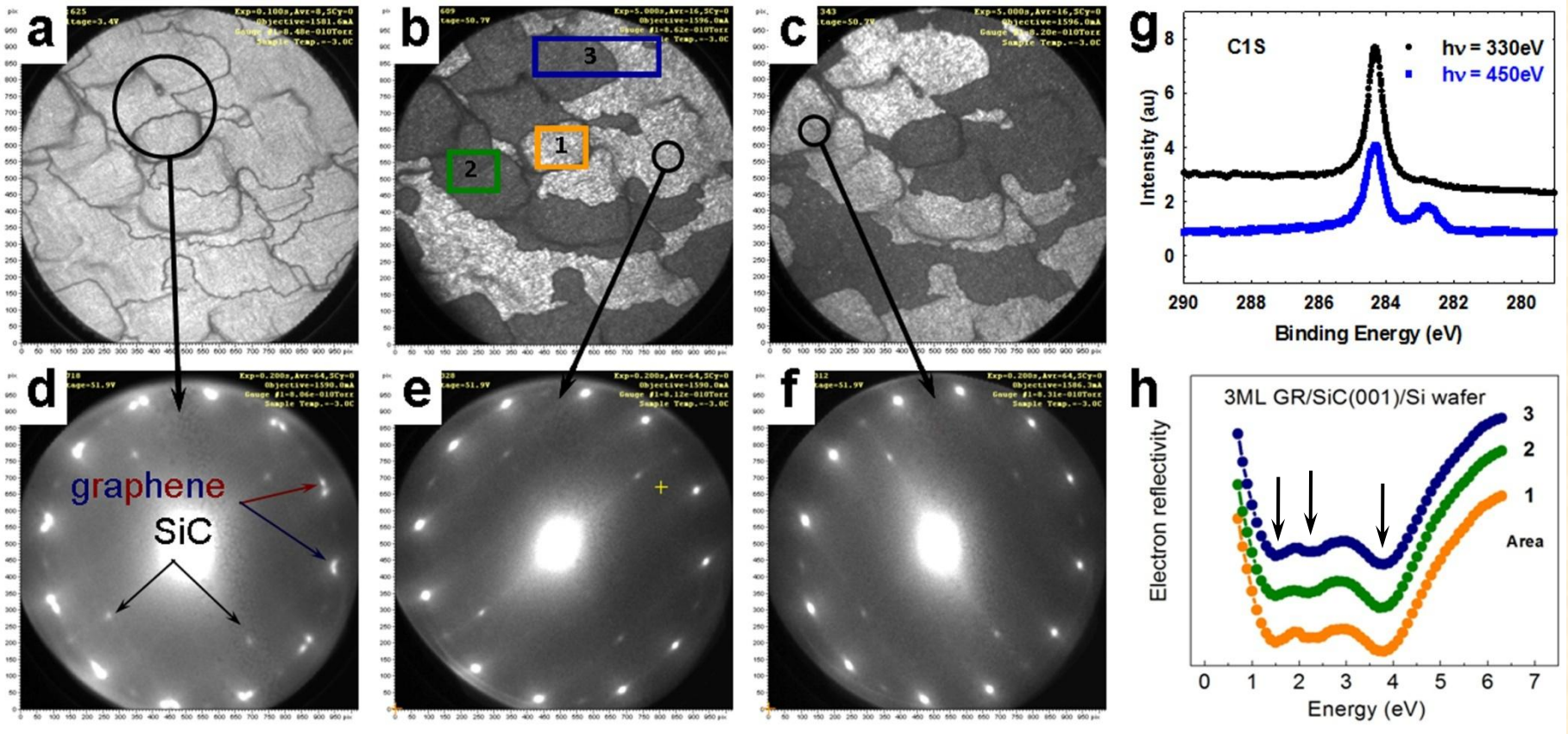

Nano Research 6 (2013) 562-570

LEED patterns from 1.5 μm surface areas (e,f) are rotated by 90° and consist of 12 non-equidistant spots

LEED pattern from 5 μm area (d) reveal 12 double spots

The reflectivity spectra (h) prove <u>uniform 3 ML thickness</u>

Dark-field images in (b) and (c) show the APD boundaries

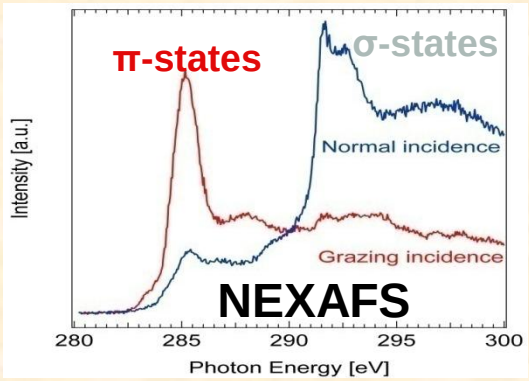

Explanation of the 12 double spots in graphene/SiC(001) LEED patterns

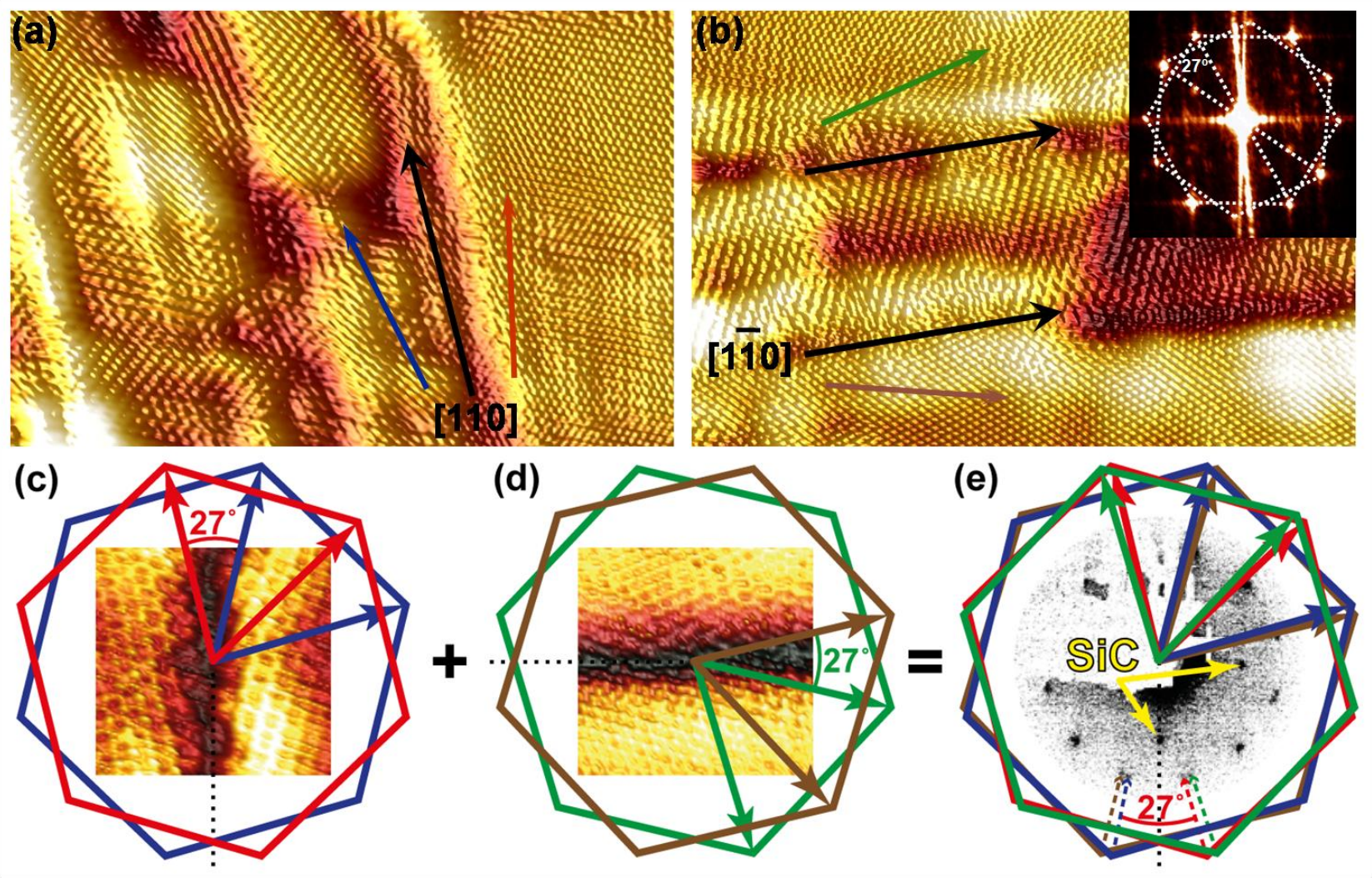

According to micro-LEED and STM data the domains are preferentially rotated by ±13.5° from two orthogonal <110> directions

Two systems of rotated domains in graphene/SiC(001)

vertical nanoribbons **horizontal nanoribbons**

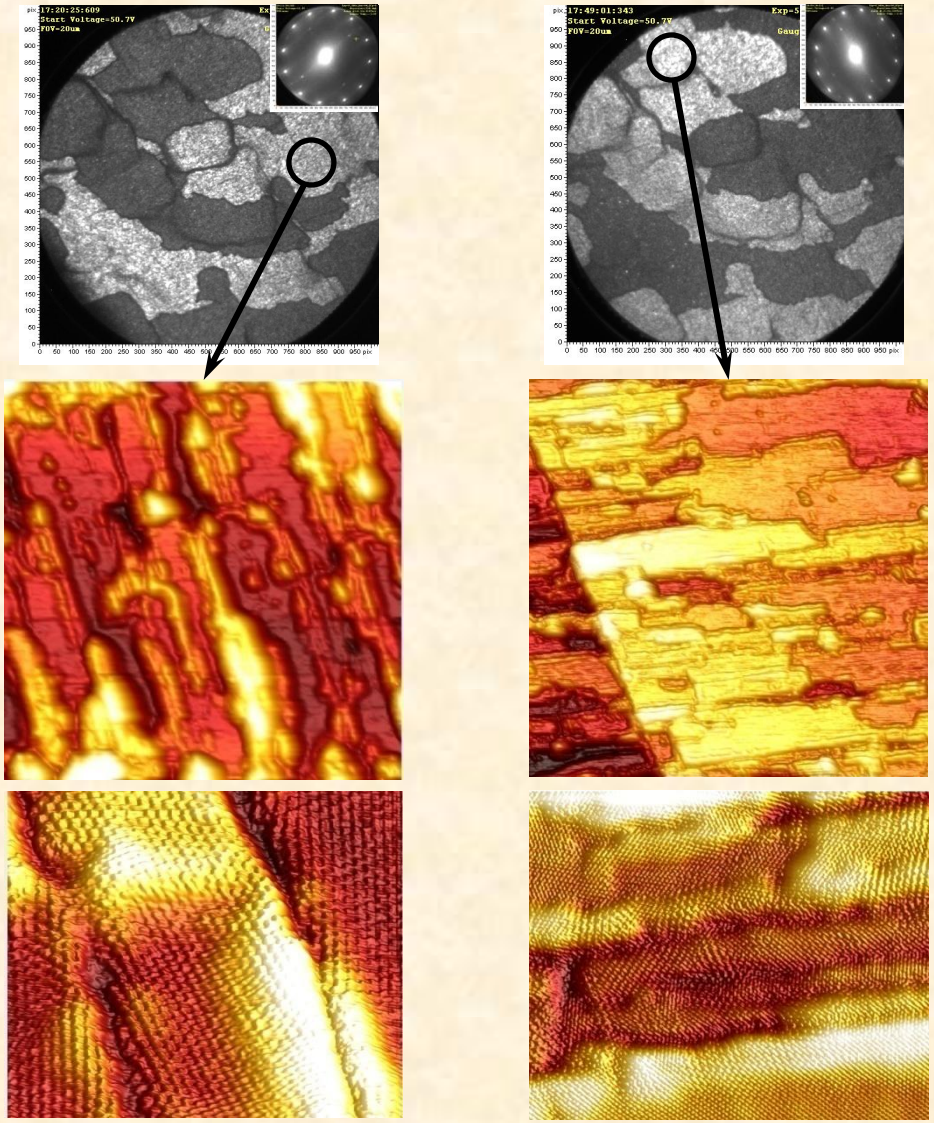

μ-LEED

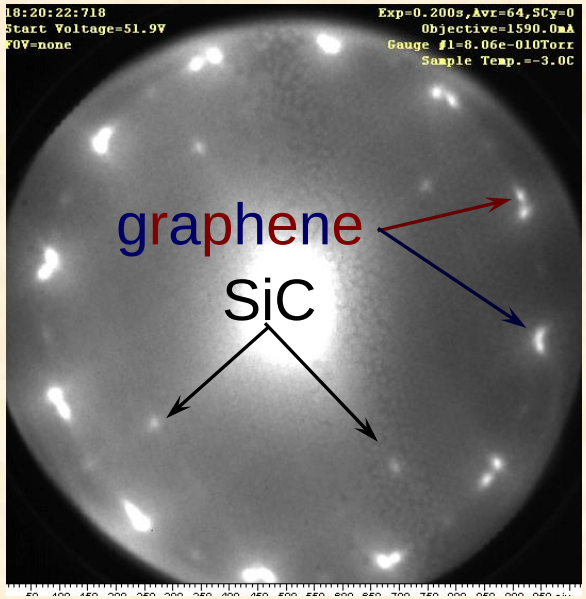

substrate spots and 12 double spots from graphene overlayer

12 double spots are caused by superposition of two LEED patterns produced by two systems of domains rotated by ±13.5º from the [110] and [1-10] directions

Atomic scale rippling of graphene/SiC(001)

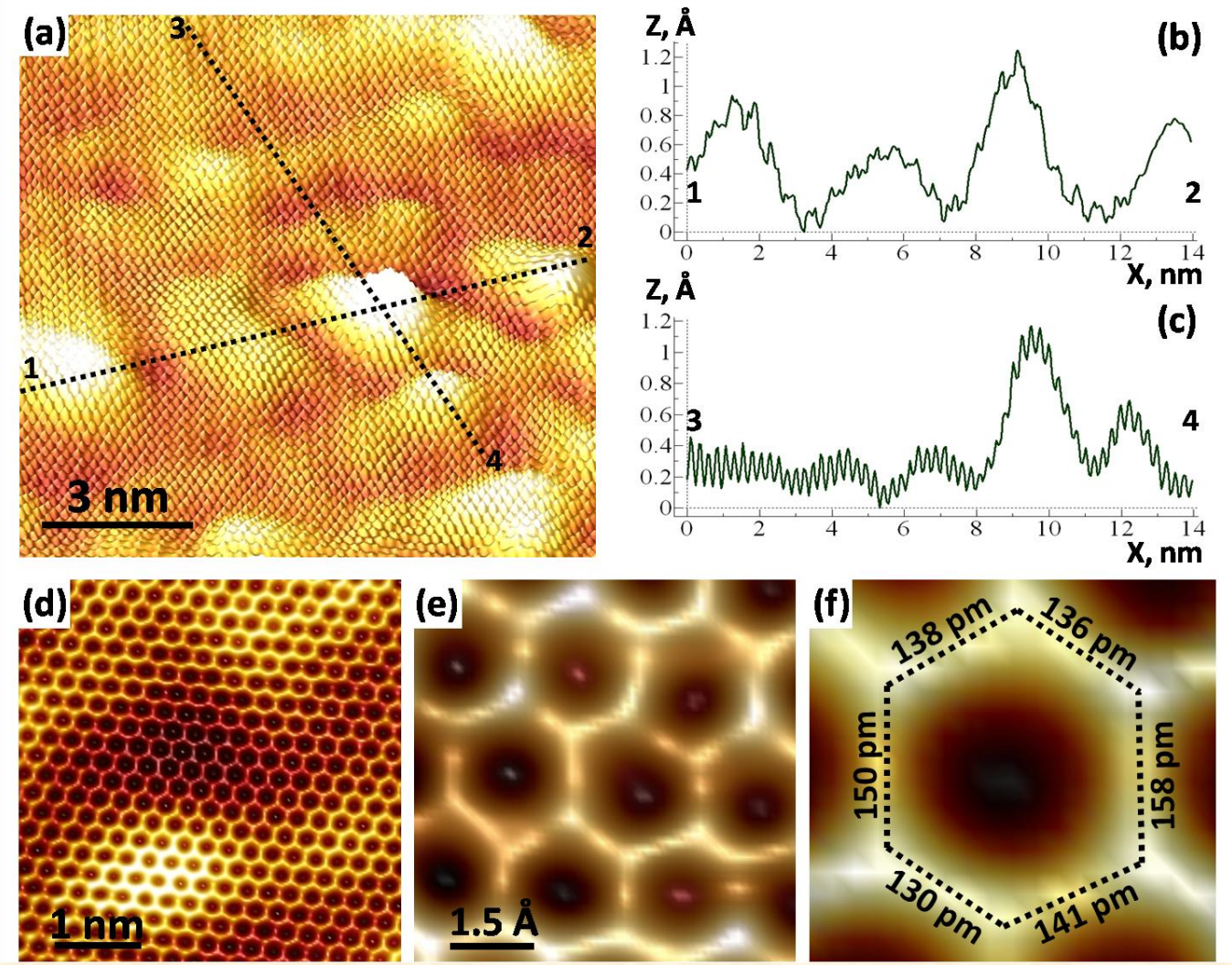

Random distortions of the carbon bonds in trilayer graphene on SiC(001) agree with the theory developed for single layer graphene

(A. Fasolino, J. Los, M. Katsnelson, Nature Mater. 6, 858 (2007))

ARPES studies of graphene/SiC(001)

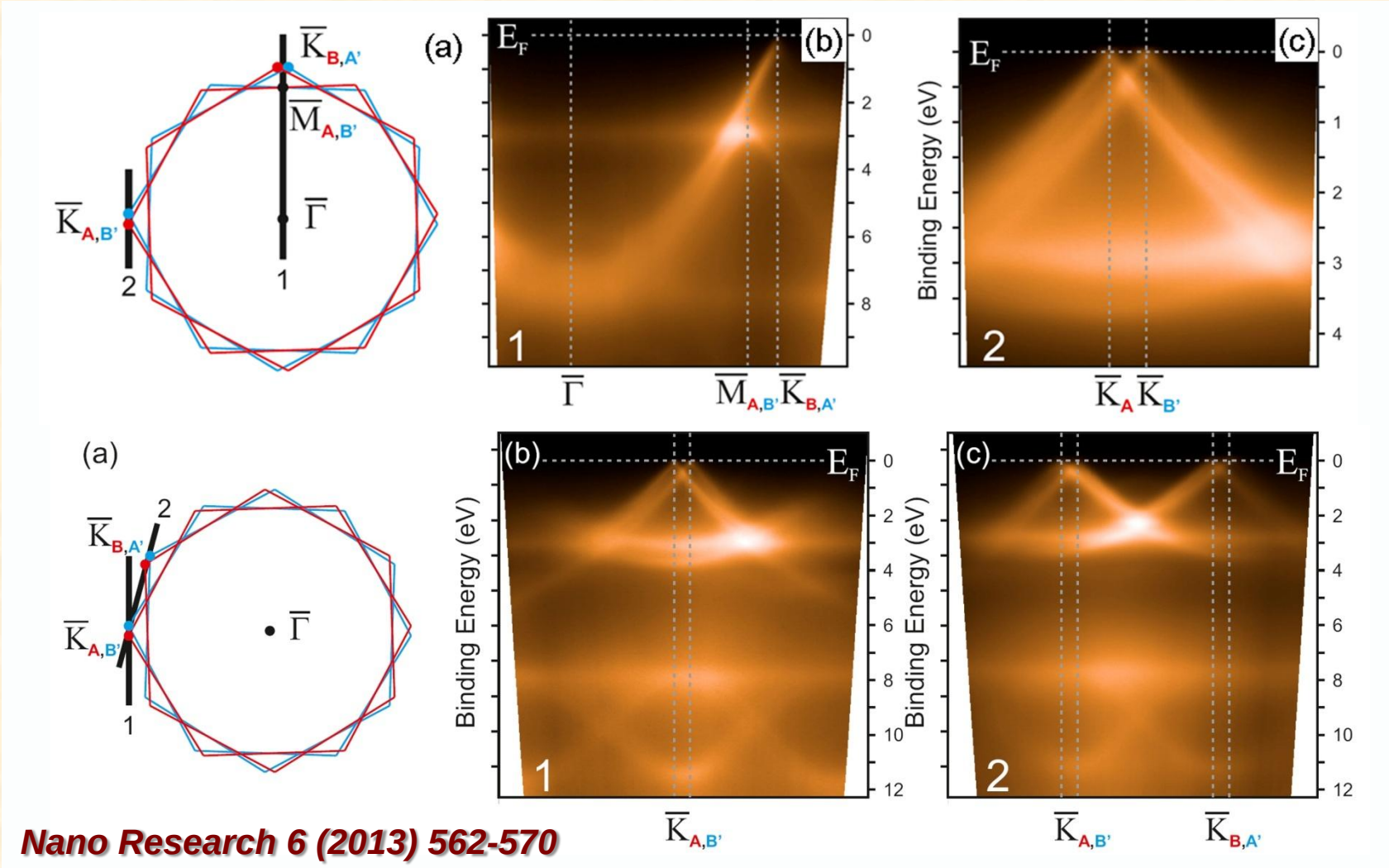

Nano Research 6 (2013) 562-570

24 Dirac cones in accordance with the rotated domain structure, nearly ideal linear dispersions, no shift of the Dirac points,

Atomic chains on SiC(001)-c(2×2) and domain boundaries in graphene

Directions of the nanodomain boundaries between rotated graphene domains (b) coincide with preferential directions of carbon atomic chains on SiC(001)-c(2×2) (a)

SiC(001)3×2 2°-off

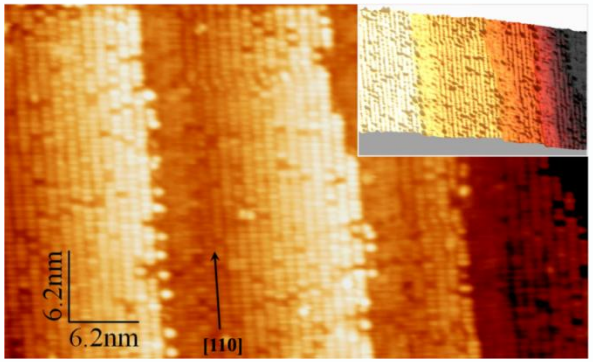

Can we control domain boundary using vicinal (stepped) substrate?

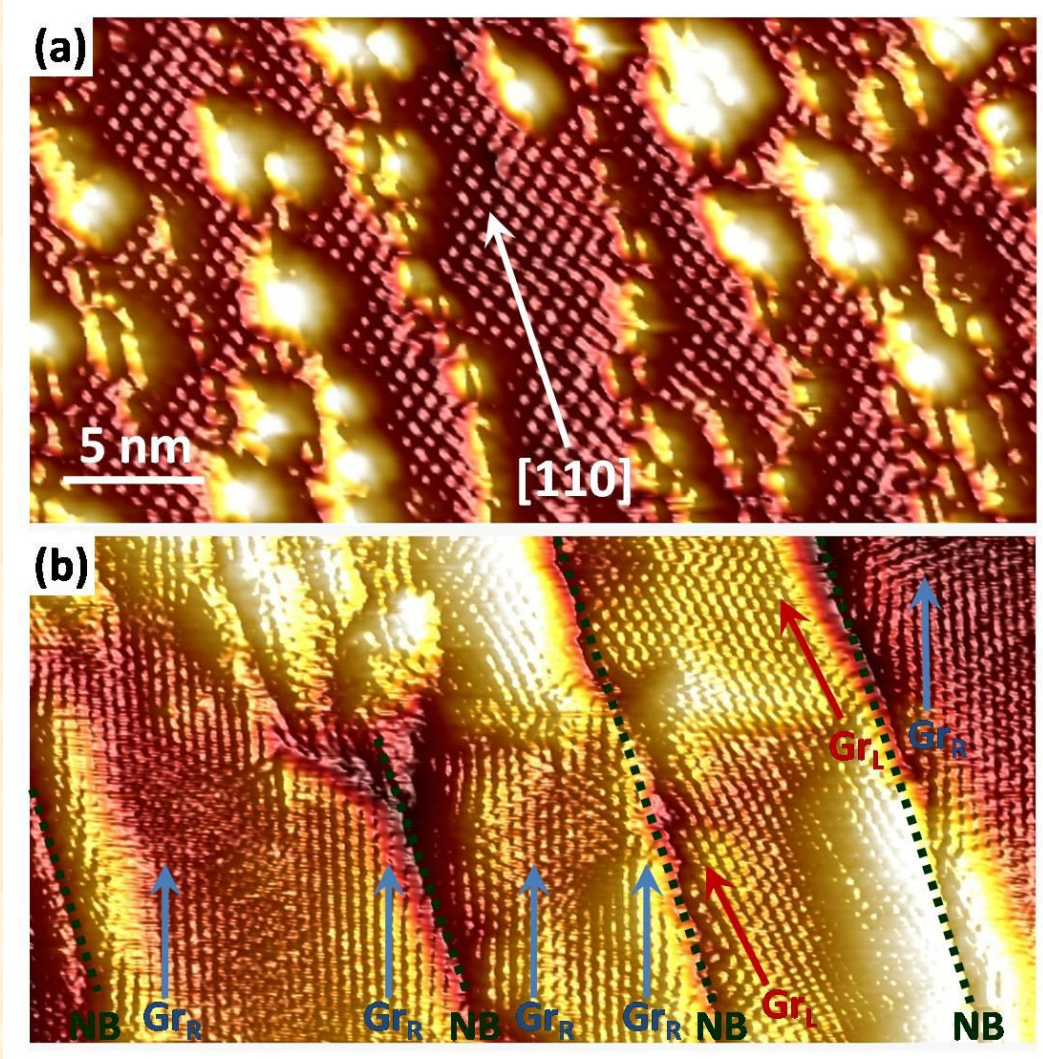

STM, LEEM, ARPES characterization of graphene grown on SiC(001) 2°-off

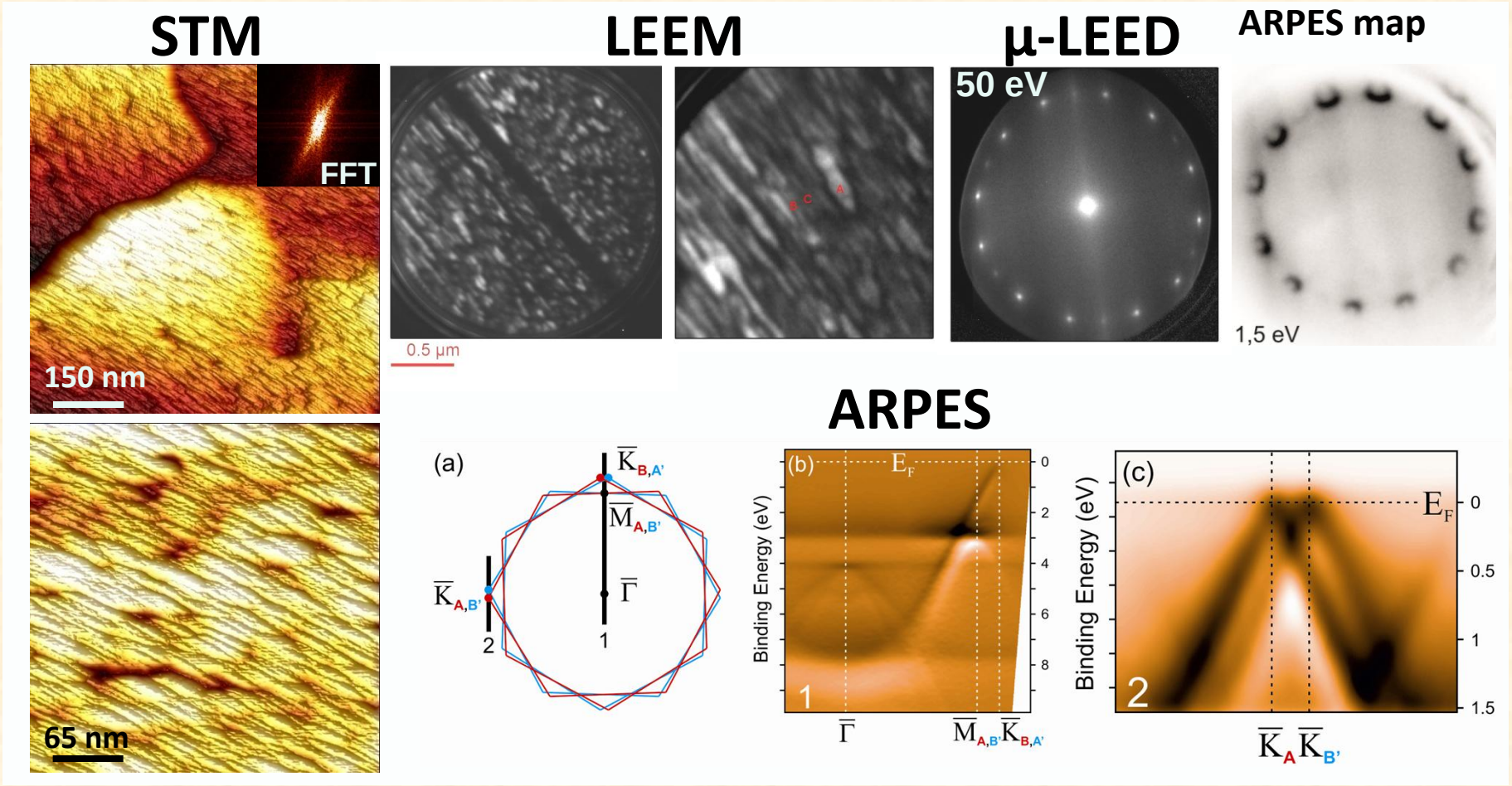

ARPES data are qualitatively the same on on-plane and vicinal (2°-, 4°-off) samples; LEEM and STM data support one preferential direction of the boundaries on the vicinal samples

Introducing energy band gap using graphene nanoribbons

PRL **98**, 206805 (2007) PHYSICAL REVIEW LETTERS week ending 18 MAY 2007

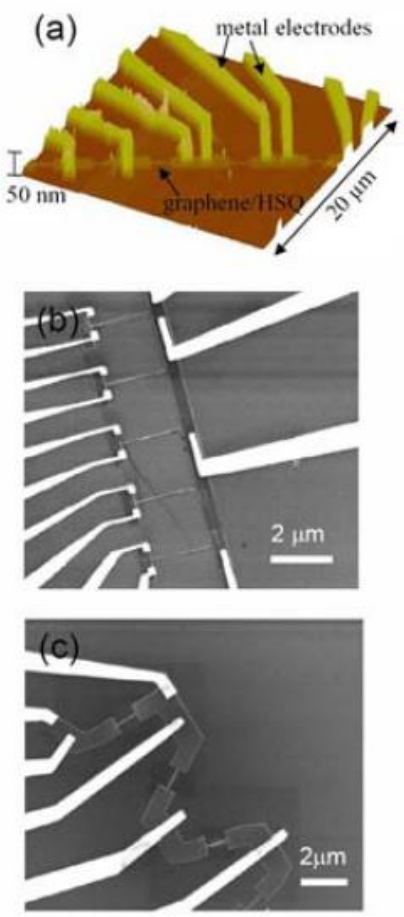

Energy Band-Gap Engineering of Graphene Nanoribbons

Melinda Y. Han,[1] Barbaros Özyilmaz,[2] Yuanbo Zhang,[2] and Philip Kim[2]
[1]*Department of Applied Physics and Applied Mathematics, Columbia University, New York, New York 10027, USA*
[2]*Department of Physics, Columbia University, New York, New York 10027, USA*
(Received 21 February 2007; published 16 May 2007)

We investigate electronic transport in lithographically patterned graphene ribbon structures where the lateral confinement of charge carriers creates an energy gap near the charge neutrality point. Individual graphene layers are contacted with metal electrodes and patterned into ribbons of varying widths and different crystallographic orientations. The temperature dependent conductance measurements show larger energy gaps opening for narrower ribbons. The sizes of these energy gaps are investigated by measuring the conductance in the nonlinear response regime at low temperatures. We find that the energy gap scales inversely with the ribbon width, thus demonstrating the ability to engineer the band gap of graphene nanostructures by lithographic processes.

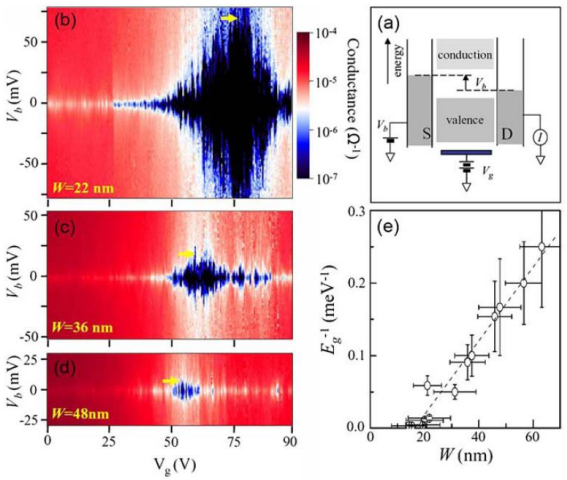

FIG. 3 (color online). (a) Schematic energy band diagram of a GNR with bias voltage V_b applied. The current I is controlled by both source-drain bias V_b and gate voltage V_g. (b)–(d) The differential conductance (dI/dV_b) of three representative GNRs from set P4 with $W = 22$, 36, and 48 nm as a function of V_b and V_g measured at $T = 1.6$ K. The light (dark) color indicates high (low) conductance as designated by the color map. The horizontal arrows represent $V_b = E_{gap}/e$. (e) E_{gap}^{-1} vs W obtained from similar analysis as (b)–(d), with a linear fit of the data.

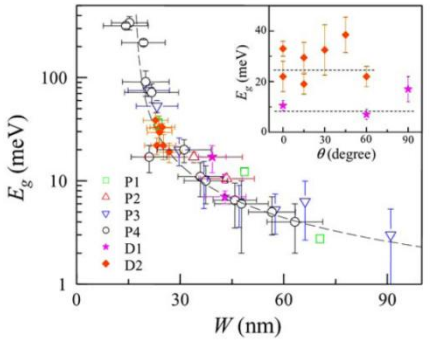

FIG. 4 (color online). E_{gap} vs W for the 6 device sets considered in this study: four (P1–P4) of the parallel type and two (D1, D2) with varying orientation. The inset shows E_{gap} vs relative angle θ for the device sets D1 and D2. Dashed lines in the inset show the value of E_{gap} as predicted by the empirical scaling of E_{gap} vs W.

Transport gap opening in nanostructured graphene on vicinal SiC(001)

4-probe transport measurements (current perpendicular to domain boundaries)

NB between rotated domains

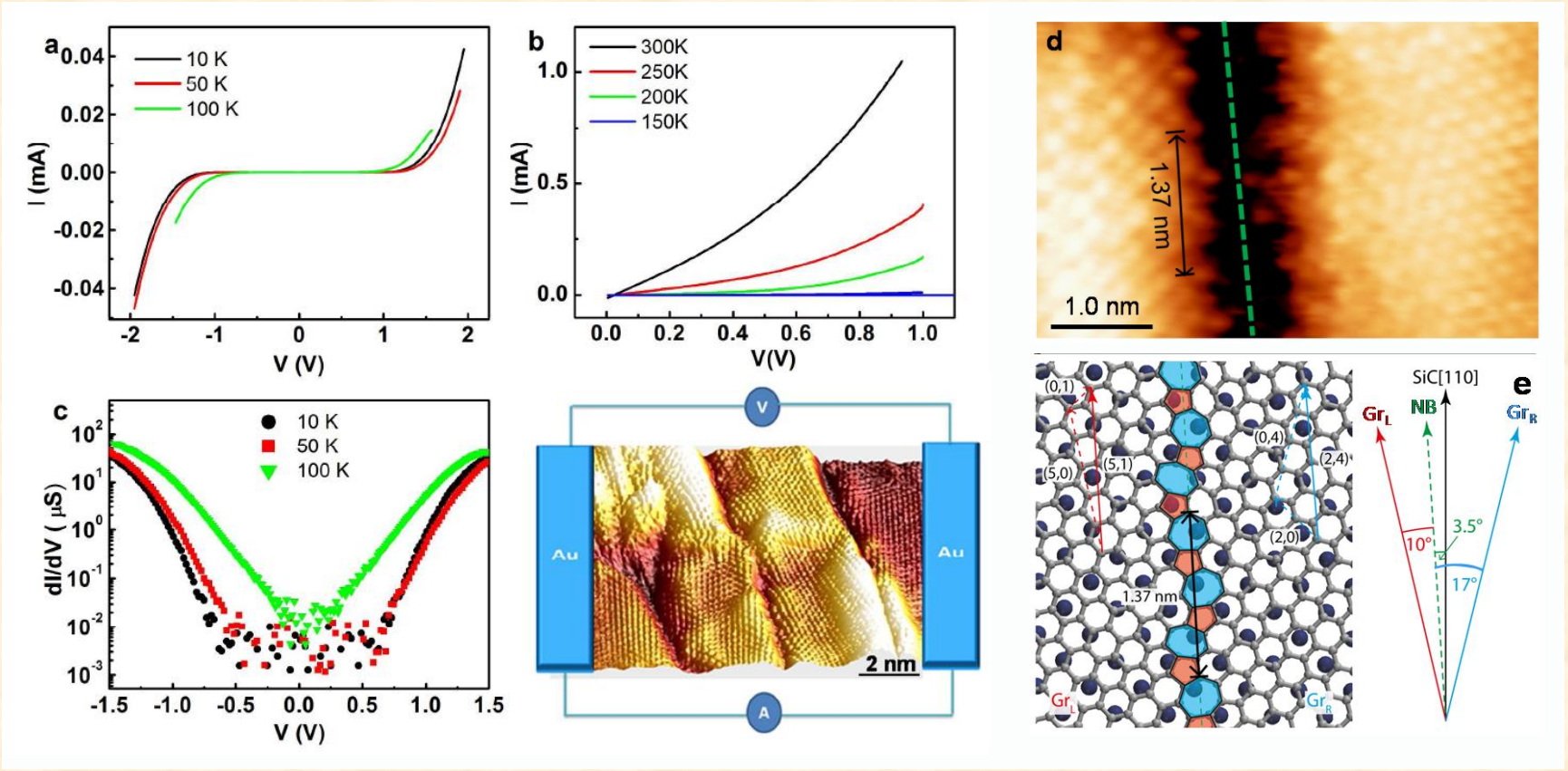

Han-Chun Wu et al., *ACS Nano, 2015*

Transport measurements along nanodomain boundaries

***I-V* measurements**

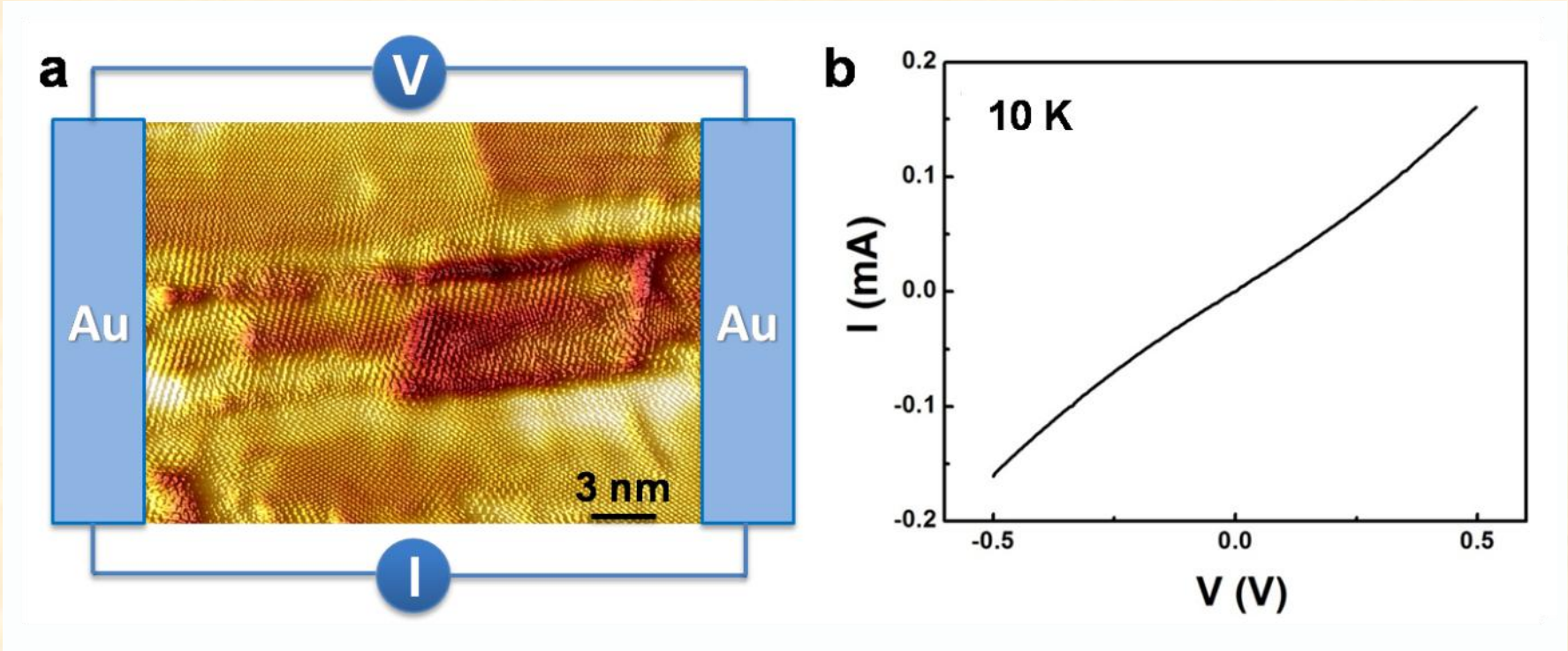

No transport gap at current parallel to nanodomain boundaries even at 10 K.

Possible explanation: *Transport gap opening in polycrystaline graphene with asymmetrically rotated domains*

LETTERS
PUBLISHED ONLINE: 22 AUGUST 2010 | DOI: 10.1038/NMAT2830
nature materials

Electronic transport in polycrystalline graphene

Oleg V. Yazyev[1,2]* and Steven G. Louie[1,2]*

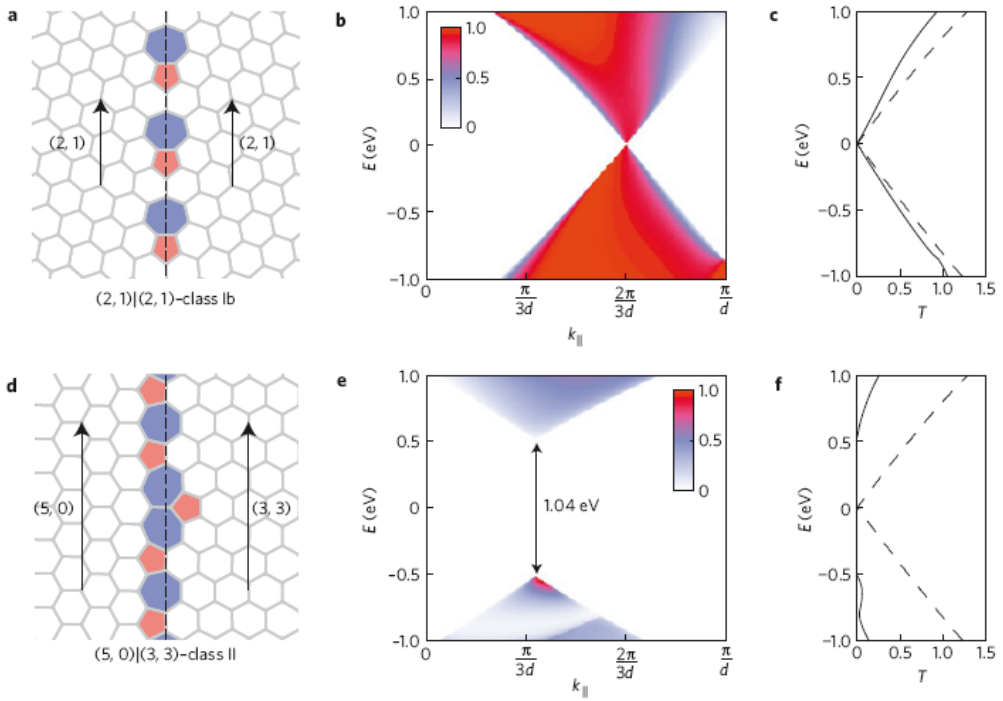

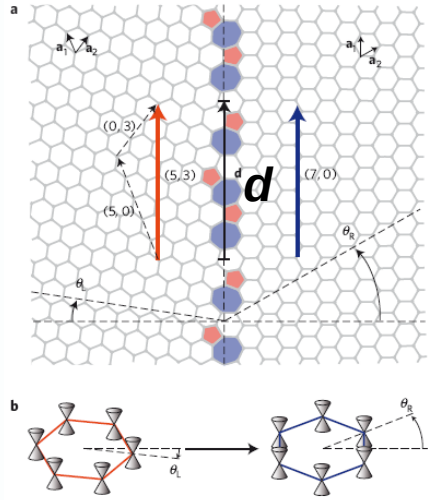

$E_g(eV)=1.38/d(nm)$

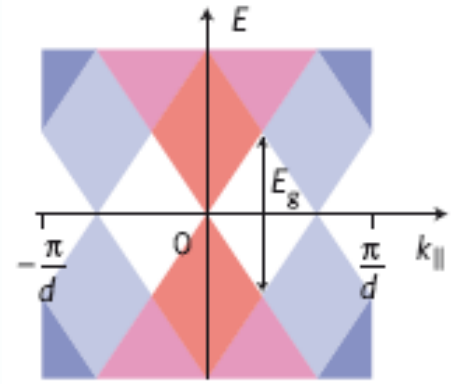

Asymmetrically rotated nanodomains

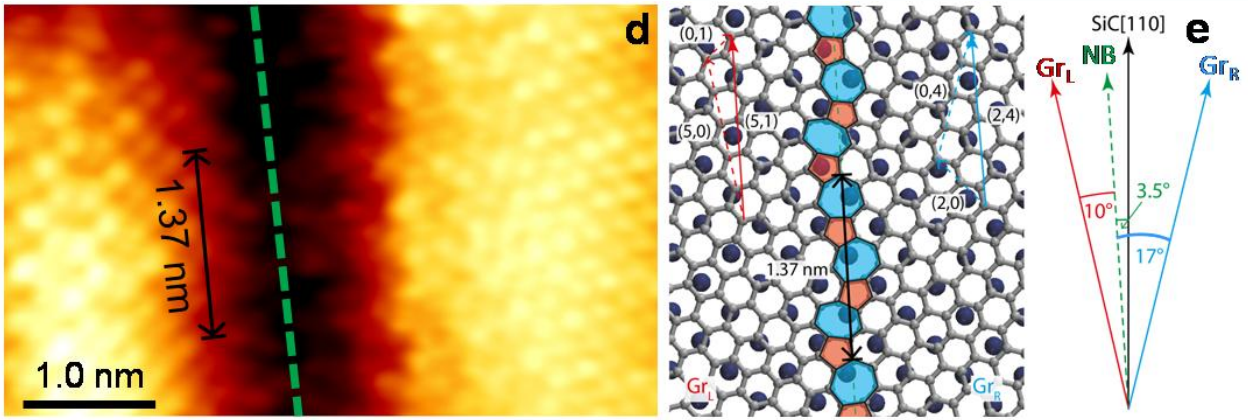

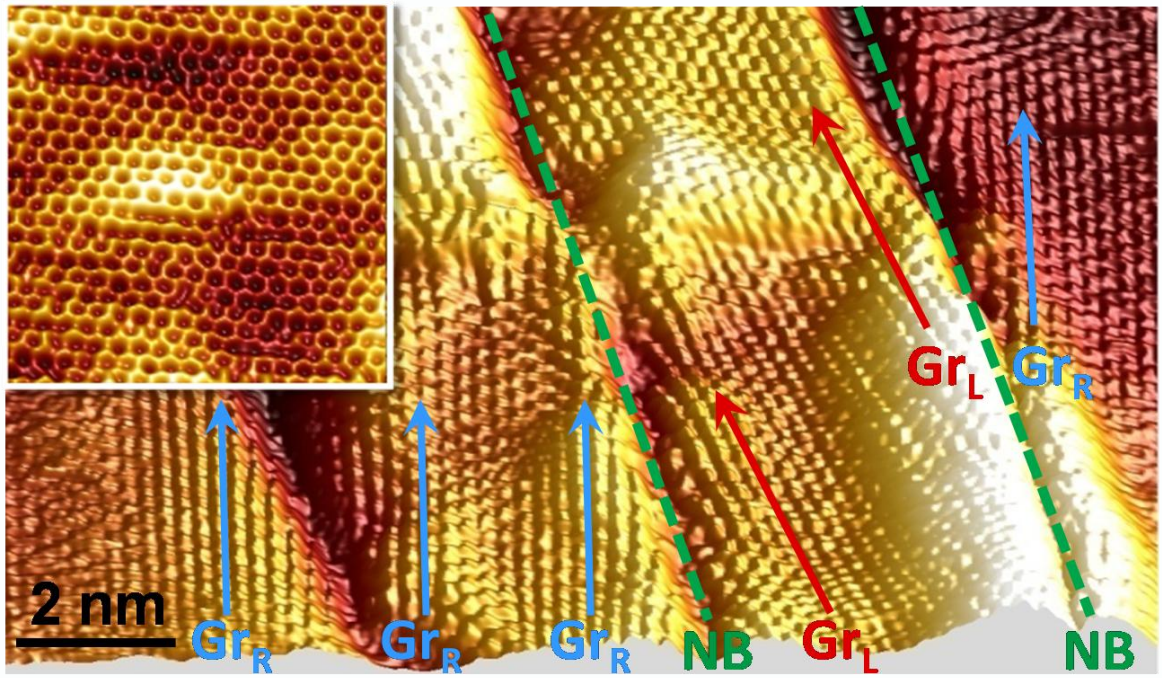

Graphene lattices in neighboring domains are rotated by 17° clockwise (Gr_R) and 10° anticlockwise (Gr_L) relative to the nanodomain boundaries

Current density distribution in graphene containing one boundary: Calculations

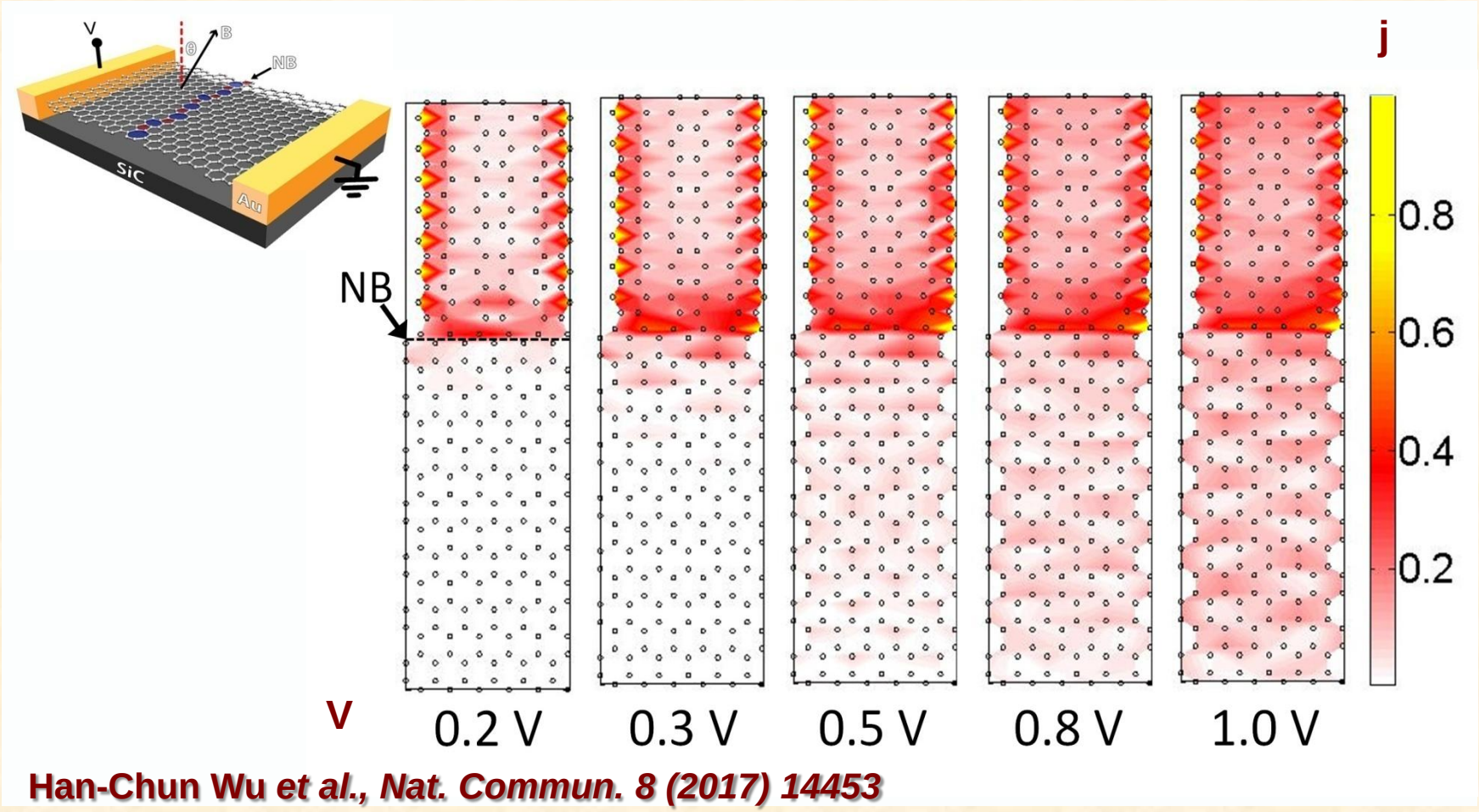

Han-Chun Wu *et al., Nat. Commun. 8 (2017) 14453*

Current distribution at different voltages calculated from first principles. The simulations indicate the presence of the transport gap and high current density along NB.

Three different nanodomain boundaries

Bent layer, no line defect

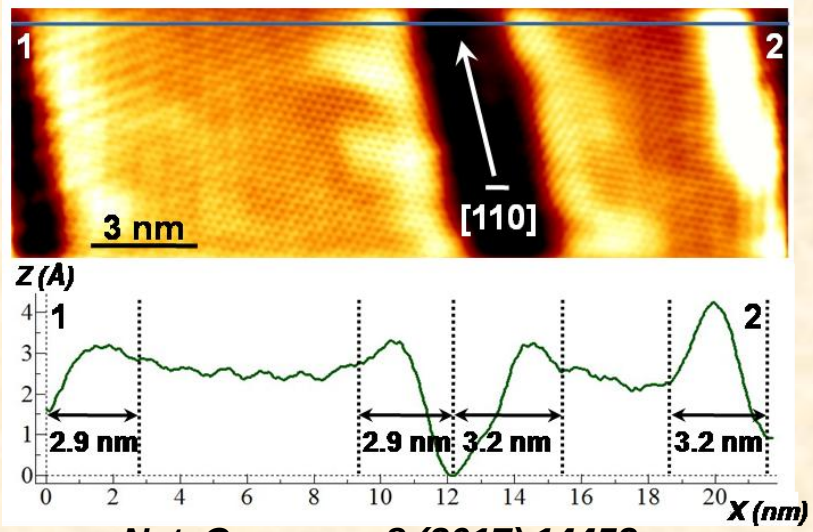

Nat. Commun. 8 (2017) 14453

Line defect, ripples near boundary

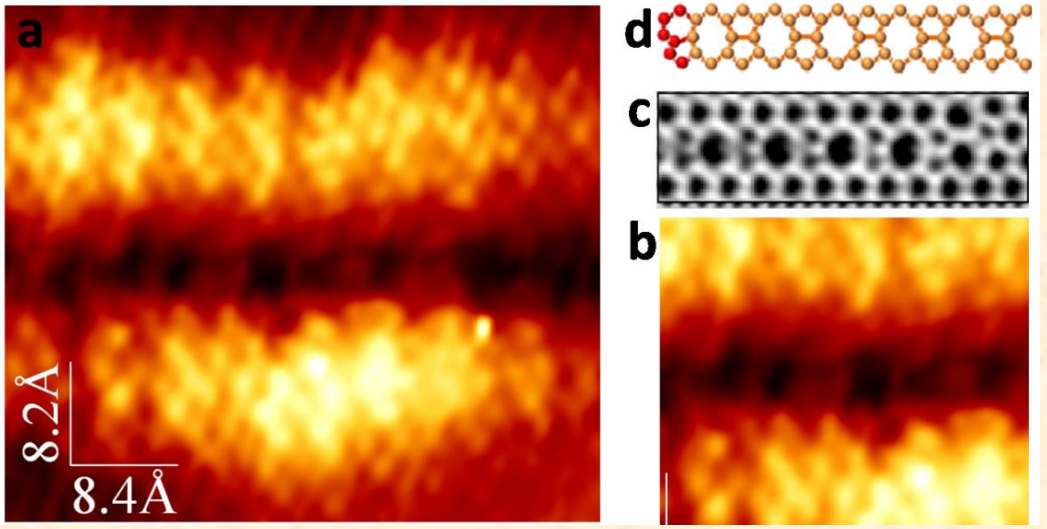

(a,b) STM images of a boundary between nanodomains with the same graphene lattice orientation **(*our experiments*)**.

(c,d) Electron microscopy image (c) and a model of domain boundary (d) *presented by* ***J.-H. Chen et al. in Phys. Rev. B 89, 121407(R) (2014)***.

Symmetrically rotated lattices

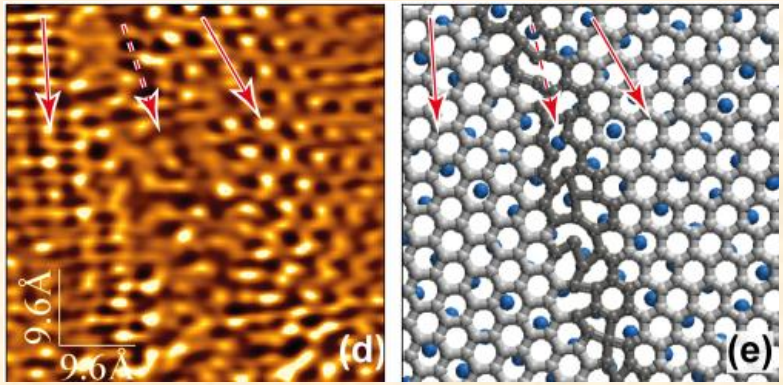

Nanotechnology, 2014

In all cases there is a nm-scale rippling near nanodomain boundaries

Role of atomic scale rippling at nanodomain boundaries

STM experiment

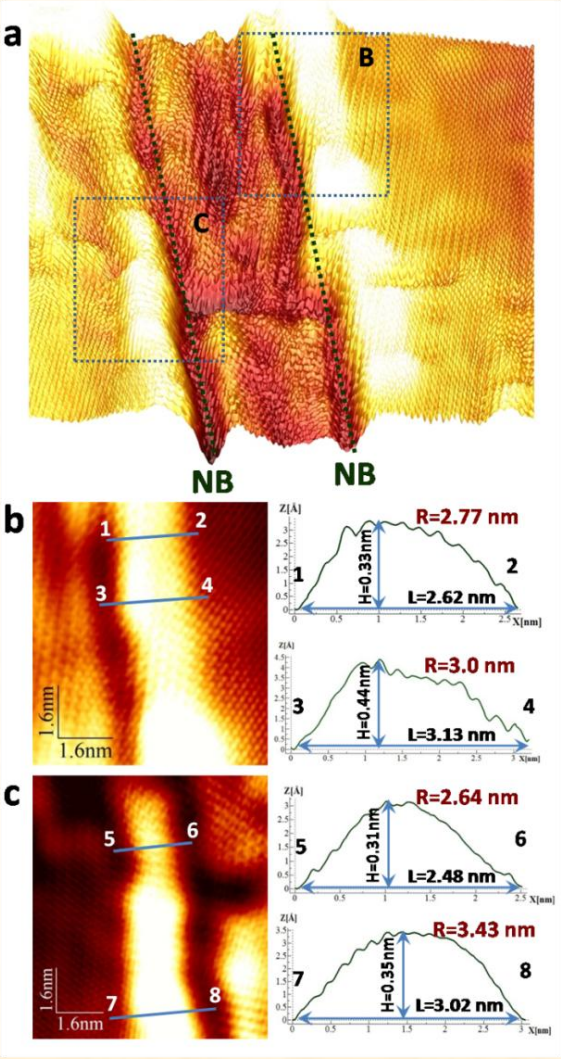

Nat. Commun. 8 (2017) 14453

According to STM, the radii of curvature of the ripples near domain boundaries are in the range of 2—5 nm.

According to calculations, transport gap can be observed even without line defects (symmetrically or asymmetrically rotated domains). Ripples can be responsible for the transport gap opening.

Calculations

name	Armchair ribbon	Zigzag ribbon
structure	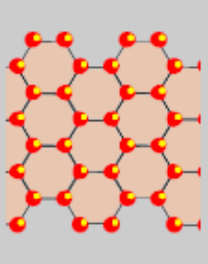	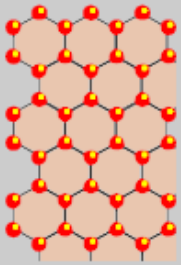
Defect type	Without line defect	Without line defect
Band structure	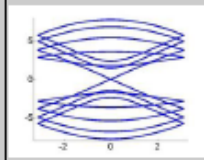	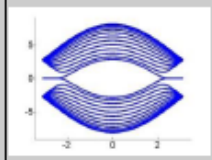
Transmission	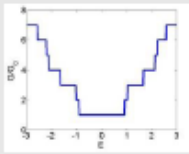	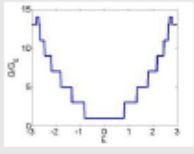

H.-C. Wu, C.-R. Chang et al., to be published

Magnetoresistance in $B_{//}$ and I-V characterization of graphene/SiC(001)

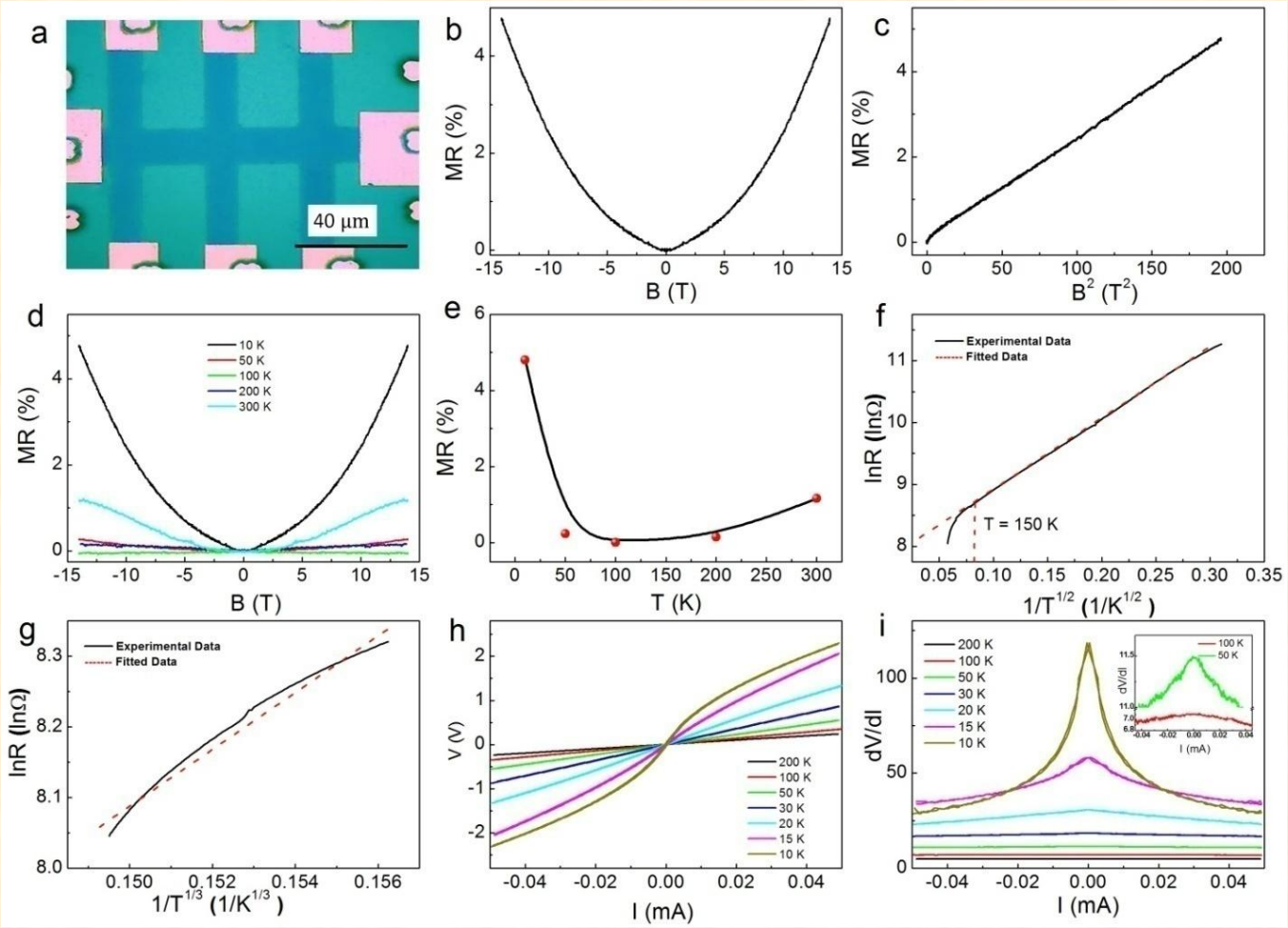

Positive in-plane MR ~ B at low and MR ~ B^2 at high magnetic fields. Switch from 2D to 1D hopping conductivity at T<150 K.

H.-C. Wu et al., Nat. Commun. 8 (2017) 14453

MR and transport properties of graphene on SiC(001) containing 1-2 boundaries

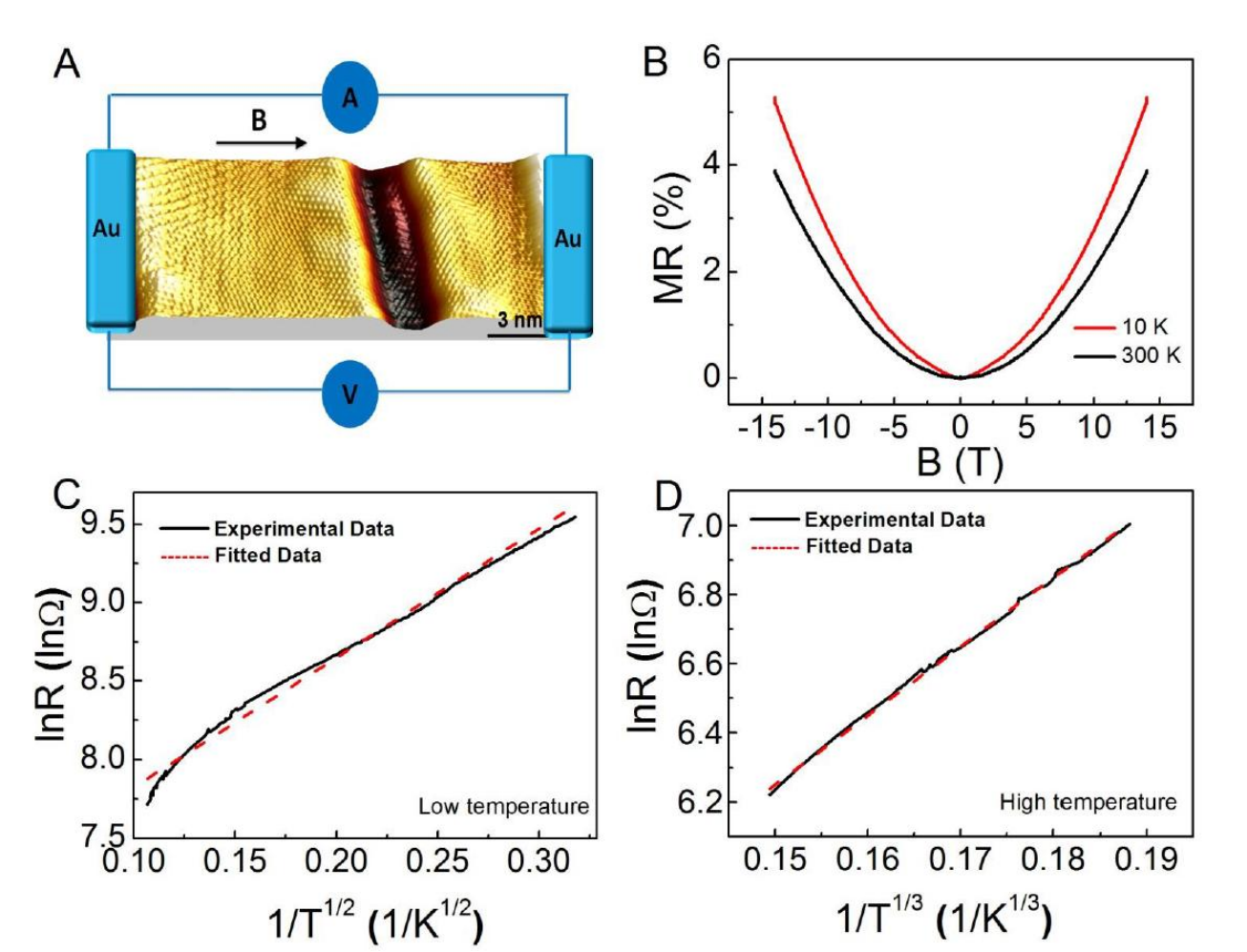

MR and transport properties in nano-gap contact are qualitatively the same as in micrometer-scale device

Charge (d) and spin density (e) distribution near nanodomain boundaries: Calculations

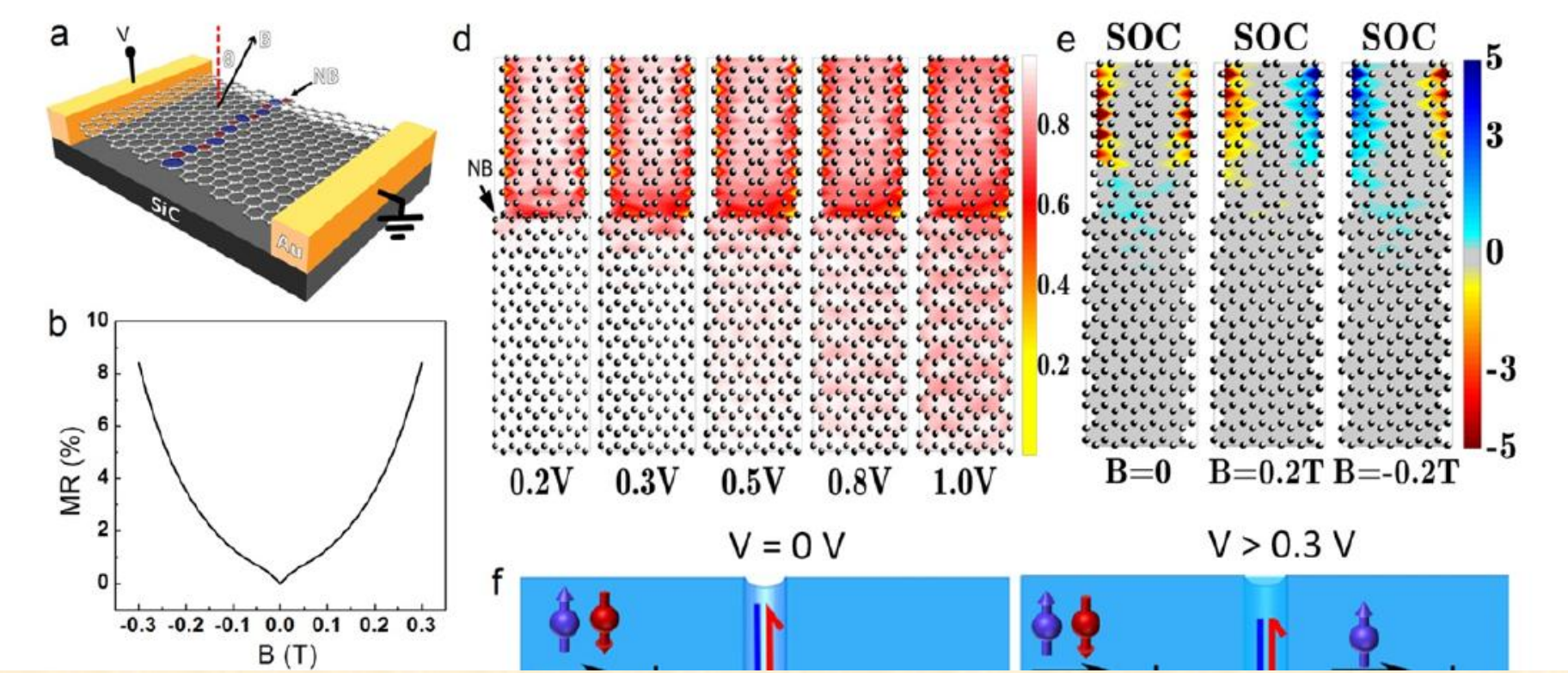

Above 150 K electrons with particular spin direction are accumulated near nanodomain boundaries field because of Zeeman splitting; at low temperature positive MR arises from NBs.

H.-C. Wu et al., Nature Communications (2017)

Немного истории

Исторический экскурс

1887 – открытие фотоэффекта (PE): Г.Герц

H. Hertz

1895 –открытие X-лучей: В.Рентген

1901 – присуждена Нобелевская премия (the FIRST) Nobel prize.

1905 – теория фотоэффекта А.Эйнштейн.

1921 –присуждена Нобелевская премия Nobel prize.

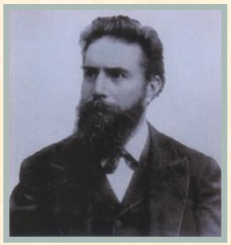

W.C. Roentgen

Karl M. G. Siegbahn, (1886 – 1978) Sweden присуждена Нобелевская премия 1924 за исследования по X-ray спектроскопии.

K.M.G. Siegbahn

Kai M. Siegbahn (SON!) (1918 -). присуждена Нобелевская премия в 1981 за развитие методов электронной спектроскопии высокого разрешения

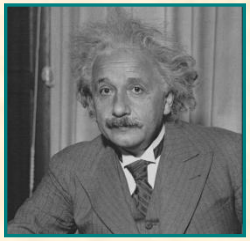

A. Einstein

1950's – huge progress in instrumentation:
- increasing the resolution of the photoelectron energy analysers,
- design of X-ray sources.
- application for surface analysis (named ESCA) by K. Siegbahn and co-workers
- also now - the discovery of the PE in gases (Turner and co-workers) and the development of the UPS (Spicer and co-workers)

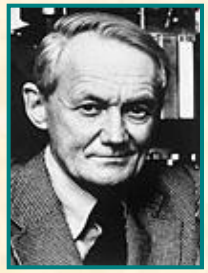

Kai M. Siegbahn

1960: occurrence of commercial XPS instruments.

Gerhardt Ertl (1936-)

присуждена Нобелевская премия
2007 Nobel prize in chemistry:

"for his studies of chemical processes on solid surfaces"

Рождение зондовой микроскопии

1971г. - **Russell Young** Изображение дифракционной решетки Прибор – Topografiner (Phys. Rev. Lett. V. 27, N 14, 1971, P. 922-924)

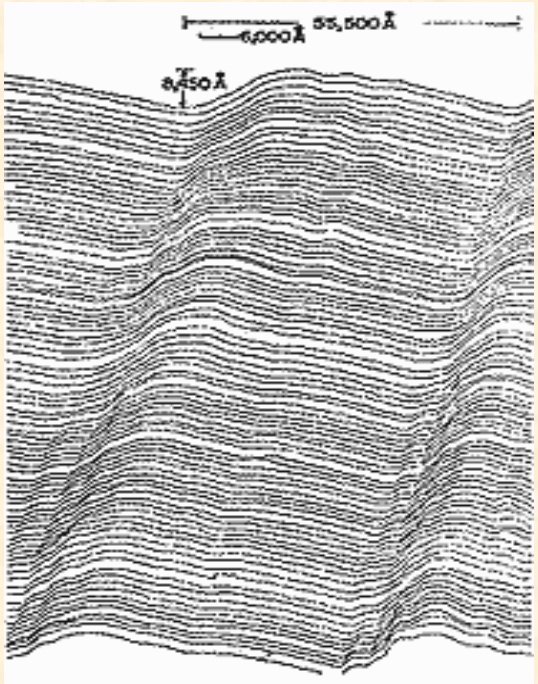

R. Young, J. Ward, F. Scire,
Rev. Sci. Instrum. 43, 999 (1972)

1986г. – Нобелевская премия (Heinrich Rohrer and Gerd K. Binnig)

Binnig и Rohrer. Патент на изобретение ***Сканирующего туннельного микроскопа*** подан Aug. 10, 1982 (Priority Sept. 20, 1979)

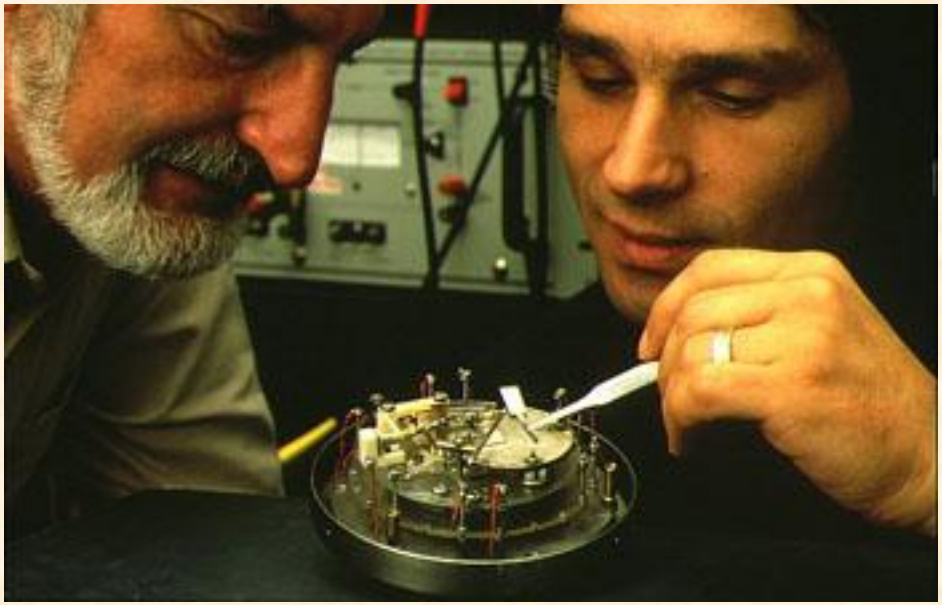

Si(111)-7×7

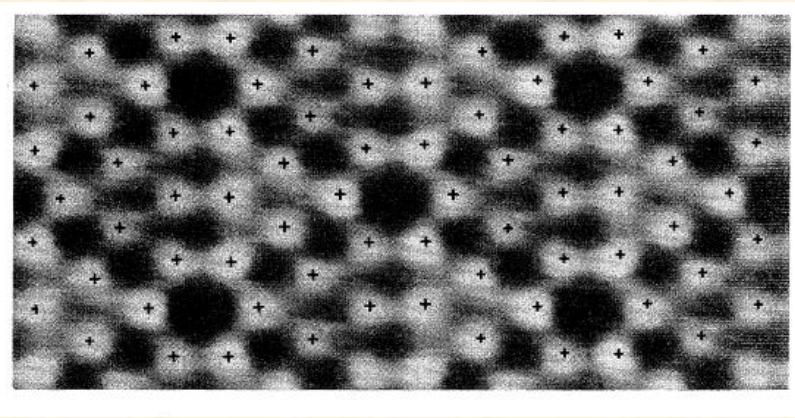

G. Binnig, H. Rohrer, *PRL, 1983*

Области применения ЭС и СЗМ

материаловедение

Тонкопленочные технологии

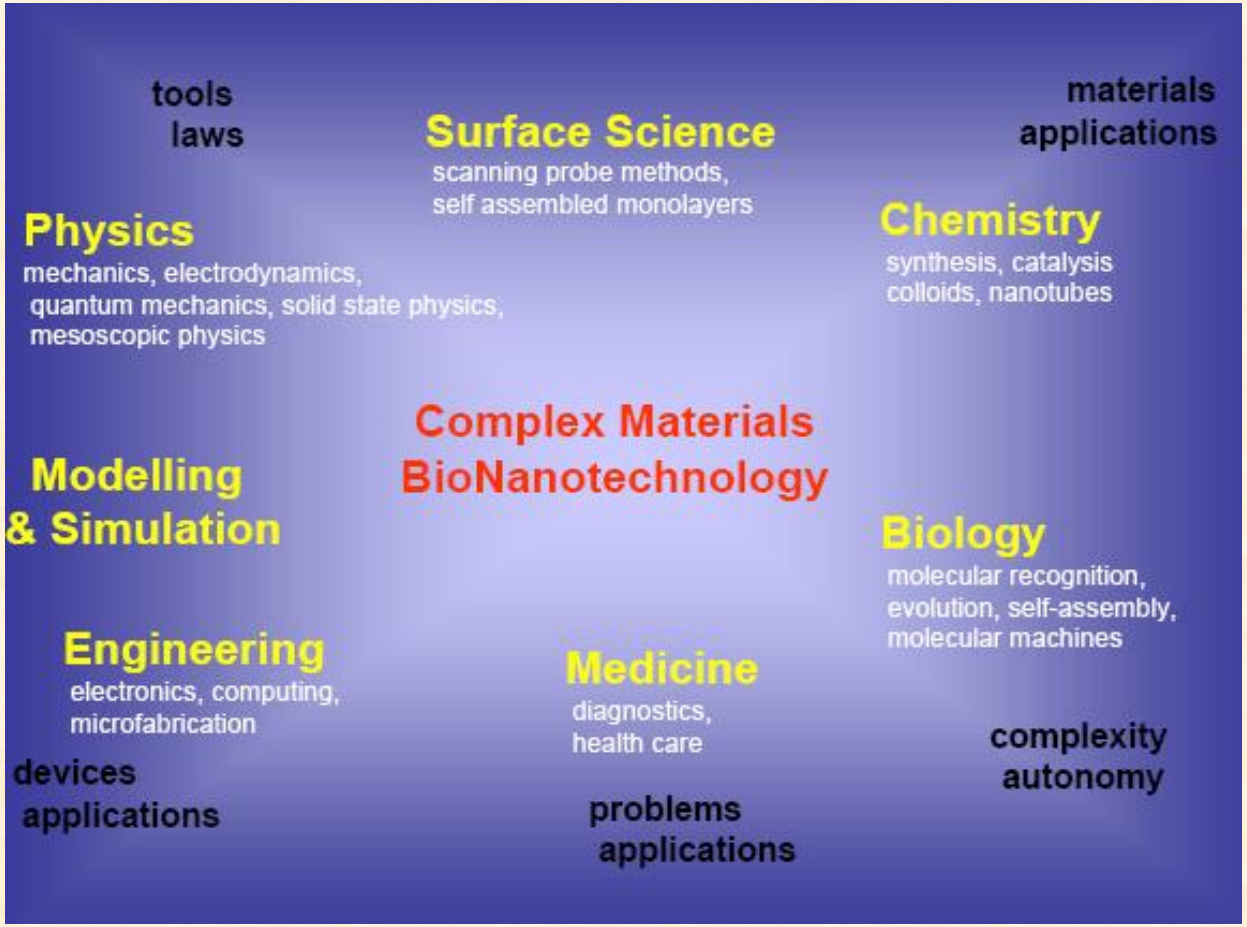

катализ

коррозия

медицина

биология

экология

Микро- и наноэлектроника

сенсоры

Спасибо за внимание!